Full title:

The *Blepharisma stoltei* macronuclear genome: towards the origins of whole genome reorganization

Short title:

Macronuclear genome of *Blepharisma stoltei* strain ATCC 30299

Minakshi Singh[1], Kwee Boon Brandon Seah[1], Christiane Emmerich[1], Aditi Singh[1], Christian Woehle[2], Bruno Huettel[2], Adam Byerly[3], Naomi Alexandra Stover[4], Mayumi Sugiura[5], Terue Harumoto[5], Estienne Carl Swart[1,*]

1. Max Planck Institute for Biology, Tuebingen, Germany
2. Max Planck Genome Center Cologne, Max Planck Institute for Plant Breeding, Cologne, Germany
3. Department of Computer Science and Information Systems, Bradley University, Peoria IL, USA
4. Department of Biology, Bradley University, Peoria, IL, USA
5. Nara Women's University, Nara, Japan

* Corresponding author

Abstract

The germ-soma distinction is a defining feature of multicellular eukaryotes. Analogous to this, ciliates, a ubiquitous microbial eukaryote lineage, have morphologically and functionally distinct nuclei, but within single cells: the germline micronucleus (MIC) and somatic macronucleus (MAC). The origins and mechanisms of the MIC to MAC transformation, especially the extensive elimination of abundant internally eliminated sequences (IESs) and transposons during genome reorganization, are great biological mysteries. *Blepharisma* represents one of the two earliest diverging ciliate classes, and has unique, dual pathways of MAC development, making it ideal for investigating the functioning, origins and evolution of these processes. Here, we report the MAC genome assembly of *Blepharisma stoltei* strain ATCC 30299 (41 Mb), arranged as numerous alternative telomere-capped minichromosomes, tens to hundreds of kilobases long. The *B. stoltei* MAC genome encodes eight PiggyBac transposase homologs liberated from transposons. All are subject to purifying selection, but just one, the putative *Blepharisma* IES excisase, has a complete catalytic amino acid triad. Numerous genes encoding other domesticated transposases are present in *B. stoltei*, and often are comparably strongly upregulated in a similar timeframe to model ciliate genome reorganization homologs. Our phylogenetic investigations suggest the PiggyBac homologs may have been ancestral ciliate IES excisases. The *B. stoltei* MAC genome, together with the upcoming MIC genome, highlights the evolution and complex interplay between transposons, domesticated transposases, and genome reorganization in the context of germline-soma differentiation within single cells.

41 # Abbreviations

42 - MIC - micronucleus
43 - MAC - macronucleus
44 - IES - interspersed eliminated sequence
45 - MDS - macronuclear-destined sequence
46 - PacBio - Pacific Biosciences
47 - CLR - continuous long read (PacBio)
48 - CCS - circular consensus sequence (PacBio)
49 - HiFi - High-fidelity read (PacBio)
50 - ATAS - alternative telomere addition site
51 - PBLE - PiggyBac-like element
52 - PGBD - PiggyBac element-derived
53 - Pgm - PiggyMac
54 - PgmL - PiggyMac-like

Introduction

Acquisition of new organelles defines and is responsible for the origins of eukaryotes [1]. Ciliates represent one of a couple of eukaryotic lineages with more than one kind of nucleus within individual cells [2]. Profound differences between the ciliate nuclei and the genomes they contain now exist, with some parallels to the germline-soma distinction in multicellular organisms [3]. Ciliate nuclear and genomic dimorphism provides a special opportunity to observe the consequences of evolution of a specialized organelle clearly derived from a general one and for studying the evolution of new, functionally differentiated genes that enable this unusual situation.

The processes responsible for large-scale developmental DNA elimination [4] in ciliate nuclei are under active study, but what the responsible ancestral molecules were remains to be determined. Knowledge of the molecules responsible for ciliate genome reorganization is dominated by *Tetrahymena* and *Paramecium* (class Oligohymenophorea), with additional input from *Oxytricha*, *Stylonychia* and *Euplotes* (class Spirotrichea) [5,6], whereas this remains to be investigated in the remaining nine or so classes. To gain fresh insights into genome reorganization and tackle questions about its origin we focused on the ciliate species *Blepharisma stoltei*. Together with its sister-class, Karyorelictea, the class Heterotrichea, to which this *B. stoltei* belongs, represent the earliest branching ciliate lineages, more distantly related to current model ciliates than those models are to each other [7]. Furthermore, *Blepharisma* exhibits distinctive alternative somatic developmental pathways, which have potential utility in disentangling processes involved in genome reorganization from preceding ones that may indirectly influence it.

Blepharisma is a distinctive genus of single-celled ciliates (Figure 1) known for the red, light-sensitive pigment, blepharismin, in the sub-pellicular membranes of representative species [8],

80 and unusual nuclear/developmental biology (Figure 2) [9]. To date molecular investigations and
81 genomics of ciliates have predominantly focused on oligohymenophoreans and spirotrichs
82 (Figure 3, Table S1). In recent years, publication of a draft genome for the heterotrich ciliate,
83 *Stentor,* has facilitated revival of this genus for investigations of cellular regeneration [10–12].
84 However, significant hurdles still need to be overcome to investigate genome reorganization in
85 *Stentor coeruleus* since requisite cell mating has not been observed in the reference somatic
86 genome strain (personal communication, Mark Slabodnick), and very high lethality has been
87 reported for other strains in which mating occurred [13]. We therefore focused on *Blepharisma*
88 which is amenable to such investigations, with controlled induction of mating, and, critically,
89 procedures for investigating cellular and nuclear development have been established from more
90 than a century of meticulous cytological research [8,14–25].
91
92 The *Blepharisma stoltei* strains used in the present study were originally isolated in Germany
93 (strain ATCC 30299) and Japan (strain HT-IV), with the former continuously cultured for over
94 fifty years, and the latter for over a decade. The cells are comparatively straightforward to
95 maintain, e.g., stable cultures can be established in a simple salt medium on a few grains of rice
96 passaged every few months. Due to their distinctive pigmentation and large size several
97 *Blepharisma* species are excellent subjects for introducing cell biology concepts to non-
98 specialists, and are thus readily available for educational purposes from commercial suppliers
99 like Carolina Biological Supply Company (USA). They are ideal subjects for behavioural and
100 developmental investigations, e.g., as voracious predators of smaller ciliates and other
101 unicellular species, and also exhibit pronounced phenotypic plasticity, including forming cysts
102 and giant, cannibal cells under suitable conditions [8].
103
104 Like all ciliates [3], *Blepharisma* cells have two types of nuclei: a macronucleus (MAC) which is
105 very large and transcriptionally active during vegetative growth, and a small, generally

106 transcriptionally inactive micronucleus (MIC), which serves as the germline. Each *Blepharisma*
107 cell has one MAC and several MICs (Figure 1A, B). In vegetative propagation (asexual
108 replication) of *Blepharisma*, cell fission results in about half of the MAC pinching off which is
109 then distributed to each of the resulting daughter cells together with the mitotically divided MICs.
110 Upon starvation, *Blepharisma* cells, like other ciliates, are also capable of conjugation and the
111 associated sexual processes. Essential for developmental investigations, the intricate ballet of
112 nuclear movements and morphological changes occurring during *Blepharisma* conjugation is
113 well-documented [9] (Figure 2). During this process about half of the MICs in each of the cells
114 undergo meiosis (meiotic MICs) and the rest do not (somatic MICs) (Figure 2B). One of the
115 meiotic MICs eventually gives rise to two haploid gametic nuclei. One gametic MIC (the
116 migratory nucleus) from each conjugating cell is exchanged with that of its partner. In parallel in
117 partnered cells, subsequent fusion of the migratory and stationary haploid nuclei generates a
118 zygotic nucleus (synkaryon), and after successive mitotic divisions gives rise to both new MICs
119 and new MACs (known as anlagen). The new MACs continue to mature, eventually growing in
120 size and DNA content [9].
121
122 Conveniently for investigations of development and genome reorganization, *Blepharisma* is one
123 of only two ciliate genera, along with *Euplotes* [26–29], where conjugation has been shown to be
124 mediated through pheromone-like substances called gamones. *Blepharisma* has two mating
125 types, distinguished by their gamone production. Mating type I cells release gamone 1, a ~30
126 kDa tyrosine-rich [30] glycoprotein [31,32]; mating type II cells release gamone 2, calcium-3-(2'-
127 formylamino-5'-hydroxybenzoyl) lactate, a small-molecule effector [33]. *Blepharisma* cells
128 commit to conjugation when complementary mating types recognize each other's gamones, with
129 the cells remaining paired while meiosis and fertilization occur and eventually new MACs begin
130 to form.
131

132 As in model ciliates, during *Blepharisma* anlagen development, MIC-specific sequences are
133 removed from a MIC genome copy to form a functional MAC genome (Seah, et al. in prep.). The
134 new MAC genomes of model ciliate species are largely free of mobile elements and other forms
135 of "junk" DNA contained in the MIC genome [34]. In the best studied ciliates, a form of genome
136 reorganization assisted by small RNAs (sRNAs) is thought to occur [5]. Specific genome
137 segments limited to the MIC, termed internally eliminated sequences (IESs), are excised by
138 domesticated transposases, and may have originated from transposons [3,5,35,36]. Large scale
139 genome-wide DNA amplification accompanies the genome reorganization process, producing
140 thousands of copies in mature MACs of larger ciliate species [3,34].
141
142 We were motivated to investigate genome reorganization in *Blepharisma*, as, unlike model
143 ciliates, these cells can produce two kinds of anlagen, and particularly because one of the two
144 pathways of their development skips the complex series of mitoses, meioses, nuclear
145 exchanges and fertilization [9] (Figure 2). Primary anlagen mature in the conventional manner
146 from zygotic nuclei. Somatic MICs which have not undergone meiosis can give rise to secondary
147 anlagen, which can develop into mature macronuclei [9]. This occurs frequently in strains with a
148 high frequency of selfing (conjugation among cells within a clonal population), in preference to
149 development of primary macronuclear anlagen [9]. This alternative pathway of MAC
150 development has also been observed experimentally after removal of primary macronuclear
151 anlagen by microsurgery [9]. As conjugation progresses, the old (maternal) MACs are
152 progressively degraded [9]. Since the *B. stoltei* MIC genome has numerous IESs which interrupt
153 genes (Seah et al. in prep.), in principle, to produce functional, mature MAC genomes, it is
154 essential that reorganization of DNA occurs in both primary and secondary anlagen.
155
156 Here we provide essential macronuclear genome and developmental, transcriptomic resources
157 for *B. stoltei* and present the first investigations of possible molecules involved in its genome

158 reorganization. Like *Stentor coeruleus* [10], *Blepharisma stoltei* genes have the shortest known
159 spliceosomal introns, predominantly 15 or 16 nt long. From long-read sequencing the *B. stoltei*
160 MAC genome appears to be organized in the form of numerous minichromosomes. Among the
161 MAC-encoded transposase genes we identified in *Blepharisma* were PiggyBac transposase
162 homologs, which, as far as we are aware, have not been reported in any ciliates other than
163 *Paramecium* and *Tetrahymena*. A few *Blepharisma* PiggyBac homologs are substantially
164 upregulated in MAC development, including one with a complete catalytic triad which is the main
165 candidate IES excisase. Raising the possibility of additional IES excisases, transposases from a
166 few different classes are also present in the MAC genome, including some with complete
167 catalytic triads. Consistent with ancient origins of genome reorganization in ciliates, *Blepharisma*
168 shares pronounced development-specific upregulation of homologs known to be involved in this
169 process, notably Dicer-like and Piwi proteins responsible for sRNA biogenesis. *Blepharisma*
170 therefore represents an invaluable outgroup for investigations of the evolution of genome
171 reorganization.
172

173 Results

174 A compact, extensively fragmented genome

175 The draft *Blepharisma stoltei* ATCC 30299 MAC genome is compact, at 41 Mb, and AT rich
176 (66%), like most sequenced ciliate MAC genomes, and relatively complete (Figure 3; Table S1,
177 2, Figure S1). From joint variant calling of reads from strains ATCC 30299 and HT-IV mapped to
178 this assembly, strain ATCC 30299 appears to be virtually homozygous, with only 1277
179 heterozygous single-nucleotide polymorphisms (SNPs) observed compared to 193725 in strain
180 HT-IV (i.e., individual heterozygosity of 3.08×10^{-5} vs. 4.67×10^{-3} respectively). Low SNP levels

were likely beneficial for the overall assembly contiguity, since heterozygosity poses significant algorithmic challenges for genome assembly software [37]. For brevity's sake, we refer to this draft genome as the *Blepharisma* MAC genome (and likewise "*Blepharisma*" for the associated strain). Though the final assembly comprises 64 telomere-to-telomere sequences, it is not possible to define conventional chromosome ends given the extensive natural fragmentation of the *Blepharisma* MAC genome (characterized in the next section), hence we refer to them simply as "contigs".

The basic telomere unit of *B. stoltei* is a permutation of CCCTAACA, like its heterotrich relative *Stentor coeruleus* [10] (Figure S2). However, a compelling candidate for a telomerase ncRNA (TERC) could not be found in either *Blepharisma* or *Stentor* using Infernal [38] and RFAM models (RF00025 - ciliate TERC; RF00024 - vertebrate TERC). Thus, it was not possible to delimit the ends of the repeat. Heterotrichs may use a different kind of ncRNA, or one which is very divergent from known TERCs. In contrast to the extremely short (20 bp) macronuclear telomeres of spirotrichs like *Oxytricha* with extreme MAC genome fragmentation [39], sequenced *Blepharisma* macronuclear telomeres are moderately long (Figure S2A), with a mode of 209 bp (i.e., 26 repeats of the 8 bp motif), extending to a few kilobases.

Approximately one in eight reads in the *Blepharisma* HiFi library were telomere-bearing and distributed across the entire genome (Figure 4A), using a moderately strict definition of possessing at least three consecutive telomeric repeats. In contrast, the telomere-bearing reads of the model ciliate *Tetrahymena thermophila* predominantly map to chromosome ends (Figure S3A), and only one in fifty nine *Tetrahymena* CLR reads are telomere-bearing, as identified by three consecutive telomeric subunit repeats (i.e., 3×CCCCAA).

206 Typically, only a minority of mapped reads are telomere-bearing at individual internal contig
207 positions, and so we term them alternative telomere addition sites (ATASs) (Figure 4A). We
208 identified a total of 46705 potential ATASs in *Blepharisma* by mapping PacBio HiFi reads onto
209 the MAC reference, and searching for partially mapped reads that contained telomeric repeats in
210 the unmapped (clipped) segments without any intervening sequence between the mapped
211 segment and the beginning/end of the telomeric repeat. The majority of these sites (38686) were
212 represented by only one mapped HiFi read.
213
214 The expected distance between telomeres, and hence the average MAC DNA molecule length,
215 is about 130 kb. This is consistent with the raw input MAC DNA lengths, which were mostly
216 longer than 10 kb and as long as 1.5 Mb (Figure S3C, D), and our observation that a small
217 fraction (1.3%) of *Blepharisma*'s HiFi reads are bound by telomeres on both ends. Excluding the
218 length of the telomeres, these telomere-bound reads may be as short as 4 kb (Figure S2B).
219 Given the frequency of telomere-bearing reads, we expect many additional two-telomere DNA
220 molecules longer than 12 kb, the approximate maximum length of the HiFi reads (Figure S3C,
221 D).
222
223 Since the lengths of the sequenced two-telomere DNA molecules on average imply that they
224 encode multiple genes, we propose classifying them as "minichromosomes". This places them
225 between the length of "nanochromosomes" of ciliates like *Oxytricha* and *Stylonychia*, which
226 typically encode single genes and are on the order of a few kilobases long [39,40], and MAC
227 chromosomes of *Paramecium tetraurelia* and *Tetrahymena thermophila* which are hundreds of
228 kilobases to megabases long [41–43]. Recently it was reported that the *Paramecium bursaria*
229 MAC genome is considerably more fragmented than those of other previously examined
230 *Paramecium* species [44]. The DNA molecules from *P. bursaria* have thus also been classified
231 as minichromosomes [44].

232

233 Alternative telomere addition sites in the MAC genome tend to be intergenic in model ciliates like
234 *Oxytricha trifallax* [39]. In *Blepharisma*, we found more intergenic ATASs (28309) than intragenic
235 ones (18396). As intergenic regions only make up 10.1 Mb of the assembly, the intergenic
236 frequency of ATASs is about five-fold higher (2.81 per 1 kb) than intragenic frequency (0.562 per
237 1 kb). The presence of intragenic ATASs raises the question how the cell tolerates or deals with
238 mRNAs encoding partial proteins transcribed from 3' truncated genes. Since the sequence data
239 was from a clonal population, it is not possible to tell how much ATAS variability there is within
240 individual cells. However, it is conceivable that their positional variation in single cells reflects
241 that of the population. In this case, together with redundancy from massive DNA amplification
242 there would likely be sufficient intact copies of every gene.

243

244 Beyond the first 2-5 bp corresponding to the junction sequences, the average base composition
245 on the chromosome flanking ATAS junctions shows an asymmetrical bias (Figure 4B). From
246 position +6 onwards there is an enrichment of T to about 40% and A to 35-39%, compared to
247 the genome-wide frequencies of 33% each. At position +19 to +23, there is a slight decrease in
248 T to 37-39%. AT values gradually decline back to about 35% each by position +150.
249 Correspondingly, G and C are depleted downstream of ATAS junctions, dropping to a minimum
250 of 8.6% and 11% respectively around position +37, compared to the genome-wide average of
251 17% each. AT enrichment and GC depletion upstream of ATAS junctions are less pronounced.

252

253 If breakage and chromosome healing were random, we would not expect such an asymmetry.
254 This suggests that there is a nucleotide bias, whether in the initiation of breaks, telomere
255 addition, or in the processing of breaks before telomere addition. However, we have not yet
256 identified any conserved motif like the 15 bp chromosome breakage site (CBS) in *Tetrahymena*
257 [45] nor a short 10-bp sequence periodicity in base composition like in *Oxytricha trifallax* [46].

258 Therefore, telomere addition in *B. stoltei* appears to involve base-pairing of short segments of
259 about 2 bp between the telomere and chromosome, with a bias centered on the “CT” in the
260 telomere unit, and an asymmetrical preference for AT-rich sequences on the chromosomal side
261 of the junction.

262 Tiny spliceosomal introns

263 The *Blepharisma stoltei* ATCC 30299 macronuclear genome is gene-dense (25,711 predicted
264 genes), with short intergenic regions, tiny introns and untranslated regions (UTRs) (Figure 5A).
265 In contrast to *Stentor* which, unusually for ciliates, uses the standard genetic code, *B. stoltei*
266 uses an alternative genetic code with UGA codons reassigned from stops to tryptophan (Figure
267 S5).
268
269 Like *Stentor* [10], most (82%) *Blepharisma* genes have no introns. In line with genome
270 compactness, during our inspections we also observed numerous overlapping poly(A)-tailed
271 RNA-seq reads on opposite strands derived from convergently transcribed gene pairs. The
272 correlation of the lengths of different noncoding region classes (intergenic regions, introns and
273 UTRs) can be explained by them being subject to common, neutral evolutionary processes [47].
274
275 *Blepharisma* introns are mostly (97%) 15 or 16 nucleotides (nt) long, like those of *Stentor*
276 (Figure 5B). Though intron reduction (7389 introns predicted in the reference *B. stoltei* MAC
277 genome, i.e., 0.29 introns per gene) is not as extreme as some other microbial eukaryotes, like
278 *Giardia lamblia* [48], where almost all have been lost, both *Blepharisma* and *Stentor* have much
279 fewer introns relative to other ciliates (e.g., intron densities of 1.6, 2.3 and 4.8 introns per gene
280 in *Paramecium*, *Oxytricha* and *Tetrahymena*, respectively [49]) and to the putative, relatively
281 intron-rich eukaryotic common ancestor [50], along with their extreme length reduction.

282

283 *Blepharisma* 15 nt introns possess a characteristic branch-point “A”, as would be expected in
284 classical models of lariat formation during mRNA splicing (Figure 5C). 16 nt introns almost
285 invariably have an “A” at either 10 or 11 nt downstream of the donor site (i.e., only one of 499
286 does not, but has “A” at 9 nt), although this is not obvious in the consensus sequence logo
287 because the position is variable (Figure S6D). Similarly, 17 nt introns all possess “A” at 10-12 nt
288 downstream of the donor site. Only a few intron bases, 5-8 and 12, of *Blepharisma*’s 15 nt
289 introns are relatively unconstrained (Figure 5C). This leaves little room for the presence of any
290 additional regulatory elements in the mRNA or underlying DNA.

291 Extensive duplications of transmembrane protein genes

292 A notable extended ~220 kb region encoding 53 genes belonging to a single orthologous group
293 (orthogroup), OG0000085 is present on Contig_1 (Figure 5A). Four additional OG0000085
294 genes are present at the opposite end of Contig_1, and 24 copies are found on other contigs,
295 often clustered together (Figure 5D). The DNA coverage across this region is lower (74×) than
296 the rest of Contig_1 (185×). Though there is uncertainty in the exact extent, given the sheer
297 volume of reads involved, the assembled sequences certainly correspond to highly repetitive
298 regions of the MAC genome. At the junction between the lower and higher coverage regions
299 more than 30 HiFi reads link the two regions of coverage, and a similar number of telomere-
300 bearing reads are in close proximity. At the junction we also observe at least two potential
301 locations of IESs, corresponding to regions that may be partially IES/partially MDS.
302

303 Large clusters of genes from particular orthogroups can be found on additional contigs (Figure
304 5D). In total 551 (2%) of predicted *B. stoltei* genes belong to the orthogroups with the largest
305 clusters per contig. Some of the largest contiguous clusters of genes from these orthogroups are

306 situated at the ends of contigs, suggesting they may have caused assembly breaks beyond
307 them. One contig, split off from other connected components in the assembly graph,
308 predominantly encodes genes from a single orthogroup (contig_64, 43× coverage; Figure 5D;
309 Figure S7). Further increases in read length and accuracy may allow assemblers to fully resolve
310 these in future. Curiously, all the orthogroups corresponding to the largest contiguous clusters of
311 genes appear to be transmembrane proteins, or decayed remnants thereof. The nature of these
312 proteins is described in Supplemental Text ("Properties of proteins encoded by extensive
313 duplications").

314 Features of gene expression during new MAC development

315 To gain an overview of the molecular processes during genome reorganization in *Blepharisma*
316 we examined gene expression trends across a developmental time series. Complementary
317 mating strains of *B. stoltei* were treated with gamones of the opposite mating type, before mixing
318 to initiate conjugation [9,51]. Samples for morphological staging and RNA-seq were taken at
319 intervals from the time of mixing ("0 hour" time point) up to 38 hours (Figure S8). The
320 progression of nuclear morphological development and the proportion of cells in each stage at
321 various time points is illustrated in Figure S9.
322
323 During conjugation in *Blepharisma*, meiosis begins around 2 h after conjugating cell pairs form
324 and continues up to around 18 h, by when gametic nuclei generated by meiosis have been
325 exchanged (Figure 2A, B, Figure S9). This is followed by karyogamy and mitotic multiplication of
326 the zygotic nucleus (22 hours). At the 26 h time point, new, developing primary MACs can be
327 observed in the conjugating pairs, in the form of large, irregular bodies (Figure 2A, Figure S9).
328 These macronuclear anlagen mature into the new MACs of the exconjugant cell by 38 h, after
329 which cell division generates two daughter cells. Smaller secondary MACs, derived directly from

330 MICs without all the intermediate nuclear stages, can also be seen from 22 hours to 30 hours,
331 but eventually disappear, giving sole way to the primary MACs (Figure 2A, Figure S9).
332
333 Examining gene expression at 26 hours, when the majority of cells are forming a new MAC
334 (Figure S9), we observe two broad trends: relatively stable constitutive gene expression (Table
335 S5; Data S3), e.g., an actin homolog (ENA accession: BSTOLATCC_MAC19444) and a
336 bacteria-like globin protein (BSTOLATCC_MAC21846), versus pronounced development-
337 specific upregulation (Table S6; Data S3), e.g., a histone (BSTOLATCC_MAC21995) an HMG
338 box protein (BSTOLATCC_MAC14030), and a translation initiation factor (eIF4E,
339 BSTOLATCC_MAC5291).
340
341 We eschewed a crude, large-scale Gene Ontology (GO) enrichment analysis in favour of close
342 scrutiny of a smaller subset of genes strongly upregulated during new MAC formation which we
343 expect are more relevant to molecular biologists. For this, computational gene annotations in
344 combination with BLASTP searches and examination of literature associated with homologs was
345 used. Ranking the relative gene expression at 26 hours vs. the average expression of starved,
346 gamone treated, and 0 hour cells, in descending order, reveals numerous genes of interest in
347 the context of genome reorganization, including homologs of proteins known to be involved in
348 genome reorganization in model ciliate species (Table S6).
349
350 Among the top 100 genes ranked this way (69× to 825× upregulation) nine contain PFAM
351 transposase domains: DDE_Tnp_1_7, DDE_3, MULE and DDE_Tnp_IS1595 (e.g.,
352 BSTOLATCC_MAC2188, BSTOLATCC_MAC14490, BSTOLATCC_MAC18054,
353 BSTOLATCC_MAC18052, respectively). We also observe small RNA (sRNA) biogenesis and
354 transport proteins, i.e., a Piwi protein (BSTOLATCC_MAC5406) and a Dicer-like protein
355 (BSTOLATCC_MAC1138; see also “Supplemental text”, “Homologs of small RNA-related

356 proteins involved in ciliate genome reorganization" and Figure S10), and a POT1 telomere-
357 binding protein homolog (POT1.4; BSTOLATCC_MAC1496; Supplemental Text "Telomere-
358 binding protein paralogs"). Numerous homologs of genes involved in DNA repair and chromatin
359 are also present among these highly developmentally upregulated genes ("Supplemental text",
360 "Development-specific upregulation of proteins associated with DNA repair and chromatin" and
361 "Supplemental text", "Development-specific histone variant upregulation"). The presence of
362 proteins involved in either transcription initiation or translation initiation among these highly
363 upregulated genes suggests a possible manner to coordinate the regulation of development-
364 specific gene expression ("Supplemental text", "Development-specific upregulation of proteins
365 associated with initiation of transcription and translation").

366 PiggyBac homologs in *Blepharisma* are candidate IES excisases

367 In *Paramecium tetraurelia* and *Tetrahymena thermophila*, PiggyBac transposases are
368 responsible for IES excision during genome reorganization occurring in the developing new
369 MAC [52,53]. These transposases appear to have been domesticated, i.e., their genes are no
370 longer contained in transposons but are encoded in the somatic genome where they provide a
371 necessary function in genome development [52,53]. PiggyBac belongs to the DDE/D-
372 superfamily of transposases due to the presence of a protein domain containing the catalytic
373 triad of 3 aspartic acid residues (DDD), where the third residue can also be a glutamate (E).
374 PiggyBac homologs typically have a DDD catalytic triad, rather than the more common DDE
375 triad of other DDE/D transposases [54]. The DDD catalytic motif is present in the PiggyMac
376 (Pgm) of *Paramecium* and the *Tetrahymena* PiggyBac homologs Tpb1 and Tpb2 [53,55].
377 Among ciliates, domesticated PiggyBac transposases have so far only been reported in the
378 model oligohymenophorean genera *Paramecium* and *Tetrahymena*, and have not been
379 detected in either the MAC or MIC genomes of the spirotrich *Oxytricha trifallax* [39,56].

380

381 We detected more transposase domains (9 distinct PFAM identifiers) in *B. stoltei* than any of the
382 other ciliate species we examined (Figure 6A). Seven of these domains are also found in at
383 least one other ciliate species. Using HMMER searches with the PFAM domain characteristic of
384 PiggyBac homologs, DDE_Tnp_1_7 (PF13843), we found eight homologs in *B. stoltei* ATCC,
385 none of which were flanked by terminal repeats identified by RepeatModeler. We also found
386 PiggyBac homologs in *B. stoltei* HT-IV and *B. japonicum* R1072. Reminiscent of *Paramecium*
387 *tetraurelia*, which, among ten PiggyMac homologs, has just one homolog with a complete
388 catalytic triad [55], the DDD triad is preserved in just a single *B. stoltei* ATCC 30299 PiggyBac
389 homolog (Figure 6B; Contig_49.g1063, BSTOLATCC_MAC17466). This gene is strongly
390 upregulated during development from 22 to 38 hours after formation of heterotypic pairs, when
391 new MACs develop and IES excision is required (Figure 6B). Furthermore, there are significant
392 similarities in the basic properties of *Blepharisma* and *Paramecium* IESs, which will be reported
393 in detail in the subsequent *B. stoltei* MIC genome paper (Seah et al., in prep.). Consequently,
394 adopting the *Paramecium* nomenclature, we refer to our primary candidate IES excisase as
395 *Blepharisma* PiggyMac (BPgm) and the other homologs as BPgm-Likes (BPgmLs).

396

397 PiggyMac homologs are also present in other heterotrich ciliates but have not yet been
398 described because of genome assembly or annotation challenges. Using BPgm as a query
399 sequence, we found convincing homologs containing the conserved catalytic DDD-motif in a
400 genome assembly of the heterotrichous ciliate *Condylostoma magnum* (TBLASTN e-value 2e-
401 24 to 2e-37). While we failed to detect the DDE_Tnp_1_7 domain in predicted genes of the
402 heterotrich *Stentor coeruleus*, we were able to detect a relatively weak adjacent TBLASTN
403 matches split across two frames in its draft MAC genome (e-value 7e-15; SteCoe_contig_741
404 positions 6558-5475). After joining ORFs corresponding to this region and translating them, we
405 obtained a more convincing DDE_Tnp_1_7 match with HMMER3 (e-value 2e-24). This either

406 corresponds to a pseudogene or a poorly assembled genomic region. It is also possible that
407 additional PiggyBac homologs were missed in unassembled *Stentor* MAC genome regions.
408
409 In addition, we searched for PiggyMac homologs in the MAC genome of the pathogenic
410 oligohymenophorean ciliate *Ichthyophthirius multifiliis* [57]. TBLASTN searches using the *T.*
411 *thermophila* Tpb2 as a query returned no hits. A HMMER search using hmmscan with a six-
412 frame translation of the *I. multifiliis* MAC genome against the PFAM-A database also did not
413 return any matches with independent E-values (i-E-value) less than 1. We note that based on
414 BUSCO analyses (Figure S1) the *I. multifiliis* genome appears to be less complete than other
415 ciliates we examined. So, a better genome assembly will be needed to investigate the possibility
416 that PiggyBac homologs are encoded elsewhere in this MAC genome.
417
418 Other than the PFAM DDE_Tnp_1_7 domain, three of the *Blepharisma* PiggyBac homologs also
419 possess a short, characteristic cysteine-rich domain (CRD) (Figure 6C). This domain is essential
420 for Pgm activity and *Paramecium* IES excision [58]. PiggyBac CRDs have been classified into
421 three different groups [58]. In *Blepharisma*, the CRD consists of five cysteine residues arranged
422 as CxxC-CxxCxxxxH-Cxxx(Y)H (where C, H, Y and x respectively denote cysteine, histidine,
423 tyrosine and any other residue). Two *Blepharisma* homologs possess this CRD without the
424 penultimate tyrosine residue, while the third contains a tyrosine residue before the final histidine.
425 This -YH feature towards the end of the CxxC-CxxCxxxxH-Cxxx(Y)H CRD is shared by all the
426 PiggyBac homologs we found in *Condylostoma*, as well as the PiggyBac-like element (PBLE)
427 from the bat *Myotis lucifugus* (Piggybat) and the human PiggyBac element-derived (PGBD)
428 proteins PGBD2 and PGBD3. In contrast, PiggyBac homologs from *Paramecium* and
429 *Tetrahymena* have a CRD with six cysteine residues arranged in the variants of the motif CxxC-
430 CxxC-Cx{2-7}Cx{3,4}H, and group together with human PGDB4 and *Spodoptera frugiperda*
431 PBLE (Figure 6C).

432

433 Previous experiments involving individual or paired gene knockdowns of most of the ten
434 *Paramecium tetraurelia* PiggyMac(-like) paralogs lead to substantial IES retention, even though
435 only one PiggyMac gene (PGM) has the complete catalytic triad, indicating that all these
436 proteins are functional [55]. To examine whether PiggyMac homologs in *Paramecium* are
437 functionally constrained we examined non-synonymous (d_N) to synonymous substitution rate
438 (d_S) ratios ($\omega = d_N/d_S$) for pairwise codon sequence alignments within and between species, with
439 the latter using two closely related *Paramecium* species (*P*. *tetraurelia* and *P*. *octaurelia*). All the
440 d_N/d_S values for pairwise comparisons of each of the catalytically incomplete *P. tetraurelia*
441 PgmLs versus the complete Pgm, were less than 1, ranging from 0.01 to 0.25 (Table S7). All
442 d_N/d_S values for pairwise comparisons between *P. tetraurelia* and *P. octaurelia* PiggyBac
443 orthologs were also substantially less than 1, ranging from 0.02 to 0.11 (Table S8). Since d_N/d_S=
444 1 indicates genes evolving neutrally [59], none of these genes are likely pseudogenes, and all
445 are subject to similar strong purifying selection.

446

447 Since only one of the eight homologs has the complete DDD catalytic triad characteristic of
448 functional PiggyBac transposases, this is the only possible catalytically active PiggyMac in *B.*
449 *stoltei*. The *in vitro* catalytic activity of the *T. ni* PiggyBac transposase is abolished when any of
450 the catalytic residues are substituted by alanine [60]. Conversely, we expect all *Blepharisma*
451 PiggyMac homologs with an incomplete catalytic triad to be catalytically inactive. In pairwise
452 comparisons of each of the catalytically incomplete homologs versus the complete one d_N/d_S
453 ranges from 0.0076 to 0.1351 (Table S9). As these estimates fall in a similar range to those
454 obtained for *Paramecium* PiggyMac/PiggyMac-likes, this indicates that the *B. stoltei* PiggyMac
455 homologs are predominantly subject to comparable purifying selection and unlikely to be
456 pseudogenes, but may have differentiated and acquired new functional roles.

457 # A common origin for most ciliate PiggyBac homologs

458 To determine whether the *Blepharisma* PiggyBac homologs share a common ciliate ancestor, or
459 whether they arose from independent acquisitions in major ciliate groups, we explored a range
460 of phylogenetic methods. We created a phylogeny of 155 sequences of DDE_Tnp_1_7 domains
461 of PiggyBac homologs which are representatives of putative domesticated transposases from
462 the genus *Blepharisma* (*B. stoltei* ATCC 30299, *B. stoltei* HT-IV, *B. japonicum*), *Condylostoma*
463 *magnum*, *Paramecium* spp., *Tetrahymena thermophila*, together with PiggyBac-like element
464 (PBLE [61]) transposases from a stramenopile species, an archaeplastid species, several
465 opisthokont species and an amoebozoan, homologs of the human PiggyBac-derived 1 gene
466 (PGBD1), PGBD3, PGBD4 and PGBD5 homologs (Figure 7; Data S1). The three BPgms from
467 the three *Blepharisma* strains whose MAC genomes we sequenced form a monophyletic clade,
468 with the BPgmLs 1 and 2 as outgroups. The BPgmLs 3,4,5,6 and 7 are grouped together with
469 the *Condylostoma* Pgms (each of which appears to have a complete catalytic triad). These two
470 clades form a heterotrich-specific group in the phylogeny. We observe that the ciliate Pgms and
471 PgmLs largely cluster to form a single clade. *T. thermophila* Tpb7 is an exception which appears
472 to group together with homologs of PGBD5 from *H. sapiens, G. gallus* and *D. rerio* but has an
473 aBayes support value of 0.84, much lower than the mode (1.0) and average (0.91) for this
474 phylogeny. The other exceptions are two fungal PBLEs and two red algal PBLEs with low
475 aBayes support within the predominantly monophyletic ciliate clade.
476
477 We applied tree topology tests to ascertain the likelihood of a monophyletic clade of ciliate Pgms
478 and PgmLs. Constrained trees were compared by different methods including bootstrap
479 proportion using the RELL method [62], a one-sided Kishino-Hasegawa test, a Shimodaira-
480 Hasegawa test [63,64], estimating confidence using expected likelihood weights [65], and an
481 approximately unbiased test [66] (Table S10). A tree with the constraint of monophyly for all

482 ciliate Pgms and PgmLs lacks support in comparison to an unconstrained tree with all the ciliate
483 Pgms and PgmLs and eukaryotic PBLEs. After excluding *T. thermophila* Tpb7, a tree
484 constrained with a clade consisting of the remaining ciliate Pgms and PgmLs is supported by all
485 tests. In other words, the ciliate PiggyBac homologs except Tpb7 likely originated in a ciliate
486 common ancestor.

487 Additional domesticated transposases

488 Three *B. stoltei* ATCC30299 MAC genome-encoded proteins possess PFAM domain DDE_1
489 (PF03184; Figure 8A). In PFAM version 35 the most common domain combinations
490 (architectures) with DDE_1, aside from proteins with just this domain detected (5898
491 sequences), are with an N-terminal PFAM domain HTH_Tnp_Tc5 (PF03221) alone (2240
492 sequences), and both an N-terminal CENP-B_N domain (PF04218) and central HTH_Tnp_Tc5
493 domain (1255 sequences). All the *B. stoltei* proteins possess the HTH_Tnp_Tc5 domain.
494 Though pairwise sequence identity is low amongst the *Blepharisma* proteins (avg. 28.3%) in
495 their multiple sequence alignment, the CENP-B_N domain in one of them appears to align
496 reasonably well to corresponding regions in the two proteins lacking this domain, suggesting
497 that it deteriorated in this pair, beyond the recognition capabilities of HMMER3 with the given
498 PFAM domain model and search parameters.
499
500 The N-terminal domains of *Homo sapiens* CENP-B proteins (corresponding to PFAM: CENP-
501 B_N, PF04218, and HTH_Tnp_Tc5) are able to bind 17 bp centromeric DNA repeats and are
502 involved in centromeric binding during chromosome segregation [67]. Potential convergent
503 domestication of transposases with these domains has been proposed for mammalian and
504 fission yeast lineages [68]. The PDC2 protein in budding yeast *Saccharomyces cerevisiae*,
505 which regulates pyruvate decarboxylase transcription [69], is considered structurally

506 homologous to human CENP-B and shares the same pair of domains, but has not been
507 reported to play a role in centromere binding [68,70]. The CENP-B_N domain abbreviation is
508 somewhat unfortunate, since the domain is also characteristic of numerous transposases with
509 no known or expected role in centromeric function, notably the Tigger and PogoR families, and
510 so presumably originated as a transposase domain [71]. As judged from searches of the UniProt
511 database, the characteristic N-terminal CENP-B DNA-binding domain (PF04218) is detectable in
512 a few protist clades (e.g., Rhodophyta and Cryptophyceae), but, among alveolates, only in
513 *Stentor coeruleus*. BLASTp matches for all three proteins in GenBank are annotated either as
514 Jerky or Tigger homologs (Jerky transposases belong to the Tigger transposase family [71]).
515 Given that none of the *B. stoltei* DDE_1 domain proteins appears to have a complete catalytic
516 triad, we think it is unlikely they are involved in transposition or IES excision.
517
518 Six MAC-encoded transposases containing the DDE_3 (PF13358) domain are present in *B.*
519 *stoltei*, all of which are substantially upregulated in MAC development (Figure 8B). Five of these
520 possess the complete DDE catalytic triad. The DDE_3 domain is characteristic of DDE
521 transposases encoded by the Telomere-Bearing Element transposons (TBEs) of *Oxytricha*
522 *trifallax* [72,73], which, despite being MIC genome-limited, are thought to be involved in IES
523 excision, rather than a domesticated PiggyMac [74]. Other DDE_3-containing transposons,
524 called Tec elements, are found in another spirotrichous ciliate, *Euplotes crassus,* but no role in
525 genome reorganization has been established for these [75]. TBEs and Tec elements do not
526 share obvious features with one another, other than both possessing an encoded protein
527 belonging to the IS630-Tc1 transposase (super)-family [76]. All six DDE_3 genes in *B. stoltei*
528 ATCC 30299 have at least 150× HiFi read coverage, consistent with the regions encoding these
529 being *bona fide* macronuclear DNA rather than MIC DNA contaminants.
530

531 The *B. stoltei* DDE_3 domain transposases appear to be more closely related to the IS630
532 family than to *Oxytricha* TBE transposases and *Euplotes* Tec transposases, and thus acquired
533 independently of them. BLASTP searches of GenBank NR with these proteins as queries,
534 returned bacterial or fungal proteins for most of the hundred top hits, and among these the most
535 common classifications are “IS630 family” transposases. One of the top hits is a MIC genome-
536 encoded protein in *Oxytricha trifallax* with a DDE_3 domain which is not a TBE transposase
537 (GenBank accession: KEJ83017.1). IS630 transposases diverge considerably from Tc1-Mariner
538 transposases, and hence are considered an outgroup to them [77]. On the other hand, IS630-
539 related transposases encoded by Anchois transposons have been detected in the *Paramecium*
540 *tetraurelia* MIC genome [35]. Since all but one of the *B. stoltei* paralogs appear to possess
541 complete catalytic triads, the possibility that they may excise a subset of IESs needs to be
542 considered.
543
544 Among other ciliates with draft MAC genomes we examined, the PFAM IS1595- and MULE
545 transposase-like domains (PF12762 and PF10551) have so far only been observed in the
546 spirotrichs *Oxytricha* and *Stylonychia* [39,40]. DDE_Tnp_IS1595 domains are characteristic of
547 the Merlin transposon superfamily and MULE is part of the Mutator transposon superfamily [54].
548 Currently no particular functions have been ascribed to these proteins in these ciliates, but they
549 are substantially upregulated during the development of these ciliates [39,56]. Both
550 transposase-like domains are found in MAC-encoded proteins in *B. stoltei* ATCC 30299 and the
551 underlying genes are also upregulated during *Blepharisma* MAC development (Figure 9A, B).
552 The genes encoding DDE_Tnp_IS1595 and MULE proteins, like the genes encoding the DDE_1
553 and DDE_3 proteins, appear to lack the flanking terminal inverted repeats characteristic of a
554 functional transposon, as identified by RepeatModeler, consistent with transposase
555 domestication. A number of members of both IS1595 and MULE transposases, including those
556 that are upregulated during new MAC formation, also appear to have complete catalytic triads.

557

558 In addition to the transposases, we also detected a family (> 30 copies) of APE-type non-LTR
559 retrotransposase genes with the two domains characteristic of such retrotransposases, i.e., an
560 APE endonuclease domain (PFAM “exo_endo_phos_2”; PF14529) and a reverse transcriptase
561 domain (PFAM “RVT_1”; PF00078) present on adjacent genes. Unlike the conventional
562 transposase-derived genes in *B. stoltei*, the expression of all these genes throughout the
563 conditions we examined is very low to negligible, and some of them also appear to be truncated
564 pseudogenes (Data S3; workbook “RVT1 + exo_endo_phos_2”). Since it is necessary to
565 understand the impact of the presence of IESs in some of these genes, their detailed analyses
566 will be reported in the context of the *Blepharisma stoltei* MIC genome, where their nature and
567 origin will be more evident.

568 Discussion

569 The genus *Blepharisma* represents one of the earliest diverging ciliate lineages, the
570 heterotrichs, forming an outgroup to the best-studied and deeply divergent oligohymenophorean
571 and spirotrich ciliates [7]. *Blepharisma* species thus provide an excellent vantage point to
572 compare unique processes that have accompanied the evolution of nuclear and genomic
573 dimorphism in ciliates, particularly the extensive genomic reorganization that occurs during the
574 new macronucleus (MAC) development. Comparisons between *Blepharisma* and other ciliates
575 also enable deeper consideration of the potential state of the ciliate common ancestor. The
576 annotated draft *B. stoltei* ATCC 30299 MAC genome and associated transcriptomic data provide
577 the basis for comparative studies of key characteristics of genome reorganization processes.

578 # A minichromosomal architecture with pronounced telomere
579 addition site variation

580 Ciliate MAC genome architectures span from longer DNA molecules in the
581 oligohymenophoreans *Paramecium tetraurelia* and *Tetrahymena thermophila*, which are more
582 similar to conventional eukaryotic chromosomes, to numerous, predominantly single-gene
583 nanochromosomes of spirotrichs like *Oxytricha trifallax* and *Euplotes crassus* [3]. The *B. stoltei*
584 ATCC 30299 MAC genome organization (and like that of *Paramecium bursaria* [44]) lies
585 between these two extremes with many minichromosomes representing numerous alternative
586 telomere addition sites. This form of natural sequence heterogeneity creates significant new
587 challenges for generating single representative consensus sequences, because genome
588 assembly methods assume chromosome boundaries are generally consistent, as they are in
589 multicellular eukaryote models, down to the terminology used to describe them [78]. Fortunately,
590 the reference *Blepharisma* MAC genome is largely homozygous, promoting contiguity in the
591 final, 41 Mb assembly of 64 two-telomere-capped contigs. Nevertheless, plenty of room for
592 refinement remains, including development of new ways to better assemble, describe and
593 organize the constituents of genomes with such extreme sequence variability.
594
595 Despite the abundance of *Blepharisma* MAC genome telomeres, we did not detect a typical
596 ncRNA gene corresponding to the telomerase RNA component (TERC) of the ribozyme
597 responsible for telomere synthesis in the MAC genome. We suspect this is due to ncRNAs
598 presenting a far greater challenge to detect than protein-coding genes and the presence of
599 highly divergent ncRNA with insufficient similarity to the handful of taxonomically-restricted
600 TERCs identified in oligohymenophorean and spirotrich ciliates and other eukaryotes so far. On
601 the other hand, five homologs of POT1, the canonical telomere-binding protein, are present

602 (Figure S4). One of these is highly upregulated when the new MAC genome is forming, and
603 presumably like model ciliates the DNA is fragmented and replicated, requiring further telomere
604 synthesis and telomere-binding proteins.

605 A potentially catalytically active PiggyMac is present in 606 *Blepharisma*

607 In current models of IES excision, MIC-limited sequences are demarcated by deposition of
608 methylation marks on histones in an sRNA-dependent process [5]. These sequences are then
609 recognized by domesticated transposases whose excision is supported by additional proteins,
610 including those that recognize these marks [5]. Together with MIC sequencing and from the
611 same time course we employed in the present study for RNA-seq we have observed abundant,
612 development-specific sRNA production in *Blepharisma* like that in other ciliates (Seah et al. in
613 prep), and so we examined the expression of potential genes responsible for their biogenesis,
614 along with other genes highly upregulated during new MAC formation. Homologs of proteins
615 implicated in ciliate genome reorganization were present among the genes most highly
616 differentially upregulated during new MAC development, notably including Dicer-like and Piwi
617 proteins, and domesticated transposases.
618
619 Following this study, we will report detailed analyses of a draft *B. stoltei* ATCC 30299 MIC
620 genome, which possesses abundant and typically TA-bound IESs (Seah et al. in prep). In
621 oligohymenophorean ciliates *Tetrahymena* and *Paramecium* there is a considerable body of
622 evidence that PiggyBac homologs are responsible for IES excision [35,52,53,55,79]. The
623 responsible IES excisases in the less-studied spirotrich ciliates, *Oxytricha*, *Stylonychia* and
624 *Euplotes*, are not as evident. In *Oxytricha* the TBE transposases are considered to be involved
625 in IES excision, but, unlike the MAC genome-encoded primary IES excisase (Tpb2) in

626 *Tetrahymena* and all the *Paramecium* PiggyMacs and PiggyMac-likes, are encoded by full-
627 length transposons present in the MIC genome, but absent from the MAC [74]. The considerable
628 heterogeneity in *Oxytricha* IES boundaries and "unscrambling" of a large subset of them [56],
629 together with the observation of pronounced developmental upregulation of numerous additional
630 MAC- and MIC-encoded transposases raises the possibility that additional transposases other
631 than those of TBEs could also be involved in IES excision [39,56]. Knowledge of IESs in other
632 ciliates is sparse (primarily confined to the phyllopharyngean *Chilodonella uncinata* [80,81]),
633 and, as far as we are aware, no specific IES excisases have been proposed for them.
634
635 Since the oligohymenophorean ciliate PiggyBac homologs are clear IES excisases, we sought
636 and found eight homologs of these genes in the *B. stoltei* ATCC 30299 MAC genome.
637 *Blepharisma* is the first ciliate genus aside from *Tetrahymena* and *Paramecium* in which such
638 proteins have been reported. Additional searches revealed clear PiggyBac homologs in
639 *Condylostoma magnum*, and a weaker pair of matches in *Stentor coeruleus*, suggesting that
640 these are a common feature of heterotrich ciliates. Reminiscent of *Paramecium tetraurelia*, in
641 which just one of the nine PiggyBac homologs, PiggyMac, has a complete DDD catalytic triad
642 [55], a single *B. stoltei* PiggyBac homolog has a complete DDD catalytic triad. The gene
643 encoding this protein in *B. stoltei* ATCC 30299 is highly upregulated during MAC development,
644 together with two other homologs that lack a complete catalytic triad. As is characteristic of
645 PiggyBac homologs, each of these three homologs also has a C-terminal, cysteine-rich, zinc
646 finger domain, which most closely resemble those of *Condylostoma magnum* homologs. The
647 organization of the heterotrich PiggyBac homolog zinc finger domains appears to be more
648 similar to that of comparable domains of *Homo sapiens* PGBD2 and PGBD3 homologs than that
649 of the zinc finger domains in *Paramecium* and *Tetrahymena* PiggyBac homologs (which are
650 more similar to the *Homo sapiens* PGBD4 zinc fingers [58]).
651

652 In *Paramecium*, since the discovery of multiple PiggyBac homologs (PiggyMac-likes), there
653 have been questions about their role, since, aside from PiggyMac, they all have incomplete
654 catalytic triads, and are thus likely catalytically inactive, but nevertheless their gene knockdowns
655 lead to pronounced IES retention [55]. It has therefore been proposed that the PiggyMac-likes
656 may function as heteromeric multi-subunit complexes in conjunction with PiggyMac during DNA
657 excision [55]. On the other hand cryo-EM structures available for moth PiggyBac transposase
658 support a model in which these proteins function as a homodimeric complex *in vitro* [82].
659 Furthermore, the primary *Tetrahymena* PiggyBac, Tpb2, is able to perform cleavage *in vitro*,
660 without the assistance of other PiggyBac homologs [53]. In other eukaryotes, domesticated
661 PiggyBacs without complete catalytic triads are thought to be retained by virtue of useful DNA-
662 binding roles [83]. One possibility for such purely DNA-binding transposases in ciliates could be
663 in competitively regulating (taming) the excision of DNA by the catalytically active transposases.
664 Future experimental analyses of the BPgm and the BPgm-likes could aid in resolving the
665 conundrums and understanding of possible interactions between catalytically active and inactive
666 transposases.

667 Domesticated PiggyBac homologs are the main candidate IES 668 excisases in *Blepharisma*

669 In addition to the PiggyBac homologs, we also found MAC genome-encoded transposases with
670 the PFAM domains “DDE_1”, “DDE_3”, “DDE_Tnp_IS1595” and “MULE” in *Blepharisma*. All the
671 genes encoding proteins with these domains lack flanking terminal repeats characteristic of
672 active transposons, suggesting these genes are further classes of domesticated transposases.
673 In *Blepharisma* and numerous other organisms, the DDE_1 domains co-occur with CENPB
674 domains. Two such proteins represent totally different proposed exaptations in mammals
675 (centromere-binding protein) and fission yeast (regulatory protein) [68–70]. Given the great

676 evolutionary distances involved, there is no specific reason to expect that the *Blepharisma*
677 homologs have either function. None of the three proteins with co-occurring DDE_1 and CENPB
678 domains have a complete catalytic triad, making it unlikely that these are active transposases or
679 IES excisases, though all three are noticeably upregulated during MAC development. Six
680 proteins with the PFAM domain DDE_3 are also encoded by *Blepharisma* MAC genes, of which
681 five possess a complete catalytic triad. DDE_3 domains are also characteristic of TBE
682 transposases in *Oxytricha* and Tec transposases in *Euplotes*. All the "DDE_3" protein genes are
683 upregulated during conjugation in *B. stoltei*, and are expressed at particularly high levels during
684 development of the new MAC. A number of DDE_Tnp_IS1595 and MULE domain-containing
685 proteins have complete catalytic triads and also show pronounced upregulation during *B. stoltei*
686 MAC development.
687
688 Upon excision, classical cut-and-paste transposases in eukaryotes typically leave behind
689 additional bases, notably including those of the target-site duplication that arose when they were
690 inserted, forming a "footprint" [84]. PiggyBac homologs are unique in performing precise,
691 "seamless" excision in eukaryotes [85], conserving the number of bases at the site of
692 transposon insertion after excision, a property that makes them popular for genetic engineering
693 [82]. *Tetrahymena* Tpb2 is the one exception among PiggyBac homologs associated with
694 imprecise excision in this eukaryote [53]. Since intragenic IESs are abundant in *Blepharisma*,
695 like *Paramecium* and unlike *Tetrahymena*, it is essential that these are excised precisely without
696 addition or removal of nucleotides, which, at best, could result in translation of additional amino
697 acids and, at worst, translation frameshifts.
698
699 Though there are clearly numerous additional domesticated transposases with complete
700 catalytic triads and whose genes are substantially upregulated during *Blepharisma*
701 development, whether they are capable of excision, and if this is precise, needs to be

established. *Tetrahymena* has distinct domesticated transposases that excise different subsets of IESs, namely those that are predominant, imprecisely excised and intergenic (by Tpb2) [53], versus those that are rare, precisely excised and intragenic (by Tpb1 and Tpb6) [79,86]. We could envisage if the additional *Blepharisma* domesticated transposases are still capable of excision, but not a precise form, an involvement in excision of a subset of the numerous intergenic IESs. Thus, while we cannot rule out the involvement of other possible domesticated transposases and PiggyMac-likes, currently *B. stoltei* PiggyMac is the primary candidate IES excisase.

A possible PiggyBac homolog ciliate common ancestor

In light of the discovery of PiggyMacs in heterotrichous ciliates, we investigated whether the last common ancestor of ciliates also possessed a PiggyMac. Phylogenetic analyses, together with tree topology tests, indicate that the oligohymenophorean and heterotrichous PiggyMacs and PiggyMac-likes form a monophyletic clade. The lack of PiggyBac homologs in other ciliate classes such as the Spirotrichea, and potentially the oligohymenophorean *Ichthyophthirius multifiliis* (with the caveat of apparent lower genome completeness), raises the question whether the PiggyMacs were lost in these lineages or were gained independently from the same source by both heterotrichs and a subset of oligohymenophoreans. We think the former is more likely. However, the alternative cannot be completely dismissed, because non-model ciliates, where the genome assembly quality allows reliable gene and domain annotations, have only been sparsely sampled.

Future directions

The *B. stoltei* ATCC 30299 MAC genome together with a corresponding MIC genome (Seah et al., in prep.) pave the way for future investigations of a peculiar, direct pathway to new MAC

725 genome development which skips the upstream complexity of meiotic and fertilization-
726 associated nuclear developmental processes of the standard pathway [9]. The pair of *B. stoltei*
727 strains we have are both now low frequency selfers, in which the conventional, indirect MAC
728 development pathway dominates. Comparisons with fresh, high frequency *Blepharisma* selfers
729 collected from the wild will facilitate comparative gene expression analyses with the direct MAC
730 development pathway, which will assist in distinguishing expression upregulation due to meiotic
731 and mitotic processes preceding indirect new MAC development. As a representative of one of
732 the two deepest branching ciliate lineages, the assembled somatic genome will facilitate
733 investigations beyond those reported here into the enigmatic origins of nuclear and genomic
734 dualism within single cells.

Materials and Methods

Strains and localities

The strains used and their original isolation localities were: *Blepharisma stoltei* ATCC 30299, Lake Federsee, Germany [24]; *Blepharisma stoltei* HT-IV, Aichi prefecture, Japan; *Blepharisma japonicum* R1072, from an isolate from Bangalore, India [22].

Cell cultivation, harvesting and cleanup

For genomic DNA isolation *B. stoltei* ATCC 30299 and HT-IV cells were cultured in Synthetic Medium for *Blepharisma* (SMB) [87] at 27˚C. Belpharismas were fed *Chlorogonium elongatum* grown in Tris-acetate phosphate (TAP) medium [88] at room temperature. *Chlorogonium* cells were pelleted at 1500 g at room temperature for 3 minutes to remove most of the TAP medium, and resuspended in 50 mL SMB. 50 ml of dense *Chlorogonium* was used to feed 1 litre of *Blepharisma* culture once every three days.

Blepharisma stoltei ATCC 30299 and HT-IV cells used for RNA extraction were cultured in Lettuce medium inoculated with *Enterbacter aerogenes* and maintained at 25˚C [89].

Blepharisma cultures were concentrated by centrifugation in pear-shaped flasks at 100 g for 2 minutes using a Hettich Rotanta 460 centrifuge with swing out buckets. Pelleted cells were washed with SMB and centrifuged again at 100 g for 2 minutes. The washed pellet was then transferred to a cylindrical tube capped with a 100 µm-pore nylon membrane at the base and immersed in SMB to filter residual algal debris from the washed cells. The cells were allowed to diffuse through the membrane overnight into the surrounding medium. The next day, the

757 cylinder with the membrane was carefully removed while attempting to minimize dislodging any
758 debris collected on the membrane. Cell density after harvesting was determined by cell counting
759 under the microscope.

760 DNA isolation, library preparation and sequencing

761 *B. stoltei* macronuclei were isolated by sucrose gradient centrifugation [4]. DNA was isolated
762 with a Qiagen 20/G genomic-tip kit according to the manufacturer's instructions. Purified DNA
763 from the isolated MACs was fragmented, size selected and used to prepare libraries according
764 to standard PacBio HiFi SMRTbell protocols. The libraries were sequenced in circular
765 consensus mode to generate HiFi reads.
766
767 Total genomic DNA from *B. stoltei* HT-IV and *B. stoltei* ATCC 30299 was isolated with the
768 SigmaAldrich GenElute Mammalian genomic DNA kit. A sequencing library was prepared with a
769 NEBnext FS DNA Library Prep Kit for Illumina and sequenced on an Illumina HiSeq 3000
770 sequencer, generating 150 bp paired-end reads.
771
772 Total genomic DNA from *B. japonicum* was isolated with the Qiagen MagAttract HMW DNA kit.
773 A long-read PacBio sequencing library was prepared using the SMRTbell® Express Template
774 Preparation Kit 2.0 according to the manufacturers' instructions and sequenced on an PacBio
775 Sequel platform with 1 SMRT cell. Independently, total genomic DNA form *B. japonicum* was
776 isolated with the SigmaAldrich GenElute Mammalian genomic DNA kit and an sequencing
777 library was prepared with the TruSeq Nano DNA Library Prep Kit (Illumina) and sequenced on
778 an Illumina NovaSeq6000 to generate 150 bp paired-end reads.

Gamone 1/ Cell-Free Fluid (CFF) isolation and conjugation activity assay

B. stoltei ATCC 30299 cells were cultured and harvested and concentrated to a density of 2000 cells/mL according to the procedure described in “Cell cultivation, Harvesting and Cleanup”. This concentrated cell culture was incubated overnight at 27˚C. The next day, the cells were harvested, and the supernatant collected and preserved at 4˚C at all times after extraction. The supernatant was then filtered through a 0.22 µm-pore filter. BSA (10 mg/mL) was added to produce the final CFF at a final BSA concentration of 0.01%.

To assess the activity of the CFF, serial dilutions of the CFF were made to obtain the gamone activity in terms of units (U) [90].The activity of the isolated CFF was 2^{10} U.

Conjugation time course and RNA isolation for high-throughput sequencing

B. stoltei cells for the complementary strains, ATCC 30299 and HT-IV, were cultivated and harvested by gentle centrifugation to achieve a final cell concentration of 2000 cells/ml for each strain. Non-gamone treated ATCC 30299 (A1) and HT-IV cells (H1) were collected (time point: -3 hours). Strain ATCC 30299 cells were then treated with synthetic gamone 2 (final concentration 1.5 µg/mL) and strain HT-IV cells were treated with cell-free fluid with a gamone 1 activity of ~2^{10} U/ml for three hours (Figure S8).

Homotypic pair formation in both cultures was checked after three hours. More than 75% of the cells in both cultures formed homotypic pairs. At this point the samples A2 (ATCC 30299) and H2 (HT-IV) were independently isolated for RNA extraction as gamone-treated control cells just

802 before mixing. For the rest of the culture, homotypic pairs in both cultures were separated by
803 pipetting them gently with a wide-bore pipette tip. Once all pairs had been separated, the two
804 cultures were mixed together. This constitutes the experiment's 0-h time point. The conjugating
805 culture was observed and samples collected for RNA isolation or cell fixation at 2 h, 6 h, 14 h,
806 18 h, 22 h, 26 h, 30 h and 38 h (Figure S8). Further details of the sample staging approach are
807 described in [9] and [51]. At each time point including samples A1, H1, A2 and H2, 7 mL of
808 culture was harvested for RNA-extraction using Trizol. The total RNA obtained was then
809 separated into a small RNA fraction < 200 nt and a fraction with RNA fragments > 200 nt using
810 the Zymo RNA Clean and Concentrator-5 kit according to the manufacturer's instructions. RNA-
811 seq libraries were prepared by BGI according to their standard protocols and sequenced on a
812 BGISeq 500 instrument.
813
814 Separate 2 mL aliquots of cells at each time point for which RNA was extracted were
815 concentrated by centrifuging gently at 100 rcf. 50 µL of the concentrated cells were fixed with
816 Carnoy's fixative (ethanol:acetic acid, 6:1), stained with DAPI and imaged to determine the state
817 of nuclear development [9].
818

819 Cell fixation and imaging

820 *B. stoltei* cells were harvested as above ("Cell cultivation"), and fixed with an equal volume of
821 "ZFAE" fixative, containing zinc sulfate (0.25 M, Sigma Aldrich), formalin, glacial acetic acid and
822 ethanol (Carl Roth), freshly prepared by mixing in a ratio of 10:2:2:5. Fixed cells were pelleted
823 (1000 g; 1 min), resuspended in 1% TritonX-100 in PHEM buffer to permeabilize (5 min; room
824 temperature), pelleted and resuspended in 2% (w/v) formaldehyde in PHEM buffer to fix further
825 (10 min; room temp.), then pelleted and washed twice with 3% (w/v) BSA in TBSTEM buffer

826 (~10 min; room temp.). For indirect immunofluorescence, washed cells were incubated with
827 primary antibody rat anti-alpha tubulin (Abcam, ab6161; 1:100 dilution in 3% w/v BSA/TBSTEM;
828 60 min; room temp.) then secondary antibody goat anti-rat IgG H&L labeled with AlexaFluor 488
829 (Abcam, ab150157, 1:500 dilution in 3% w/v BSA/TBSTEM; 20 min; room temp.). Nuclei were
830 counterstained with DAPI (1 µg/mL) in 3% (w/v) BSA/TBSTEM. A z-stack of images was
831 acquired using a confocal laser scanning microscope (Leica TCS SP8), equipped with a HC PL
832 APO 40× 1.30 Oil CS2 objective and a 1 photomultiplier tube and 3 HyD detectors, for DAPI
833 (405 nm excitation, 420-470 nm emission) and Alexa Fluor 488 (488 nm excitation, 510-530 nm
834 emission). Scanning was performed in sequential exposure mode. Spatial sampling was
835 achieved according to Nyquist criteria. ImageJ (Fiji) [91] was used to adjust image contrast and
836 brightness and overlay the DAPI and AlexaFluor 488 channels. The z-stack was temporally
837 color-coded.
838
839 For a nuclear 3D reconstruction (Figure 1B), cells were fixed in 1% (w/v) formaldehyde and
840 0.25% (w/v) glutaraldehyde. Nuclei were stained with Hoechst 33342 (Invitrogen) (5 µM in the
841 culture media), and imaged with a confocal laser scanning microscope (Zeiss, LSM780)
842 equipped with an LD C-Apochromat 40x/1,1 W Korr objective and a 32 channel GaAsP array
843 detector, with 405 nm excitation and 420-470 nm emission. Spatial sampling was achieved
844 according to Nyquist criteria. The IMARIS (Bitplane) software v8.0.2 was used for three-
845 dimensional reconstructions and contrast adjustments.
846
847 For scanning electron microscopy (SEM) cells were fixed in 0.5% osmium tetroxide/2%
848 formaldehyde/2.5% glutaraldehyde in 0.06x PHEM for 5-10 minutes at room temperature. Cells
849 were post-fixed with 2% formaldehyde/2.5% glutaraldehyde in 0.06x PHEM for 4-6 hours at
850 room temperature. Subsequently, samples were dehydrated in a graded ethanol series with 1
851 day per step followed by critical point drying (Polaron) with CO_2. Finally, the cells were sputter-

852 coated with a 4 nm thick layer of platinum (CCU-010, Safematic) and examined with a field
853 emission scanning electron microscope (Regulus 8230, Hitachi High Technologies) at an
854 accelerating voltage of 3 kV.
855

856 Genome assembly

857 Two MAC genome assemblies for *B. stoltei* ATCC 30299 (70× and 76× coverage) were
858 produced with Flye (version 2.7-b1585) [92] for the two separate PacBio Sequel II libraries
859 (independent replicates) using default parameters and the switches: --pacbio-hifi -g 45m. The
860 approximate genome assembly size was chosen based on preliminary Illumina genome
861 assemblies of approximately 40 Mb. Additional assemblies using the combined coverage (145×)
862 of the two libraries were produced using either Flye version 2.7-b1585 or 2.8.1-b1676, and the
863 same parameters. Two rounds of extension and merging were then used, first comparing the
864 70× and 76× assemblies to each other, then comparing the 145× assembly to the former
865 merged assembly. Assembly graphs were all relatively simple, with few tangles to be resolved
866 (Figure S7). Minimap2 [93] was used for pairwise comparison of the assemblies using the
867 parameters: -x asm5 --frag=yes --secondary=no, and the resultant aligned sequences were
868 visually inspected and manually merged or extended where possible using Geneious (version
869 2020.1.2) [94].
870
871 Visual inspection of read mapping to the combined assembly was then used to trim off contig
872 ends where there was little correspondence between the assembly consensus and the mapped
873 reads - which we classify as "cruft". Read mapping to cruft regions was often lower or uneven,
874 suggestive of repeats. Alternatively, these features could be due to trace MIC sequences, or
875 sites of alternative chromosome breakage during development which lead to sequences that are

876 neither purely MAC nor MIC. A few contigs with similar dubious mapping of reads at internal
877 locations, which were also clear sites of chromosome fragmentation (evident by abundant
878 telomere-bearing reads in the vicinity) were split apart and trimmed back as for the contig ends.
879 Telomere-bearing reads mapped to the non-trimmed region nearest to the trimmed site were
880 then used to define contig ends, adding representative telomeric repeats from one of the
881 underlying sequences mapped to each of the ends. The main genome assembly with gene
882 predictions can be obtained from the European Nucleotide Archive (ENA) (PRJEB40285;
883 accession GCA_905310155). “Cruft” sequences are also available from the same project
884 accession.
885
886 Two separate assemblies were generated for *Blepharisma japonicum.* A genome assembly for
887 *Blepharisma japonicum* strain R1072 was generated from Illumina reads, using SPAdes
888 genome assembler (v3.14.0) [95]. An assembly with PacBio Sequel long reads was produced
889 with Ra (v0.2.1) [96], which uses the Overlap-Layout-Consensus paradigm. The assembly
890 produced with Ra was more contiguous, with 268 contigs, in comparison to 1510 contigs in the
891 SPAdes assembly, and was chosen as the reference assembly for *Blepharisma japonicum*
892 (ENA accession: ERR6474383).
893
894 *Condylostoma magnum* genomic reads (study accession PRJEB9019) from a previous study
895 [97] were reassembled to improve contiguity and remove bacterial contamination. Reads were
896 trimmed with bbduk.sh from the BBmap package v38.22
897 (https://sourceforge.net/projects/bbmap/), using minimum PHRED quality score 2 (both ends)
898 and k-mer trimming for Illumina adapters and Phi-X phage sequence (right end), retaining only
899 reads ≥25 bp. Trimmed reads were error-corrected and reassembled with SPAdes v3.13.0 [95]
900 using k-mer values 21, 33, 55, 77, 99. To identify potential contaminants, the unassembled
901 reads were screened with phyloFlash v3.3b1 [98] against SILVA v132 [99]; the coding density

902 under the standard genetic code and prokaryotic gene model were also estimated using
903 Prodigal v2.6.3 [100]. Plotting the coverage vs. GC% of the initial assembly showed that most of
904 the likely bacterial contigs (high prokaryotic coding density, lower coverage, presence of
905 bacterial SSU rRNA sequences) had >=40% GC, so we retained only contigs with <40% GC as
906 the final *C. magnum* genome bin. The final assembly is available from the ENA bioproject
907 PRJEB48875 (accession GCA_920105805).
908
909 All assemblies were inspected with the quality assessment tool QUAST [101].

910 Variant calling

911 Illumina total genomic DNA-seq libraries for *B. stoltei* strains ATCC 30299 (ENA accession:
912 ERR6061285) and HT-IV (ERR6064674) were mapped to the ATCC 30299 reference assembly
913 with bowtie2 v2.4.2 [102]. Alignments were tagged with the MC tag (CIGAR string for mate/next
914 segment) using samtools [103] fixmate. The BAM file was sorted and indexed, read groups were
915 added with bamaddrg (commit 9baba65, https://github.com/ekg/bamaddrg), and duplicate reads
916 were removed with Picard MarkDuplicates v2.25.1 (http://broadinstitute.github.io/picard/).
917 Variants were called from the combined BAM file with freebayes v1.3.2 [104] in diploid mode,
918 with maximum coverage 1000 (option -g). The resultant VCF file was combined and indexed
919 with bcftools v1.12 [103], then filtered to retain only SNPs with quality score > 20, and at least
920 one alternate allele.

921 Annotation of alternative telomere addition sites

922 Alternative telomere addition sites (ATASs) were annotated by mapping PacBio HiFi reads to
923 the curated reference MAC assembly described above, using minimap2 and the following flags:
924 -x asm20 --secondary=no --MD. We expect reads representing alternative telomere additions to

925 have one portion mapping to the assembly (excluding telomeric regions), with the other portion
926 containing telomeric repeats being soft-clipped in the BAM record. For each mapped read with a
927 soft-clipped segment, we extracted the clipped sequence, and the coordinates and orientation of
928 the clip relative to the reference. We searched for ≥ 24 bp tandem direct repeats of the telomere
929 unit (i.e., ≥3 repeats of the 8 bp unit) in the clipped segment with NCRF v1.01.02 [105], which
930 can detect tandem repeats in the presence of noise, e.g., from sequencing error. The orientation
931 of the telomere sequence, the distance from the end of the telomeric repeat to the clip junction
932 ('gap'), and the number of telomere-bearing reads vs. total mapped reads at each junction were
933 also recorded. Junctions with zero gap between telomere repeat and clip junction were
934 annotated as ATASs. The above procedure was implemented in the MILTEL module of the
935 software package BleTIES v0.1.3 [106].
936
937 MILTEL output was processed with Python scripts depending on Biopython [107], pybedtools
938 [108], Bedtools [109], and Matplotlib [110], to summarize statistics of junction sequences and
939 telomere permutations at ATAS junctions, and to extract genomic sequences flanking ATASs for
940 sequence logos. Logos were drawn with Weblogo v3.7.5 [111], with sequences oriented such
941 that the telomere would be added on the 5' end of the ATAS junctions.
942
943 To calculate the expected minichromosome length, we assumed that ATASs were independent
944 and identically distributed in the genome following a Poisson distribution. About 47×10^3 ATASs
945 were annotated, supported on average by a single read. Given a genome of 42 Mbp at 145×
946 coverage, the expected rate of encountering an ATAS is 47×10^3 / (145 × 42 Mbp), so the
947 distance between ATASs (i.e., the minichromosome length) is exponentially distributed with
948 expectation (145 × 42 Mbp) / 47×10^3 = 130 kbp.

949 ## RNA-seq read mapping

950 To permit correct mapping of tiny introns RNA-seq data was mapped to the *B. stoltei* ATCC
951 30299 MAC genome using a version of HISAT2 [112] with modified source code, with the static
952 variable minIntronLen in hisat2.cpp lowered to 9 from 20 (change available in the HISAT2 github
953 fork: https://github.com/Swart-lab/hisat2/; commit hash 86527b9). HISAT2 was run with default
954 parameters and parameters --min-intronlen 9 --max-intronlen 500. It should be noted that RNA-
955 seq from timepoints in which *B. stoltei* ATCC 30299 and *B. stoltei* HT-IV cells were mixed
956 together were only mapped to the former genome assembly, and so reads for up to three alleles
957 may map to each of the genes in this assembly.

958 ## Genetic code prediction

959 We used the program PORC (Prediction Of Reassigned Codons; available from
960 https://github.com/Swart-lab/PORC) previously written to predict genetic codes in protist
961 transcriptomes [97] to predict the *B. stoltei* genetic code. This program was used to translate the
962 draft *B. stoltei* ATCC 30299 genome assembly in all six frames (with the standard genetic
963 code). Like the program FACIL [113] that inspired PORC, the frequencies of amino acids in
964 PFAM (version 34.0) protein domain profiles aligned to the six frame translation by HMMER
965 3.1b2 [114] (default search parameters; domains used for prediction with conditional E-values <
966 1e-20), and correspondingly also to the underlying codon, are used to infer the most likely amino
967 acid encoded by each codon (Figure S5).

968 ## Gene prediction

969 We created a wrapper program, Intronarrator, to predict genes in *Blepharisma* and other
970 heterotrichs, accommodating their tiny introns. Intronarrator can be downloaded and installed

971 together with dependencies via Conda from GitHub (https://github.com/Swart-lab/Intronarrator).
972 Intronarrator directly infers introns from spliced RNA-seq reads mapped by HISAT2 from the
973 entire developmental time course we generated. RNA-seq reads densely cover almost the entire
974 *Blepharisma* MAC genome, aside from intergenic regions, and most potential protein-coding
975 genes (Figure 5A). After predicting the introns and removing them to create an intron-minus
976 genome, Intronarrator runs AUGUSTUS (version 3.3.3) using its intronless model. It then adds
977 back the introns to the intronless gene predictions to produce the final gene predictions.
978
979 Introns are inferred from "CIGAR" string annotations in mapped RNA-seq BAM files, using the
980 regular expression "[0-9]+M([0-9][0-9])N[0-9]+M" to select spliced reads. For intron inference we
981 only used primary alignments with: MAPQ >= 10; just a single "N", indicating one potential
982 intron, per read; and at least 6 mapped bases flanking both the 5' and 3' intron boundaries (to
983 limit spurious chance matches of a few bases that might otherwise lead to incorrect intron
984 prediction). The most important parameters for Intronarrator are a cut-off of 0.2 for the fraction of
985 spliced reads covering a potential intron, and a minimum of 10 or more spliced reads to call an
986 intron. The splicing fraction cut-off was chosen based on the overall distribution of splicing
987 (Figure S6A-C). From our visual examination of mapped RNA-seq reads and gene predictions,
988 values less than this were typically "cryptic" excision events [115] which remove potentially
989 essential protein-coding sequences, rather than genuine introns. Intronarrator classifies an
990 intron as sense (7389 in total, excluding alternative splicing), when the majority of reads
991 (irrespective of splicing) mapping to the intron are the same strand, and antisense (554 in total)
992 when they are not. The most frequently spliced intron was chosen in rare cases of overlapping
993 alternative intron splicing.
994
995 To eliminate spurious prediction of protein-coding genes overlapping ncRNA genes, we also
996 incorporated ncRNA prediction in Intronarrator. Infernal [38] (default parameters; e-value < 1e-6)

997 was used to predict a restricted set of conserved ncRNAs models (i.e., tRNAs, rRNAs, SRP, and
998 spliceosomal RNAs) from RFAM 14.0 [116]. These ncRNAs were hard-masked (with "N"
999 characters) before AUGUSTUS gene prediction. Both Infernal ncRNA predictions (excluding
1000 tRNAs) and tRNA-scan SE 2.0 [117] (default parameters) tRNA predictions are annotated in the
1001 *B. stoltei* ATCC 30299 assembly deposited in the European Nucleotide Archive.
1002
1003 Since we found that *Blepharisma stoltei*, like *Blepharisma japonicum* [97], uses a non-standard
1004 genetic code, with UGA codon translated as tryptophan, gene predictions use the "The Mold,
1005 Protozoan, and Coelenterate Mitochondrial Code and the Mycoplasma/Spiroplasma Code
1006 (transl_table=4)" from the NCBI genetic codes. The default AUGUSTUS gene prediction
1007 parameters override alternative (mitochondrial) start codons permitted by NCBI genetic code 4,
1008 other than ATG. So, all predicted *B. stoltei* gene coding sequences begin with ATG.
1009
1010 RNA-seq read mapping relative to gene predictions of Contig_1 of *B. stoltei* ATCC30299 was
1011 visualized with PyGenomeTracks [118].

1012 Assessment of genome completeness

1013 A BUSCO (version 4.0.2) [119] analysis of the assembled MAC genomes of *B. stoltei* and *B.*
1014 *japonicum* was performed on the set of predicted proteins (BUSCO mode -prot) using the
1015 BUSCO Alveolata database. The completeness of the *Blepharisma* genomes was compared to
1016 the protein-level BUSCO analysis of the published genome assemblies of ciliates *T.*
1017 *thermophila*, *P. tetraurelia*, *S. coeruleus* and *I. multifiliis* (Figure S1).

1018 ## Gene annotation

1019 Pannzer2 [120] (default parameters) and EggNog (version 2.0.1) [121] were used for gene
1020 annotation. Annotations were combined and are available from the Max Planck Society's Open
1021 Research Repository, Edmond (https://dx.doi.org/10.17617/3.8c). Protein domain annotations
1022 were performed using hmmscan from HMMER3 (version 3.3, Nov 2019) [114] vs. the PFAM
1023 database (Pfam-A.full, 33.0, retrieved on June 23, 2020) with default parameters.

1024 ## Gene expression analysis

1025 Features from RNA-seq reads mapped to the *B. stoltei* ATCC 30299 genome over the
1026 developmental time-course were extracted using featureCounts from the Subread package
1027 [122]. Further analysis was performed using the R software environment. Genes with a total
1028 read count of less than 50, across all timepoints, were filtered out of the dataset. The remaining
1029 genes were passed as a DGElist object to edgeR [123]. Each time point, representing one
1030 library, was normalized for library size using the edgeR function calcNormFactors. The
1031 normalized read counts were transformed into TPM (transcripts per million) values [124,125].
1032 The TPM-values for different genes were compared across timepoints to examine changes in
1033 gene expression. Heatmaps showing log2(TPM) changes across timepoints were plotted using
1034 the tidyverse collection of R packages (https://www.tidyverse.org/) and RColorBrewer
1035 (https://rdrr.io/cran/RColorBrewer/). Tabulated gene expression estimates together with protein
1036 annotations are available from Edmond (https://dx.doi.org/10.17617/3.8c).

1037 ## Sequence visualization and analysis

1038 Nucleotide and amino acid sequences were visualized using Geneious Prime (Biomatters Ltd.)
1039 [94]. Multiple sequence alignments were performed with MAFFT version 7.450 [126,127].
1040 Phylogenetic trees were constructed with PhyML version 3.3.20180621 [128].

1041 ## Orthogroup inference and analysis of orthogroup clusters

1042 OrthoFinder version 2.5.2 with default parameters (i.e., using Diamond for searching, MAFFT for
1043 multiple alignment and FastTree for phylogenies) was used to define orthogroups, i.e., sets of
1044 genes descended from the last common ancestor of the chosen species. Proteomes for the
1045 following ciliate species were used: *Tetrahymena thermophila*, *Oxytricha trifallax*, *Stentor*
1046 *coeruleus* (data from ciliate.org [129]); *Euplotes octocarinatus* (EOGD [130]); *Paramecium*
1047 *tetraurelia*, *Paramecium caudatum* (data from ParameciumDB [131]); plus *Perkinsus marinus*
1048 ATCC 50983 (GenBank accession: AAXJ00000000) as a non-ciliate outgroup. Orthogroup
1049 clusters are available as Data S2, or from Edmond (https://dx.doi.org/10.17617/3.8c).

1050 ## d_N/d_S estimation

1051 We generated pairwise coding sequence alignments of PiggyMac paralog nucleotide sequences
1052 from *P. tetraurelia* and *P. octaurelia* using MAFFT version 7.450 [127] [126] (algorithm: “auto”,
1053 scoring matrix: 200PAM/k=2, gap open penalty 1.53, offset value 0.123) using the “translation
1054 align” panel of Geneious Prime (version 2020.1.2) [94]. PAML version 4.9 [132] was used to
1055 estimate d_N/d_S values in pairwise mode (runmode = -2, seqtype = 1, CodonFreq = 2). For
1056 *Blepharisma stoltei*, we generated pairwise coding sequence alignments of the *Blepharisma*
1057 PiggyMac homolog, BPgm (Contig_49.g1063; BSTOLATCC_MAC17466), with the *Blepharisma*
1058 Pgm-likes (BPgmLs) using ClustalW 2.1 [133] (Genetic code: *Blepharisma*, Protein alignment

1059 options: ClustalW alignment, Cost matrix: BLOSUM, Gap open cost: 10, Gap open penalty: 0.1)
1060 using “translation align” panel of Geneious Prime (version 2020.1.2). PAML version 4.9 was
1061 used to estimate dN/dS values in pairwise mode (runmode = -2, seqtype = 1, CodonFreq = 2).

1062 Phylogenetic analysis

1063 Protein sequences of PBLEs and PGDBs were obtained from Bouallègue et al [61]. Protein
1064 sequences of *Paramecium* and *Tetrahymena* Pgms and PgmLs were obtained from
1065 ParameciumDB [131] (PGM, PGMLs1-5) and ciliate.org [129] (Tpb1, Tpb2, Tpb7, LIA5),
1066 respectively. *Condylostoma* and *Blepharisma* Pgms and PgmLs were obtained from genome
1067 assemblies (accessions GCA_920105805 and GCA_905310155, respectively). Other PiggyBac
1068 protein sequences (*T. ni, D. purpureum*) were obtained from Uniprot [134]. Sequence
1069 manipulation was done using Geneious (Biomatters Ltd.). The Geneious plug-in for
1070 InterProScan [135] was used to identify DDE_Tnp_1_7 domains using the PFAM-A database
1071 [136]. The DDE_Tnp_1_7 domains were extracted and aligned using the MAFFT plug-in
1072 (v7.450) for Geneious [127] (Algorithm: Auto, Scoring matrix: BLOSUM62, Gap open penalty:
1073 1.53, Offset value: 0.123). The best-fit model of evolution for each alignment was identified
1074 using ModelTest-NG [137] (modeltest-ng -i <input_file>.phy -d aa -p 4 -T phyml -o
1075 <output_file>.out). The best model according to Bayesian criteria (BIC) were used to create
1076 phylogenetic trees using PhyML [128] [phyml -i <input_file>.phy -d aa -m LG -f m -v 0 -a e -c 4 -
1077 o tlr]. Phylogenetic trees thus generated were visualized with FigTree (v1.4.4) (Andrew
1078 Rambaut, http://tree.bio.ed.ac.uk/). Tree topology tests were performed using IQtree (v2.1.4-
1079 beta) [138] (iqtree -s <input file> -m LG+G4 -z <unconstrained and constrained treefiles> -n 0 -
1080 zb 10000 -au -nt AUTO).

1081 ## Repeat annotation

1082 Interspersed repeat element families were predicted with RepeatModeler v2.0.1 (default
1083 settings, random number seed 12345) with the following dependencies: rmblast v2.9.0+
1084 (http://www.repeatmasker.org/RMBlast.html), TRF 4.09 (Benson, 1999), RECON (Bao and
1085 Eddy, 2002), RepeatScout 1.0.6 (Price et al., 2005), RepeatMasker v4.1.1
1086 (http://www.repeatmasker.org/RMDownload.html). Repeat families were also classified in the
1087 pipeline by RepeatClassifier v2.0.1 through comparison against RepeatMasker's repeat protein
1088 database and the Dfam database. Consensus sequences of the predicted repeat families,
1089 produced by RepeatModeler, were then used to annotate repeats with RepeatMasker, using
1090 rmblast as the search engine.
1091
1092 Terminal inverted repeats (TIRs) of selected repeat element families were identified by aligning
1093 the consensus sequence from RepeatModeler, and/or selected full-length elements, with their
1094 respective reverse complements using MAFFT (Katoh and Standley, 2013) (plugin version
1095 distributed with Geneious). TIRs from the Dfam DNA transposon termini signatures database
1096 (v1.1, https://www.dfam.org/releases/dna_termini_1.1/dna_termini_1.1.hmm.gz) (Storer et al.,
1097 2021) were searched with hmmsearch (HMMer v3.2.1) against the IES sequences, to identify
1098 matches to TIR signatures of major transposon subfamilies.
1099

1100 # Data availability

1101 The draft *Blepharisma stoltei* ATCC 30299 macronuclear genome assembly is accessible from
1102 bleph.ciliate.org and from the European Nucleotide Archive (ENA) bioproject PRJEB40285
1103 under the accession GCA_905310155. PacBio CCS reads (ERR5873783 and ERR5873334)

1104 and subreads (ERR5962314) used to assemble the genome are also available from ENA.
1105 Illumina DNA-seq data for the *B. stoltei* ATCC 30299 and HT-IV strains is available from
1106 accessions ERR6061285 and ERR6064674, respectively. The RNA-seq developmental time
1107 course is available from the bioproject PRJEB45374 (accessions ERR6049461-ERR6049485).
1108
1109 Illumina and PacBio Sequel sequencing data for *Blepharisma japonicum* strain R1702 is
1110 available from the ENA bioproject PRJEB46921 (Illumina accessions: ERR6473251,
1111 ERR6474356; PacBio accession: ERR6474383).
1112

1113 Acknowledgements

1114 This paper is dedicated in memory of Akio Miyake and his decades of inspirational *Blepharisma*
1115 research. We thank Federico Buonanno for the provision of *B. stoltei* ATCC 30299 cells and
1116 culturing advice, Christa Lanz and the MPI for Biology's genome center, Jürgen Berger for SEM
1117 imaging, and Sebastien Colin and the MPI for Biology's Light Microscopy Facility for the 3D
1118 nuclear reconstruction.
1119

1120 Bibliography

1121 1. Martin WF, Garg S, Zimorski V. Endosymbiotic theories for eukaryote origin. Philos
1122 Trans R Soc Lond B Biol Sci. 2015;370: 20140330. doi:10.1098/rstb.2014.0330

1123 2. Orias E. On the evolution of the karyorelict ciliate life cycle: heterophasic ciliates and the
1124 origin of ciliate binary fission. BioSystems. 1991;25: 67–73. doi:10.1016/0303-
1125 2647(91)90013-B

1126 3. Prescott DM. The DNA of ciliated protozoa. Microbiol Rev. 1994;58: 233–267.
1127 doi:10.1128/mr.58.2.233-267.1994

1128 4. Lauth MR, Spear BB, Heumann J, Prescott DM. DNA of ciliated protozoa: DNA
1129 sequence diminution during macronuclear development of Oxytricha. Cell. 1976;7: 67–
1130 74. doi:10.1016/0092-8674(76)90256-7

1131 5. Chalker DL, Meyer E, Mochizuki K. Epigenetics of ciliates. Cold Spring Harb Perspect
1132 Biol. 2013;5: a017764. doi:10.1101/cshperspect.a017764

1133 6. Vogt A, Goldman AD, Mochizuki K, Landweber LF. Transposon domestication versus
1134 mutualism in ciliate genome rearrangements. PLoS Genet. 2013;9: e1003659.
1135 doi:10.1371/journal.pgen.1003659

1136 7. Lynn DH, editor. The Ciliated Protozoa. Dordrecht: Springer Netherlands; 2010.
1137 doi:10.1007/978-1-4020-8239-9

1138 8. Giese AC. Blepharisma: The Biology of a Light-sensitive Protozoan. illustrated ed.
1139 Stanford University Press; 1973.

1140 9. Miyake A, Rivola V, Harumoto T. Double paths of macronucleus differentiation at
1141 conjugation in Blepharisma japonicum. Eur J Protistol. 1991;27: 178–200.
1142 doi:10.1016/S0932-4739(11)80340-8

1143 10. Slabodnick MM, Ruby JG, Reiff SB, Swart EC, Gosai S, Prabakaran S, et al. The
1144 Macronuclear Genome of Stentor coeruleus Reveals Tiny Introns in a Giant Cell. Curr
1145 Biol. 2017;27: 569–575. doi:10.1016/j.cub.2016.12.057

1146 11. Slabodnick MM, Marshall WF. Stentor coeruleus. Curr Biol. 2014;24: R783-4.
1147 doi:10.1016/j.cub.2014.06.044

1148 12. Zhang KS, Blauch LR, Huang W, Marshall WF, Tang SKY. Microfluidic guillotine reveals
1149 multiple timescales and mechanical modes of wound response in Stentor coeruleus.

1150 BMC Biol. 2021;19: 63. doi:10.1186/s12915-021-00970-0

1151 13. Rapport EW, Rapport DJ, Berger J, Kupers V. Induction of conjugation in Stentor
1152 coeruleus. Trans Am Microsc Soc. 1976;95: 220–224. doi:10.2307/3225068

1153 14. Miyake A, Harumoto T. Asymmetrical cell division in Blepharisma japonicum: difference
1154 between daughter cells in mating-type expression. Exp Cell Res. 1990;190: 65–68.
1155 doi:10.1016/0014-4827(90)90144-y

1156 15. Terazima MN, Harumoto T. Defense function of pigment granules in the ciliate
1157 Blepharisma japonicum against two predatory protists, Amoeba proteus (Rhizopodea)
1158 and Climacostomum virens (Ciliata). Zool Sci. 2004;21: 823–828. doi:10.2108/zsj.21.823

1159 16. Kumazawa H. Homopolar Grafting in Blepharisma japonicum. Journal of Experimental
1160 Zoology. 1979;207: 1–16.

1161 17. Sugiura M, Shiotani H, Suzaki T, Harumoto T. Behavioural changes induced by the
1162 conjugation-inducing pheromones, gamone 1 and 2, in the ciliate Blepharisma
1163 japonicum. Eur J Protistol. 2010;46: 143–149. doi:10.1016/j.ejop.2010.01.002

1164 18. Young D. Macronuclear reorganization in Blepharisma undulans. Doctoral dissertation.
1165 1937.

1166 19. Friedl E, Miyake A, Heckmann K. Requirement of successive protein syntheses for the
1167 progress of meiosis in Blepharisma. Exp Cell Res. 1983;145: 105–113.
1168 doi:10.1016/s0014-4827(83)80013-5

1169 20. Miyake A, Tulli M, Nobili R. Requirement of protein synthesis in the initiation of meiosis
1170 and other nuclear changes in conjugation of Blepharisma. Exp Cell Res. 1979;120: 87–
1171 93. doi:10.1016/0014-4827(79)90539-1

1172 21. Inaba F. Conjugation between two strains of *Blepharisma*. J Protozool. 1965;12: 146–
1173 151. doi:10.1111/j.1550-7408.1965.tb01828.x

1174 22. Harumoto T, Miyake A, Ishikawa N, Sugibayashi R, Zenfuku K, Iio H. Chemical defense
1175 by means of pigmented extrusomes in the ciliate Blepharisma japonicum. Eur J Protistol.
1176 1998;34: 458–470. doi:10.1016/S0932-4739(98)80014-X

1177 23. Kobayashi M, Miura M, Takusagawa M, Sugiura M, Harumoto T. Two possible barriers
1178 blocking conjugation between different megakaryotypes of Blepharisma. Zool Sci.
1179 2015;32: 53–61. doi:10.2108/zs140151

1180 24. Repak AJ. Encystment and Excystment of the Heterotrichous Ciliate Blepharisma stoltei
1181 Isquith. Journal of Protozoology. 1968;5: 407–412.

1182 25. Salvini M, Durante M, Nobili R. Characterization of macronuclear DNA in Blepharisma
1183 japonicum. Protoplasma. 1983;117: 82–88. doi:10.1007/BF01281787

1184 26. Kimball RF. The nature and inheritance of mating types in euplotes patella. Genetics.
1185 1942;27: 269–285.

1186 27. Katashima RYO. Mating Types in *Euplotes eurystomus*. J Protozool. 1959;6: 75–83.
1187 doi:10.1111/j.1550-7408.1959.tb03930.x

1188 28. Luporini P, Miceli C, Ortenzi C. Evidence that the ciliate Euplotes raikovi releases
1189 mating-inducing factors (gamones). J Exp Zool. 1983;226: 1–9.
1190 doi:10.1002/jez.1402260102

1191 29. Vallesi A, Giuli G, Bradshaw RA, Luporini P. Autocrine mitogenic activity of pheromones
1192 produced by the protozoan ciliate Euplotes raikovi. Nature. 1995;376: 522–524.
1193 doi:10.1038/376522a0

1194 30. Braun V, Miyake A. Composition of blepharmone, a conjugation-inducing glycoprotein of
1195 the ciliate Blepharisma. FEBS Lett. 1975;53: 131–134. doi:10.1016/0014-
1196 5793(75)80003-2

1197 31. Miyake A, Beyer J. Blepharmone: a conjugation-inducing glycoprotein in the ciliate

1198 blepharisma. Science. 1974;185: 621–623. doi:10.1126/science.185.4151.621

1199 32. Sugiura M, Harumoto T. Identification, characterization, and complete amino acid
1200 sequence of the conjugation-inducing glycoprotein (blepharmone) in the ciliate
1201 Blepharisma japonicum. Proc Natl Acad Sci USA. 2001;98: 14446–14451.
1202 doi:10.1073/pnas.221457698

1203 33. Kubota T, Tokoroyama T, Tsukuda Y, Koyama H, Miyake A. Isolation and structure
1204 determination of blepharismin, a conjugation initiating gamone in the ciliate blepharisma.
1205 Science. 1973;179: 400–402. doi:10.1126/science.179.4071.400

1206 34. Klobutcher LA, Herrick G. Developmental genome reorganization in ciliated protozoa:
1207 the transposon link. Prog Nucleic Acid Res Mol Biol. 1997;56: 1–62. doi:10.1016/S0079-
1208 6603(08)61001-6

1209 35. Arnaiz O, Mathy N, Baudry C, Malinsky S, Aury J-M, Denby Wilkes C, et al. The
1210 Paramecium germline genome provides a niche for intragenic parasitic DNA:
1211 evolutionary dynamics of internal eliminated sequences. PLoS Genet. 2012;8:
1212 e1002984. doi:10.1371/journal.pgen.1002984

1213 36. Klobutcher LA, Herrick G. Consensus inverted terminal repeat sequence of Paramecium
1214 IESs: resemblance to termini of Tc1-related and Euplotes Tec transposons. Nucleic
1215 Acids Res. 1995;23: 2006–2013. doi:10.1093/nar/23.11.2006

1216 37. Chin C-S, Peluso P, Sedlazeck FJ, Nattestad M, Concepcion GT, Clum A, et al. Phased
1217 diploid genome assembly with single-molecule real-time sequencing. Nat Methods.
1218 2016;13: 1050–1054. doi:10.1038/nmeth.4035

1219 38. Nawrocki EP, Kolbe DL, Eddy SR. Infernal 1.0: inference of RNA alignments.
1220 Bioinformatics. 2009;25: 1335–1337. doi:10.1093/bioinformatics/btp157

1221 39. Swart EC, Bracht JR, Magrini V, Minx P, Chen X, Zhou Y, et al. The Oxytricha trifallax

1222 macronuclear genome: a complex eukaryotic genome with 16,000 tiny chromosomes.
1223 PLoS Biol. 2013;11: e1001473. doi:10.1371/journal.pbio.1001473

1224 40. Aeschlimann SH, Jönsson F, Postberg J, Stover NA, Petera RL, Lipps H-J, et al. The
1225 draft assembly of the radically organized Stylonychia lemnae macronuclear genome.
1226 Genome Biol Evol. 2014;6: 1707–1723. doi:10.1093/gbe/evu139

1227 41. Zagulski M, Nowak JK, Le Mouël A, Nowacki M, Migdalski A, Gromadka R, et al. High
1228 coding density on the largest Paramecium tetraurelia somatic chromosome. Curr Biol.
1229 2004;14: 1397–1404. doi:10.1016/j.cub.2004.07.029

1230 42. Sheng Y, Duan L, Cheng T, Qiao Y, Stover NA, Gao S. The completed macronuclear
1231 genome of a model ciliate Tetrahymena thermophila and its application in genome
1232 scrambling and copy number analyses. Sci China Life Sci. 2020;63: 1534–1542.
1233 doi:10.1007/s11427-020-1689-4

1234 43. Aury J-M, Jaillon O, Duret L, Noel B, Jubin C, Porcel BM, et al. Global trends of whole-
1235 genome duplications revealed by the ciliate Paramecium tetraurelia. Nature. 2006;444:
1236 171–178. doi:10.1038/nature05230

1237 44. Cheng Y-H, Liu C-FJ, Yu Y-H, Jhou Y-T, Fujishima M, Tsai IJ, et al. Genome plasticity in
1238 Paramecium bursaria revealed by population genomics. BMC Biol. 2020;18: 180.
1239 doi:10.1186/s12915-020-00912-2

1240 45. Yao MC, Yao CH, Monks B. The controlling sequence for site-specific chromosome
1241 breakage in Tetrahymena. Cell. 1990;63: 763–772. doi:10.1016/0092-8674(90)90142-2

1242 46. Cavalcanti ARO, Dunn DM, Weiss R, Herrick G, Landweber LF, Doak TG. Sequence
1243 features of Oxytricha trifallax (class Spirotrichea) macronuclear telomeric and
1244 subtelomeric sequences. Protist. 2004;155: 311–322. doi:10.1078/1434461041844196

1245 47. Lynch M. The origins of eukaryotic gene structure. Mol Biol Evol. 2006;23: 450–468.

1246 doi:10.1093/molbev/msj050

1247 48. Roy SW, Hudson AJ, Joseph J, Yee J, Russell AG. Numerous fragmented spliceosomal
1248 introns, AT-AC splicing, and an unusual dynein gene expression pathway in Giardia
1249 lamblia. Mol Biol Evol. 2012;29: 43–49. doi:10.1093/molbev/msr063

1250 49. Bondarenko VS, Gelfand MS. Evolution of the Exon-Intron Structure in Ciliate Genomes.
1251 PLoS ONE. 2016;11: e0161476. doi:10.1371/journal.pone.0161476

1252 50. Csuros M, Rogozin IB, Koonin EV. A detailed history of intron-rich eukaryotic ancestors
1253 inferred from a global survey of 100 complete genomes. PLoS Comput Biol. 2011;7:
1254 e1002150. doi:10.1371/journal.pcbi.1002150

1255 51. Sugiura M, Tanaka Y, Suzaki T, Harumoto T. Alternative gene expression in type I and
1256 type II cells may enable further nuclear changes during conjugation of Blepharisma
1257 japonicum. Protist. 2012;163: 204–216. doi:10.1016/j.protis.2011.07.007

1258 52. Baudry C, Malinsky S, Restituito M, Kapusta A, Rosa S, Meyer E, et al. PiggyMac, a
1259 domesticated piggyBac transposase involved in programmed genome rearrangements in
1260 the ciliate Paramecium tetraurelia. Genes Dev. 2009;23: 2478–2483.
1261 doi:10.1101/gad.547309

1262 53. Cheng C-Y, Vogt A, Mochizuki K, Yao M-C. A domesticated piggyBac transposase plays
1263 key roles in heterochromatin dynamics and DNA cleavage during programmed DNA
1264 deletion in Tetrahymena thermophila. Mol Biol Cell. 2010;21: 1753–1762.
1265 doi:10.1091/mbc.e09-12-1079

1266 54. Yuan Y-W, Wessler SR. The catalytic domain of all eukaryotic cut-and-paste
1267 transposase superfamilies. Proc Natl Acad Sci USA. 2011;108: 7884–7889.
1268 doi:10.1073/pnas.1104208108

1269 55. Bischerour J, Bhullar S, Denby Wilkes C, Régnier V, Mathy N, Dubois E, et al. Six

1270 domesticated PiggyBac transposases together carry out programmed DNA elimination in
1271 Paramecium. eLife. 2018;7. doi:10.7554/eLife.37927

1272 56. Chen X, Bracht JR, Goldman AD, Dolzhenko E, Clay DM, Swart EC, et al. The
1273 architecture of a scrambled genome reveals massive levels of genomic rearrangement
1274 during development. Cell. 2014;158: 1187–1198. doi:10.1016/j.cell.2014.07.034

1275 57. Coyne RS, Hannick L, Shanmugam D, Hostetler JB, Brami D, Joardar VS, et al.
1276 Comparative genomics of the pathogenic ciliate Ichthyophthirius multifiliis, its free-living
1277 relatives and a host species provide insights into adoption of a parasitic lifestyle and
1278 prospects for disease control. Genome Biol. 2011;12: R100. doi:10.1186/gb-2011-12-10-
1279 r100

1280 58. Guérineau M, Bessa L, Moriau S, Lescop E, Bontems F, Mathy N, et al. The unusual
1281 structure of the PiggyMac cysteine-rich domain reveals zinc finger diversity in PiggyBac-
1282 related transposases. Mob DNA. 2021;12: 12. doi:10.1186/s13100-021-00240-4

1283 59. Yang Z, Nielsen R. Estimating synonymous and nonsynonymous substitution rates
1284 under realistic evolutionary models. Mol Biol Evol. 2000;17: 32–43.
1285 doi:10.1093/oxfordjournals.molbev.a026236

1286 60. Mitra R, Fain-Thornton J, Craig NL. piggyBac can bypass DNA synthesis during cut and
1287 paste transposition. EMBO J. 2008;27: 1097–1109. doi:10.1038/emboj.2008.41

1288 61. Bouallègue M, Rouault J-D, Hua-Van A, Makni M, Capy P. Molecular Evolution of
1289 piggyBac Superfamily: From Selfishness to Domestication. Genome Biol Evol. 2017;9:
1290 323–339. doi:10.1093/gbe/evw292

1291 62. Kishino H, Miyata T, Hasegawa M. Maximum likelihood inference of protein phylogeny
1292 and the origin of chloroplasts. J Mol Evol. 1990;31: 151–160. doi:10.1007/BF02109483

1293 63. Kishino H, Hasegawa M. Evaluation of the maximum likelihood estimate of the

1294 evolutionary tree topologies from DNA sequence data, and the branching order in
1295 hominoidea. J Mol Evol. 1989;29: 170–179. doi:10.1007/BF02100115

1296 64. Ota R, Waddell PJ, Hasegawa M, Shimodaira H, Kishino H. Appropriate likelihood ratio
1297 tests and marginal distributions for evolutionary tree models with constraints on
1298 parameters. Mol Biol Evol. 2000;17: 798–803.
1299 doi:10.1093/oxfordjournals.molbev.a026358

1300 65. Strimmer K, Rambaut A. Inferring confidence sets of possibly misspecified gene trees.
1301 Proc Biol Sci. 2002;269: 137–142. doi:10.1098/rspb.2001.1862

1302 66. Shimodaira H. An approximately unbiased test of phylogenetic tree selection. Syst Biol.
1303 2002;51: 492–508. doi:10.1080/10635150290069913

1304 67. Tanaka Y, Nureki O, Kurumizaka H, Fukai S, Kawaguchi S, Ikuta M, et al. Crystal
1305 structure of the CENP-B protein-DNA complex: the DNA-binding domains of CENP-B
1306 induce kinks in the CENP-B box DNA. EMBO J. 2001;20: 6612–6618.
1307 doi:10.1093/emboj/20.23.6612

1308 68. Casola C, Hucks D, Feschotte C. Convergent domestication of pogo-like transposases
1309 into centromere-binding proteins in fission yeast and mammals. Mol Biol Evol. 2008;25:
1310 29–41. doi:10.1093/molbev/msm221

1311 69. Hohmann S. Characterisation of PDC2, a gene necessary for high level expression of
1312 pyruvate decarboxylase structural genes in Saccharomyces cerevisiae. Mol Gen Genet.
1313 1993;241: 657–666. doi:10.1007/BF00279908

1314 70. Mojzita D, Hohmann S. Pdc2 coordinates expression of the THI regulon in the yeast
1315 Saccharomyces cerevisiae. Mol Genet Genomics. 2006;276: 147–161.
1316 doi:10.1007/s00438-006-0130-z

1317 71. Gao B, Wang Y, Diaby M, Zong W, Shen D, Wang S, et al. Evolution of pogo, a separate

1318 superfamily of IS630-Tc1-mariner transposons, revealing recurrent domestication events
1319 in vertebrates. Mob DNA. 2020;11: 25. doi:10.1186/s13100-020-00220-0

1320 72. Witherspoon DJ, Doak TG, Williams KR, Seegmiller A, Seger J, Herrick G. Selection on
1321 the protein-coding genes of the TBE1 family of transposable elements in the ciliates
1322 Oxytricha fallax and O. trifallax. Mol Biol Evol. 1997;14: 696–706.
1323 doi:10.1093/oxfordjournals.molbev.a025809

1324 73. Williams K, Doak TG, Herrick G. Developmental precise excision of Oxytricha trifallax
1325 telomere-bearing elements and formation of circles closed by a copy of the flanking
1326 target duplication. EMBO J. 1993;12: 4593–4601. doi:10.1002/j.1460-
1327 2075.1993.tb06148.x

1328 74. Nowacki M, Higgins BP, Maquilan GM, Swart EC, Doak TG, Landweber LF. A functional
1329 role for transposases in a large eukaryotic genome. Science. 2009;324: 935–938.
1330 doi:10.1126/science.1170023

1331 75. Jahn CL, Doktor SZ, Frels JS, Jaraczewski JW, Krikau MF. Structures of the Euplotes
1332 crassus Tec1 and Tec2 elements: identification of putative transposase coding regions.
1333 Gene. 1993;133: 71–78. doi:10.1016/0378-1119(93)90226-s

1334 76. Doak TG, Doerder FP, Jahn CL, Herrick G. A proposed superfamily of transposase
1335 genes: transposon-like elements in ciliated protozoa and a common “D35E” motif. Proc
1336 Natl Acad Sci USA. 1994;91: 942–946. doi:10.1073/pnas.91.3.942

1337 77. Dupeyron M, Baril T, Bass C, Hayward A. Phylogenetic analysis of the Tc1/mariner
1338 superfamily reveals the unexplored diversity of pogo-like elements. Mob DNA. 2020;11:
1339 21. doi:10.1186/s13100-020-00212-0

1340 78. Lewin HA, Graves JAM, Ryder OA, Graphodatsky AS, O’Brien SJ. Precision
1341 nomenclature for the new genomics. Gigascience. 2019;8.

1342 doi:10.1093/gigascience/giz086

1343 79. Feng L, Wang G, Hamilton EP, Xiong J, Yan G, Chen K, et al. A germline-limited
1344 piggyBac transposase gene is required for precise excision in Tetrahymena genome
1345 rearrangement. Nucleic Acids Res. 2017;45: 9481–9502. doi:10.1093/nar/gkx652

1346 80. Zufall RA, Sturm M, Mahon BC. Evolution of germline-limited sequences in two
1347 populations of the ciliate Chilodonella uncinata. J Mol Evol. 2012;74: 140–146.
1348 doi:10.1007/s00239-012-9493-4

1349 81. Zufall RA, Katz LA. Micronuclear and macronuclear forms of beta-tubulin genes in the
1350 ciliate Chilodonella uncinata reveal insights into genome processing and protein
1351 evolution. J Eukaryot Microbiol. 2007;54: 275–282. doi:10.1111/j.1550-
1352 7408.2007.00267.x

1353 82. Chen Q, Luo W, Veach RA, Hickman AB, Wilson MH, Dyda F. Structural basis of
1354 seamless excision and specific targeting by piggyBac transposase. Nat Commun.
1355 2020;11: 3446. doi:10.1038/s41467-020-17128-1

1356 83. Sarkar A, Sim C, Hong YS, Hogan JR, Fraser MJ, Robertson HM, et al. Molecular
1357 evolutionary analysis of the widespread piggyBac transposon family and related
1358 “domesticated” sequences. Mol Genet Genomics. 2003;270: 173–180.
1359 doi:10.1007/s00438-003-0909-0

1360 84. van Luenen HG, Colloms SD, Plasterk RH. The mechanism of transposition of Tc3 in C.
1361 elegans. Cell. 1994;79: 293–301. doi:10.1016/0092-8674(94)90198-8

1362 85. Elick TA, Bauser CA, Fraser MJ. Excision of the piggyBac transposable element in vitro
1363 is a precise event that is enhanced by the expression of its encoded transposase.
1364 Genetica. 1996;98: 33–41. doi:10.1007/BF00120216

1365 86. Cheng C-Y, Young JM, Lin C-YG, Chao J-L, Malik HS, Yao M-C. The piggyBac

1366 transposon-derived genes TPB1 and TPB6 mediate essential transposon-like excision
1367 during the developmental rearrangement of key genes in Tetrahymena thermophila.
1368 Genes Dev. 2016;30: 2724–2736. doi:10.1101/gad.290460.116

1369 87. Miyake A, Beyer J. Cell interaction by means of soluble factors (gamones) in conjugation
1370 of Blepharisma intermedium. Exp Cell Res. 1973;76: 15–24. doi:10.1016/0014-
1371 4827(73)90413-8

1372 88. Andersen RA. Algal Culturing Techniques. 1st Edition. 2004.

1373 89. Miyake A, Harumoto T, Salvi B, Rivola V. Defensive function of pigment granules in
1374 Blepharisma japonicum. Eur J Protistol. 1990;25: 310–315. doi:10.1016/S0932-
1375 4739(11)80122-7

1376 90. Miyake A. Cell interaction by gamones in blepharisma. Sexual interactions in eukaryotic
1377 microbes. Elsevier; 1981. pp. 95–129. doi:10.1016/B978-0-12-524160-1.50010-2

1378 91. Schindelin J, Arganda-Carreras I, Frise E, Kaynig V, Longair M, Pietzsch T, et al. Fiji: an
1379 open-source platform for biological-image analysis. Nat Methods. 2012;9: 676–682.
1380 doi:10.1038/nmeth.2019

1381 92. Kolmogorov M, Yuan J, Lin Y, Pevzner PA. Assembly of long, error-prone reads using
1382 repeat graphs. Nat Biotechnol. 2019;37: 540–546. doi:10.1038/s41587-019-0072-8

1383 93. Li H. Minimap2: pairwise alignment for nucleotide sequences. Bioinformatics. 2018;34:
1384 3094–3100. doi:10.1093/bioinformatics/bty191

1385 94. Kearse M, Moir R, Wilson A, Stones-Havas S, Cheung M, Sturrock S, et al. Geneious
1386 Basic: an integrated and extendable desktop software platform for the organization and
1387 analysis of sequence data. Bioinformatics. 2012;28: 1647–1649.
1388 doi:10.1093/bioinformatics/bts199

1389 95. Prjibelski A, Antipov D, Meleshko D, Lapidus A, Korobeynikov A. Using SPAdes de novo

1390 assembler. Curr Protoc Bioinformatics. 2020;70: e102. doi:10.1002/cpbi.102

1391 96. Vaser R, Sikic M. Yet another de novo genome assembler. BioRxiv. 2019.
1392 doi:10.1101/656306

1393 97. Swart EC, Serra V, Petroni G, Nowacki M. Genetic Codes with No Dedicated Stop
1394 Codon: Context-Dependent Translation Termination. Cell. 2016;166: 691–702.
1395 doi:10.1016/j.cell.2016.06.020

1396 98. Gruber-Vodicka HR, Seah BKB, Pruesse E. phyloFlash: Rapid Small-Subunit rRNA
1397 Profiling and Targeted Assembly from Metagenomes. mSystems. 2020;5.
1398 doi:10.1128/mSystems.00920-20

1399 99. Quast C, Pruesse E, Yilmaz P, Gerken J, Schweer T, Yarza P, et al. The SILVA
1400 ribosomal RNA gene database project: improved data processing and web-based tools.
1401 Nucleic Acids Res. 2013;41: D590-6. doi:10.1093/nar/gks1219

1402 100. Hyatt D, Chen G-L, Locascio PF, Land ML, Larimer FW, Hauser LJ. Prodigal: prokaryotic
1403 gene recognition and translation initiation site identification. BMC Bioinformatics.
1404 2010;11: 119. doi:10.1186/1471-2105-11-119

1405 101. Gurevich A, Saveliev V, Vyahhi N, Tesler G. QUAST: quality assessment tool for
1406 genome assemblies. Bioinformatics. 2013;29: 1072–1075.
1407 doi:10.1093/bioinformatics/btt086

1408 102. Langmead B, Salzberg SL. Fast gapped-read alignment with Bowtie 2. Nat Methods.
1409 2012;9: 357–359. doi:10.1038/nmeth.1923

1410 103. Danecek P, Bonfield JK, Liddle J, Marshall J, Ohan V, Pollard MO, et al. Twelve years of
1411 SAMtools and BCFtools. Gigascience. 2021;10. doi:10.1093/gigascience/giab008

1412 104. Garrison E, Marth G. Haplotype-based variant detection from short-read sequencing. v2
1413 ed. arXiv; 2012 Jul p. arXiv:1207.3907 [q-bio.GN]. Available:

https://arxiv.org/abs/1207.3907

105. Harris RS, Cechova M, Makova KD. Noise-cancelling repeat finder: uncovering tandem repeats in error-prone long-read sequencing data. Bioinformatics. 2019;35: 4809–4811. doi:10.1093/bioinformatics/btz484

106. Seah BKB, Swart EC. BleTIES: Annotation of natural genome editing in ciliates using long read sequencing. BioRxiv. 2021. doi:10.1101/2021.05.18.444610

107. Cock PJA, Antao T, Chang JT, Chapman BA, Cox CJ, Dalke A, et al. Biopython: freely available Python tools for computational molecular biology and bioinformatics. Bioinformatics. 2009;25: 1422–1423. doi:10.1093/bioinformatics/btp163

108. Dale RK, Pedersen BS, Quinlan AR. Pybedtools: a flexible Python library for manipulating genomic datasets and annotations. Bioinformatics. 2011;27: 3423–3424. doi:10.1093/bioinformatics/btr539

109. Quinlan AR, Hall IM. BEDTools: a flexible suite of utilities for comparing genomic features. Bioinformatics. 2010;26: 841–842. doi:10.1093/bioinformatics/btq033

110. Hunter JD. Matplotlib: A 2D Graphics Environment. Comput Sci Eng. 2007;9: 90–95. doi:10.1109/MCSE.2007.55

111. Crooks GE, Hon G, Chandonia JM, Brenner SE. WebLogo: a sequence logo generator. Genome Res. 2004;14: 1188–1190. doi:10.1101/gr.849004

112. Kim D, Paggi JM, Park C, Bennett C, Salzberg SL. Graph-based genome alignment and genotyping with HISAT2 and HISAT-genotype. Nat Biotechnol. 2019;37: 907–915. doi:10.1038/s41587-019-0201-4

113. Dutilh BE, Jurgelenaite R, Szklarczyk R, van Hijum SAFT, Harhangi HR, Schmid M, et al. FACIL: Fast and Accurate Genetic Code Inference and Logo. Bioinformatics. 2011;27: 1929–1933. doi:10.1093/bioinformatics/btr316

1438 114. Eddy SR. Accelerated profile HMM searches. PLoS Comput Biol. 2011;7: e1002195.
1439 doi:10.1371/journal.pcbi.1002195

1440 115. Saudemont B, Popa A, Parmley JL, Rocher V, Blugeon C, Necsulea A, et al. The fitness
1441 cost of mis-splicing is the main determinant of alternative splicing patterns. Genome Biol.
1442 2017;18: 208. doi:10.1186/s13059-017-1344-6

1443 116. Kalvari I, Argasinska J, Quinones-Olvera N, Nawrocki EP, Rivas E, Eddy SR, et al. Rfam
1444 13.0: shifting to a genome-centric resource for non-coding RNA families. Nucleic Acids
1445 Res. 2018;46: D335–D342. doi:10.1093/nar/gkx1038

1446 117. Chan PP, Lin BY, Mak AJ, Lowe TM. tRNAscan-SE 2.0: Improved Detection and
1447 Functional Classification of Transfer RNA Genes. BioRxiv. 2019. doi:10.1101/614032

1448 118. Lopez-Delisle L, Rabbani L, Wolff J, Bhardwaj V, Backofen R, Grüning B, et al.
1449 pyGenomeTracks: reproducible plots for multivariate genomic datasets. Bioinformatics.
1450 2021;37: 422–423. doi:10.1093/bioinformatics/btaa692

1451 119. Waterhouse RM, Seppey M, Simão FA, Manni M, Ioannidis P, Klioutchnikov G, et al.
1452 BUSCO applications from quality assessments to gene prediction and phylogenomics.
1453 Mol Biol Evol. 2018;35: 543–548. doi:10.1093/molbev/msx319

1454 120. Törönen P, Medlar A, Holm L. PANNZER2: a rapid functional annotation web server.
1455 Nucleic Acids Res. 2018;46: W84–W88. doi:10.1093/nar/gky350

1456 121. Huerta-Cepas J, Szklarczyk D, Heller D, Hernández-Plaza A, Forslund SK, Cook H, et
1457 al. eggNOG 5.0: a hierarchical, functionally and phylogenetically annotated orthology
1458 resource based on 5090 organisms and 2502 viruses. Nucleic Acids Res. 2019;47:
1459 D309–D314. doi:10.1093/nar/gky1085

1460 122. Liao Y, Smyth GK, Shi W. featureCounts: an efficient general purpose program for
1461 assigning sequence reads to genomic features. Bioinformatics. 2014;30: 923–930.

1462 doi:10.1093/bioinformatics/btt656

1463 123. Robinson MD, McCarthy DJ, Smyth GK. edgeR: a Bioconductor package for differential
1464 expression analysis of digital gene expression data. Bioinformatics. 2010;26: 139–140.
1465 doi:10.1093/bioinformatics/btp616

1466 124. Li B, Ruotti V, Stewart RM, Thomson JA, Dewey CN. RNA-Seq gene expression
1467 estimation with read mapping uncertainty. Bioinformatics. 2010;26: 493–500.
1468 doi:10.1093/bioinformatics/btp692

1469 125. Wagner GP, Kin K, Lynch VJ. Measurement of mRNA abundance using RNA-seq data:
1470 RPKM measure is inconsistent among samples. Theory Biosci. 2012;131: 281–285.
1471 doi:10.1007/s12064-012-0162-3

1472 126. Katoh K, Misawa K, Kuma K, Miyata T. MAFFT: a novel method for rapid multiple
1473 sequence alignment based on fast Fourier transform. Nucleic Acids Res. 2002;30: 3059–
1474 3066. doi:10.1093/nar/gkf436

1475 127. Katoh K, Standley DM. MAFFT multiple sequence alignment software version 7:
1476 improvements in performance and usability. Mol Biol Evol. 2013;30: 772–780.
1477 doi:10.1093/molbev/mst010

1478 128. Guindon S, Dufayard J-F, Lefort V, Anisimova M, Hordijk W, Gascuel O. New algorithms
1479 and methods to estimate maximum-likelihood phylogenies: assessing the performance
1480 of PhyML 3.0. Syst Biol. 2010;59: 307–321. doi:10.1093/sysbio/syq010

1481 129. Stover NA, Punia RS, Bowen MS, Dolins SB, Clark TG. Tetrahymena Genome
1482 Database Wiki: a community-maintained model organism database. Database (Oxford).
1483 2012;2012: bas007. doi:10.1093/database/bas007

1484 130. Wang R-L, Miao W, Wang W, Xiong J, Liang A-H. EOGD: the Euplotes octocarinatus
1485 genome database. BMC Genomics. 2018;19: 63. doi:10.1186/s12864-018-4445-z

1486 131. Arnaiz O, Meyer E, Sperling L. ParameciumDB 2019: integrating genomic data across
1487 the genus for functional and evolutionary biology. Nucleic Acids Res. 2020;48: D599–
1488 D605. doi:10.1093/nar/gkz948

1489 132. Yang Z. PAML 4: phylogenetic analysis by maximum likelihood. Mol Biol Evol. 2007;24:
1490 1586–1591. doi:10.1093/molbev/msm088

1491 133. Larkin MA, Blackshields G, Brown NP, Chenna R, McGettigan PA, McWilliam H, et al.
1492 Clustal W and Clustal X version 2.0. Bioinformatics. 2007;23: 2947–2948.
1493 doi:10.1093/bioinformatics/btm404

1494 134. UniProt Consortium. UniProt: the universal protein knowledgebase in 2021. Nucleic
1495 Acids Res. 2021;49: D480–D489. doi:10.1093/nar/gkaa1100

1496 135. Jones P, Binns D, Chang H-Y, Fraser M, Li W, McAnulla C, et al. InterProScan 5:
1497 genome-scale protein function classification. Bioinformatics. 2014;30: 1236–1240.
1498 doi:10.1093/bioinformatics/btu031

1499 136. Mistry J, Chuguransky S, Williams L, Qureshi M, Salazar GA, Sonnhammer ELL, et al.
1500 Pfam: The protein families database in 2021. Nucleic Acids Res. 2021;49: D412–D419.
1501 doi:10.1093/nar/gkaa913

1502 137. Darriba D, Posada D, Kozlov AM, Stamatakis A, Morel B, Flouri T. ModelTest-NG: A
1503 New and Scalable Tool for the Selection of DNA and Protein Evolutionary Models. Mol
1504 Biol Evol. 2020;37: 291–294. doi:10.1093/molbev/msz189

1505 138. Minh BQ, Schmidt HA, Chernomor O, Schrempf D, Woodhams MD, von Haeseler A, et
1506 al. IQ-TREE 2: New Models and Efficient Methods for Phylogenetic Inference in the
1507 Genomic Era. Mol Biol Evol. 2020;37: 1530–1534. doi:10.1093/molbev/msaa015

1508 139. Suzuki S. Parthenogenetic conjugation in Blepharisma undulans japonicus Suzuki. Bull
1509 Yamagata Univ Natural Sci. 1957;4: 69–84.

1510 140. Kriventseva EV, Kuznetsov D, Tegenfeldt F, Manni M, Dias R, Simão FA, et al. OrthoDB
1511 v10: sampling the diversity of animal, plant, fungal, protist, bacterial and viral genomes
1512 for evolutionary and functional annotations of orthologs. Nucleic Acids Res. 2019;47:
1513 D807–D811. doi:10.1093/nar/gky1053

1514 141. Wick RR, Schultz MB, Zobel J, Holt KE. Bandage: interactive visualization of de novo
1515 genome assemblies. Bioinformatics. 2015;31: 3350–3352.
1516 doi:10.1093/bioinformatics/btv383

1517

1518 # Figure captions

1519 **Figure 1. *Blepharisma* cells and properties of ciliate MAC genomes**. **A.** *B. stoltei* ATCC
1520 30299 cell stained with anti-alpha tubulin-Alexa488 (depth-color coded red to yellow) and DAPI
1521 (cyan). **B.** Snapshot of a 3D reconstruction (Imaris, Bitplane) from CLSM images of Hoechst
1522 33342 (dsDNA dye, Invitrogen™) fluorescence (Ex405 nm / Em420-470 nm). **C.** Scanning
1523 electron microscope (SEM) image of a *B. stoltei* ATCC 30299 cell (false color).
1524

1525 **Figure 2. Nuclear development during *Blepharisma stoltei* conjugation. A.** Cell
1526 development cycle with inset showing the four main kinds of nuclei, highlighted with arrows.
1527 Illustration of various cell stages adapted from [139]). Detailed staging collected for an RNA-seq
1528 time course is provided in Figure S9. **B.** Schematic of nuclear processes occurring during
1529 conjugation (classified according to, and modified from [9]). Nuclear events occurring before and
1530 up to, but not including fusion of the gametic nuclei (syngamy) are classified into sixteen pre-
1531 gamic stages where the MICs undergo meiosis and the haploid products of meiotic MICs are
1532 exchanged between the conjugating cells, followed by karyogamy. After karyogamy, cells are
1533 classified into 10 stages S (synkaryon), D1 (1st mitosis), I1 (1st interphase), D2 (2nd mitosis), I2
1534 (2nd interphase), D3 (3rd mitosis), I3 (3rd interphase), D4 (4th mitosis), E1 (1st embryonic stage),
1535 E2 (2nd embryonic stage). After E2, the exconjugants divide further and are classified into 6
1536 stages of cell division (CD1-6) which we did not follow here.
1537

1538 **Figure 3. Basic properties of ciliate MAC genomes.** In cell diagrams MACs are green and
1539 MICs are small black dots in close proximity to MACs. Citations for genome properties are in
1540 Data S1.
1541
1542

1543 **Figure 4**. **Alternative telomere addition sites. A.** Mapping of a subset telomere-containing
1544 HiFi reads to a *B. stoltei* MAC genome contig region, with alternative telomere addition sites
1545 (ATASs) shown by blue (5') or mauve (3') arrows. Pink bars at read ends indicate soft-masking
1546 by minimap2, typically of telomeric repeats. **B.** Mean base frequencies in +/- 1 kbp flanking
1547 ATAS junctions.
1548
1549 **Figure 5. A gene-dense somatic genome with tiny introns. A.** HiFi (DNA) and RNA-seq
1550 coverage across a representative *B. stoltei* ATCC30299 MAC genome contig (Contig_1). Y
1551 scale is linear for HiFi reads and logarithmic (base 10) for RNA-seq. Plus strand (relative to the
1552 contig) RNA-seq coverage is green; minus strand RNA-seq coverage is blue. Between the RNA-
1553 seq coverage graphs each arrow represents a predicted gene, colored green when transcribed
1554 from the sense strand and blue from the antisense one. Two orthogroups classified by
1555 OrthoFinder are shown in orange and pink, respectively. **B.** Distribution of intron lengths from
1556 predicted genes. **C.** Sequence logos for 15 bp introns (splicing frequency > 0.5). **D.** Clustered
1557 orthogroups (Data S2) in the *B. stoltei* MAC genome.
1558
1559 **Figure 6. MAC genome-encoded transposases in ciliates and properties of a putative**
1560 ***Blepharisma* IES excisase. A.** Presence/absence matrix of PFAM transposase domains
1561 detected in predicted MAC genome-encoded ciliate proteins. Ciliate classes are indicated before
1562 the binomial species names. Note that *Ichthyophthirius multifiliis* is not shown because no
1563 domains with i-E-values < 1e-4 were detected. PiggyBac homolog phylogeny with PFAM
1564 domain architecture and gene expression heatmap for *Blepharisma*. **B**. DDE_Tnp_1_7 domain
1565 phylogeny with PFAM domain architecture and gene expression heatmap for *Blepharisma*. **C.**
1566 Cysteine-rich domains of PiggyBac homologs. PBLE transposases: Ago (*Aphis gossypii*); Bmo
1567 (*Bombyx mori*); Cag (*Ctenoplusia agnata*); Har (*Helicoverpa armigera*); Hvi (*Heliothis virescens*);
1568 PB-Tni (*Trichoplusia ni*); Mlu (PiggyBat from *Myotis lucifugus*); PLE-wu (*Spodoptera frugiperda*).

1569 Domesticated PGBD transposases: Oni (*Oreochromis niloticus*); Pny (*Pundamilia nyererei*);
1570 Lia5, Tpb1, Tpb2, Tpb6 and Tpb7 (*Tetrahymena thermophila*); Pgm, PgmL1, PgmL2,
1571 PgmL3a/b/c, PgmL4a/b, PgmL5a/b (*Paramecium tetraurelia*); Tru (*Takifugu rubripes*); Pgbd2,
1572 Pgbd3 and Pgbd4 (*Homo sapiens*).
1573
1574 **Figure 7. Phylogeny of ciliate PiggyBac homologs, eukaryotic PBLEs and PGBD5**
1575 **homologs.** Colors indicate eukaryotic lineages: purple=Alveolata, green=Stramenopiles,
1576 cyan=Archaeplastida, yellow=Opisthokonta, blue=Amoebozoa. Clade highlighted in pink
1577 represents all heterotrich Pgms and PgmLs. aBayes values generated by PhyML are
1578 represented as line widths and branch colors. aBayes values lower than 0.9 are represented in
1579 red-grey, with lower values appearing more red. The tree is rooted at the PiggyBac-like element
1580 of *Entamoeba invadens.*
1581
1582 **Figure 8. DDE_1 and DDE_3 domain transposases in *Blepharisma*. A.** DDE_1 domain
1583 phylogeny with PFAM domain architecture and gene expression heatmap for *Blepharisma*. **B.**
1584 DDE_3 domain phylogeny with PFAM domain architecture and gene expression heatmap for
1585 *Blepharisma*.
1586
1587 **Figure 9. DDE_Tnp_IS1595 and MULE domain transposases in *Blepharisma*. A.**
1588 DDE_Tnp_IS1595 domain phylogeny with PFAM domain architecture and gene expression
1589 heatmap for *Blepharisma*. **B.** MULE domain phylogeny with PFAM domain architecture and
1590 gene expression heatmap for *Blepharisma*.
1591
1592
1593

Supplementary figure captions

Figure S1. Analysis of assembly completeness by Benchmarking Universal Single-Copy Orthologs (BUSCO). Completeness of the *B. stoltei* ATCC 30299 MAC assembly was estimated by the percentage of BUSCOs found in the assembly with reference to the OrthoDB v10 alveolate database [140]. The nature of the ortholog-matches is indicated by characters followed by counts: C (complete orthologs) - light blue, D (duplicated orthologs) - dark blue, F (fragmented orthologs) - yellow and M (missing orthologs) - red.

Figure S2. Properties of minichromosomes, telomeres, and alternative telomere addition sites. A. Length distribution of telomeres of telomere-bearing HiFi reads. **B.** Length distribution of HiFi reads delimited by telomeres. **C**. Diagram of a telomere-bearing read mapped onto genome reference at an ATAS. Sequence which is ambiguously chromosomal or telomeric is "junction sequence"; junction coordinate which maximizes telomere repeat length on the read is the "first identifiable breakpoint"; the coordinate maximizing alignment length to reference is the "last identifiable breakpoint". The last telomeric unit permutation at the last identifiable breakpoint is underlined (length 8 bp). **D.** Sequence logos of chromosomal sequence at ATAS junctions, sorted by which permutation of the telomeric repeat is present (plot labels). Logos are aligned to the "last identifiable breakpoint" between positions 20 and 21; telomeric repeats on telomere-bearing reads begin to the left of the breakpoint. **E**. Frequencies of 2-mers in whole genome (blue), in telomeres (green), and at ATAS junctions (chromosomal side after last identifiable breakpoint, orange). **F.** Histogram of junction sequence lengths for ATASs in *B. stoltei*. **G.** Counts of each telomere repeat permutation at ATAS junctions (last identifiable breakpoint).

1619 **Figure S3**. **Femto Pulse analyses of *B. stoltei* MAC DNA and mapping of *T. thermophila***
1620 **telomere-bearing reads. A.** Mapping of PacBio CLR reads with 3 consecutive telomeric
1621 repeats to a representative *T. thermophila* MAC chromosome (Chr_001 from ciliate.org). **B.**
1622 Length distribution of input MAC DNA sizes prior to fragmentation and library preparation
1623 (Femto Pulse; LM = lower maker) - replicate 1. RFU=relative fluorescent units. **C.** Length
1624 distribution of input MAC DNA sizes prior to fragmentation and library preparation (Femto Pulse;
1625 LM = lower maker) - replicate 2.
1626
1627 **Figure S4. POT1 paralog phylogeny, PFAM domain architecture, and gene expression in**
1628 ***Blepharisma*.** Diagram elements as described in Figure 6B.
1629
1630 **Figure S5. *Blepharisma stoltei* genetic code.** Prediction for *B. stoltei* ATCC 30299 MAC
1631 genome by PORC; codons that are stops in the standard genetic code are highlighted in orange.
1632
1633 **Figure S6. Intron splicing. A.** Distribution of intron splicing fraction of candidate sense introns
1634 in the *B. stoltei* MAC genome. **B**. Distribution of intron splicing fractions of introns according to
1635 intron lengths. **C.** Distribution of intron splicing fraction of candidate antisense introns. **D.**
1636 Sequence logos for all predicted 16 nt introns, and 16 nt introns with “A” at either position -7 or -
1637 6 (counting from the 3’ end). The number of introns underlying the logos are indicated to the
1638 right. **E.** Distribution of intron splicing fractions of introns according to intron lengths. **F.** Sample
1639 of RNA-seq reads mapped to a GT-GG intron from gene BSTOLATCC_MAC21551
1640 (Contig_57.g761). Translation in alternative reading frames downstream of the predicted intron
1641 leads to premature stop codons soon after the intron.
1642
1643 **Figure S7**. ***B. stoltei* ATCC30299 MAC genome assembly graph.** Bandage [141]
1644 representation of Flye 2.8.1 assembly graph. Edges corresponding to contigs are colored by

1645 coverage (brightest pink = 160×, black=0×).

1646

1647 **Figure S8. Experimental approach for conjugation RNA-seq time series.** Complementary
1648 mating type strains of *Blepharisma stoltei* were harvested and cleaned by starving overnight.
1649 The cleaned cultures were treated in a time-staggered format, with gamones of the
1650 complementary mating type, where gamone 2 was a solution of the synthetic gamone 2 calcium
1651 salt and gamone 1 was provided as the cell-free fluid (CFF) harvested from mating-type I cells.
1652 Two sets of time-staggered gamone-treated cultures were used for the time series. Set I,
1653 indicated by the solid line, was mixed and used to observe and collect samples at 0 hours, 2
1654 hours, 6 hours, 26 hours and 30 hours after mixing. Set II, indicated by the dashed lines, was
1655 mixed and used to observe and collect samples at 14 hours, 18 hours, 22 hours and 38 hours
1656 after mixing. Test tubes indicate Trizol samples prepared for RNA-extraction which were stored
1657 at -80 ˚C before processing. Cells collected for imaging were obtained shortly before the
1658 remainder were transferred into Trizol.

1659

1660 **Figure S9. Developmental staging of *B. stoltei* for RNA-seq. A.** The classification of nuclear
1661 morphology into stages has been done according to previous descriptions [9]. Nuclear events
1662 occurring before and up to, but not including fusion of the gametic nuclei (syngamy) are
1663 classified into sixteen stages indicated by roman numerals. These are the pre-gamic stages of
1664 conjugation where the MICs undergo meiosis and the haploid products of meiotic MICs are
1665 exchanged between the conjugating cells. Stages after syngamy are classified into 10 stages,
1666 stage S (synkaryon), D1 (1st mitosis), I1(1st interphase), D2 (2nd mitosis), I2 (2nd interphase),
1667 D3 (3rd mitosis), I3 (3rd interphase), D4 (4th mitosis), E1 (1st embryonic stage), E2 (2nd
1668 embryonic stage). After E2, the exconjugants divide further and are classified into 6 stages of
1669 cell division (CD1-6) which we did not follow here. Illustration of various cell stages adapted from
1670 [139]). Stacked bars show the proportion of cells at each time point at different stages of

1671 development, preceded by the number of cells inspected (n).

1672

1673 **Figure S10. Small RNA-related proteins in *Blepharisma*. A.** ResIII, Helicase_c and

1674 Ribonuclease_3 domain phylogeny with PFAM domain architecture and gene expression

1675 heatmap for *Blepharisma*. **B.** PIWI domain phylogeny with PFAM domain architecture and gene

1676 expression heatmap for *B. stoltei*.

1677

1678 **Figure S11. Histones and histone-domain-containing proteins in *Blepharisma*.** Gene

1679 expression heatmaps are shown as in previous figures, are clustered according to major histone

1680 type as classified using HistoneDB domain models. Domains from PFAM and HistoneDB are

1681 shown to the right.

Figure 1.

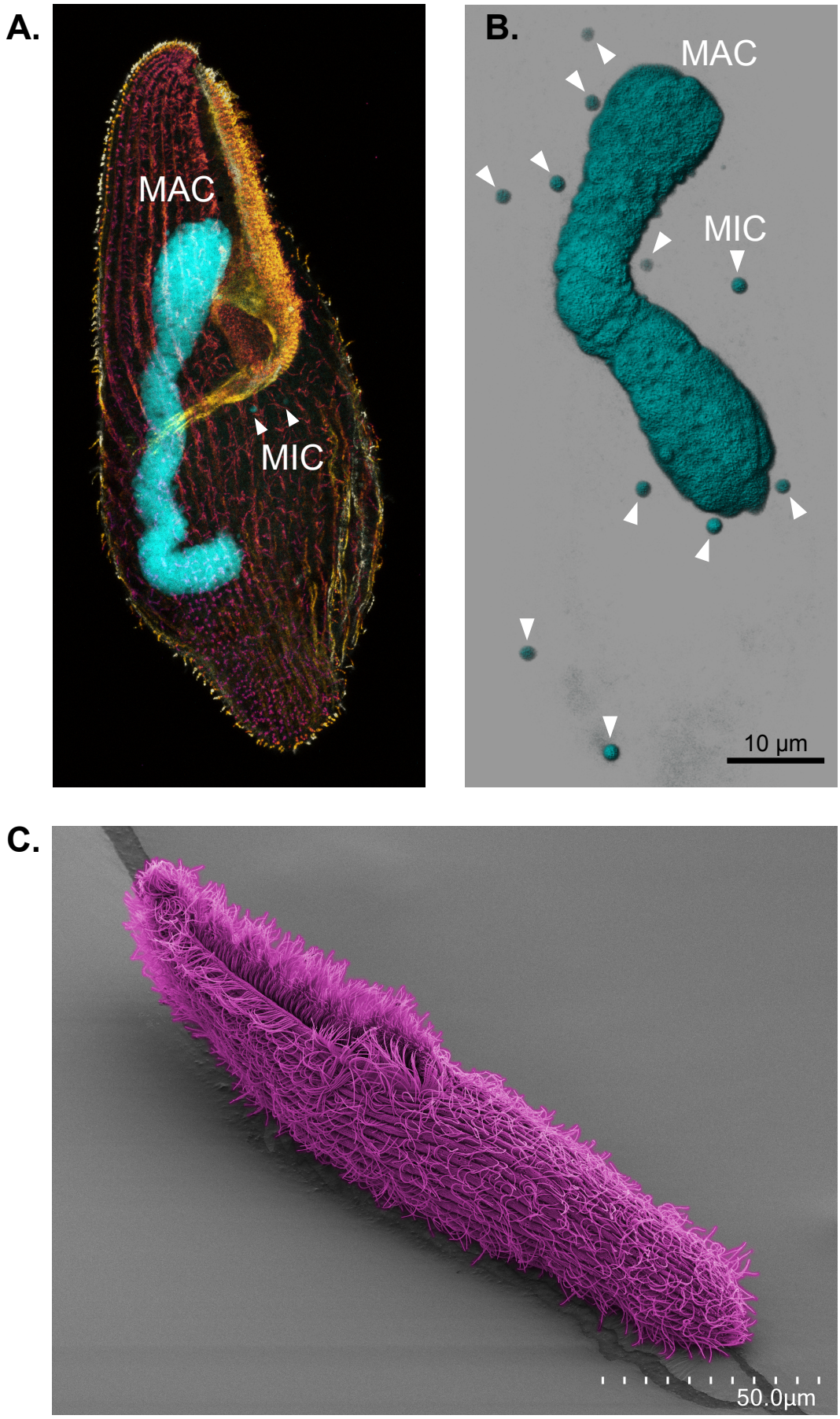

Figure 2.

A.

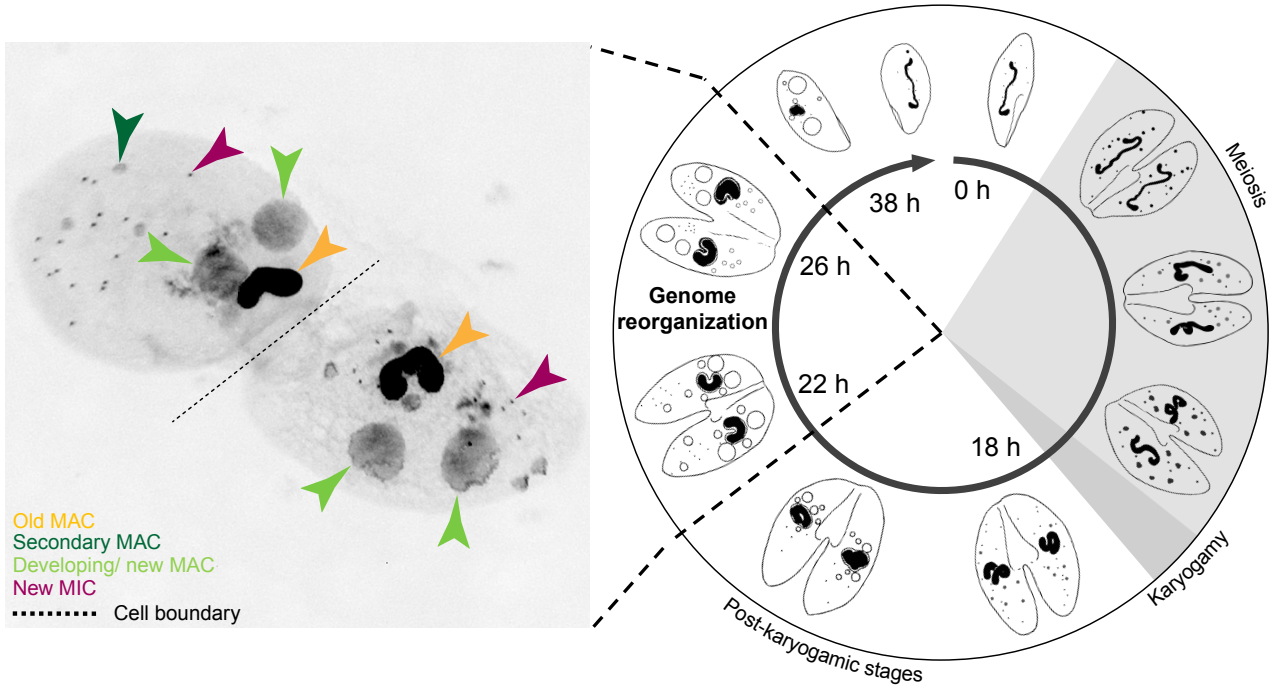
Old MAC
Secondary MAC
Developing/ new MAC
New MIC
Cell boundary
0 h
38 h
26 h
22 h
18 h
Genome reorganization
Meiosis
Karyogamy
Post-karyogamic stages

B.

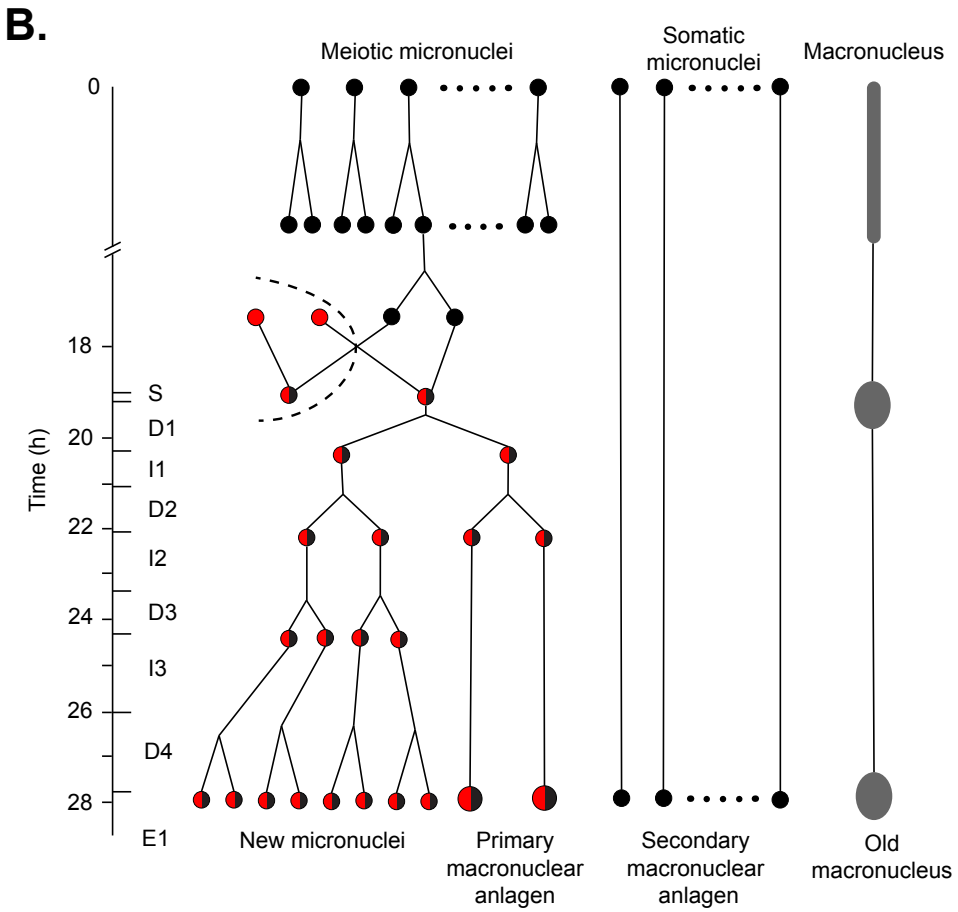
Meiotic micronuclei
Somatic micronuclei
Macronucleus
Time (h)
0
18
20
22
24
26
28
S
D1
I1
D2
I2
D3
I3
D4
E1
New micronuclei
Primary macronuclear anlagen
Secondary macronuclear anlagen
Old macronucleus

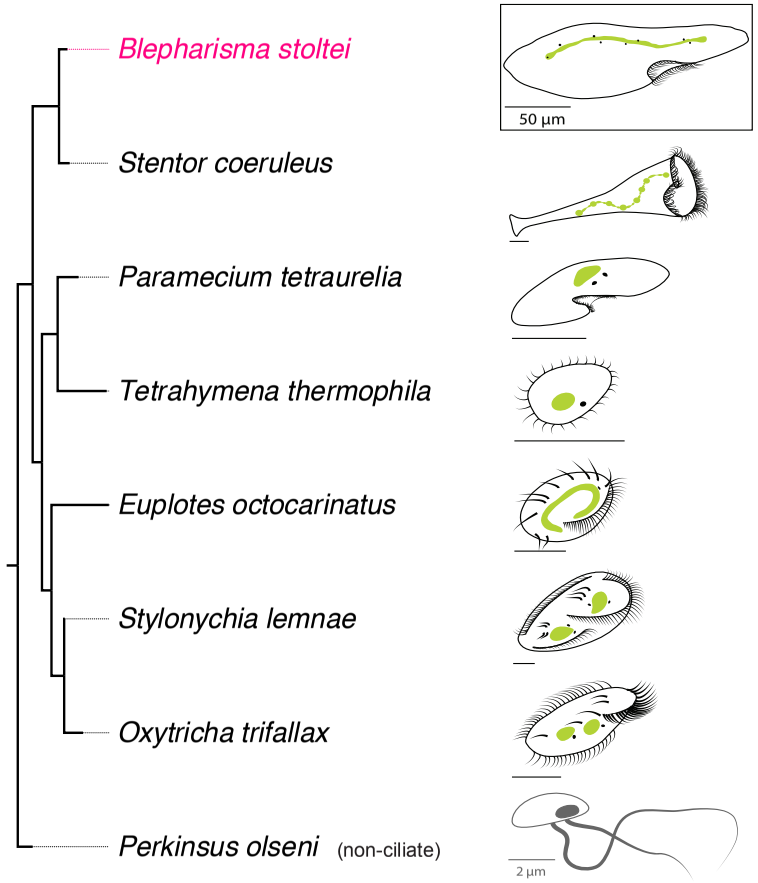

Species	Genome size (~Mb)	Genome architecture	Genes (zygosity)	Codon reassignments		
				UAA	UAG	UGA
***Blepharisma stoltei* (ATCC 302099)**	**41**	**Mini-chromosomes**	**25726 (n)**	*	*	**W**
Stentor coeruleus	77	?	31426 (?)	*	*	*
Paramecium tetraurelia	72	Chromosomes	39642 (n)	Q	Q	*
Tetrahymena thermophila	103	Chromosomes	26258 (n)	Q	Q	*
Euplotes octocarinatus	88	Nano-chromosomes	29076 (n)	*	*	C
Stylonychia lemnae	52	Nano-chromosomes	15102 (n)	Q	Q	*
Oxytricha trifallax	50	Nano-chromosomes	18400 (n)	Q	Q	*
Perkinsus olseni	63	Chromosomes	17342 (4n)	*	*	*

Figure 3.

Figure 4.

A.

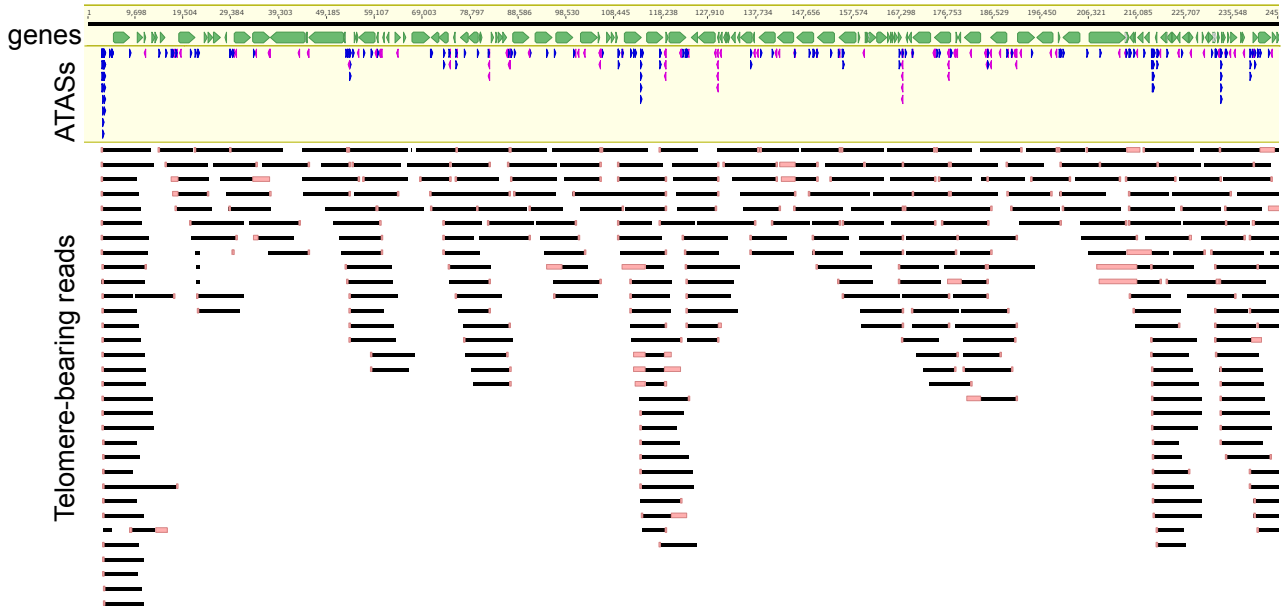
genes
ATASs
Telomere-bearing reads

B.

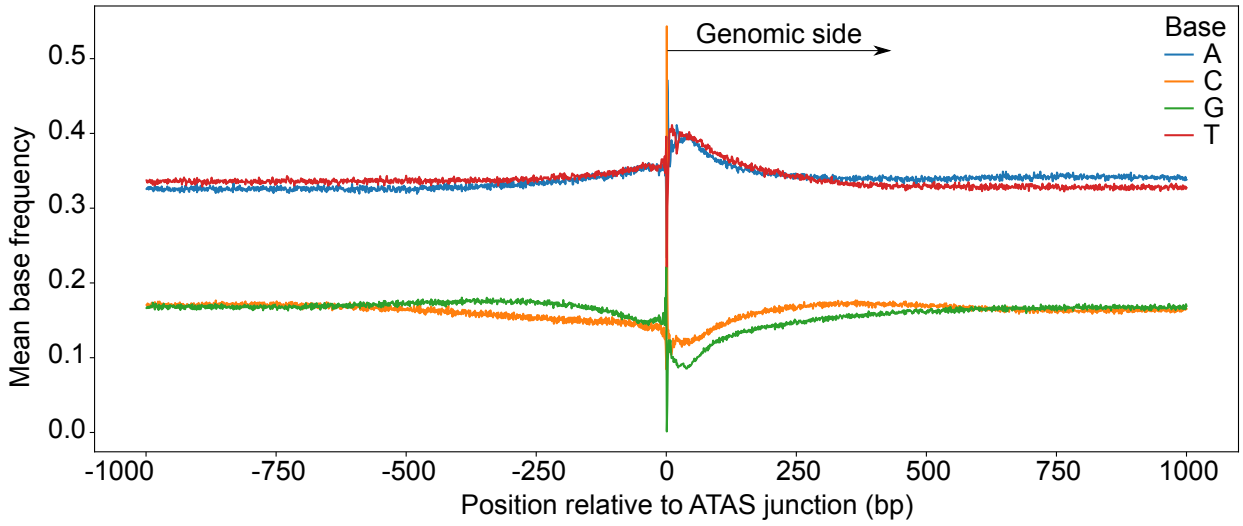
Genomic side
Base
A
C
G
T
Mean base frequency
0.0
0.1
0.2
0.3
0.4
0.5
-1000
-750
-500
-250
0
250
500
750
1000
Position relative to ATAS junction (bp)

Figure 5.

A.

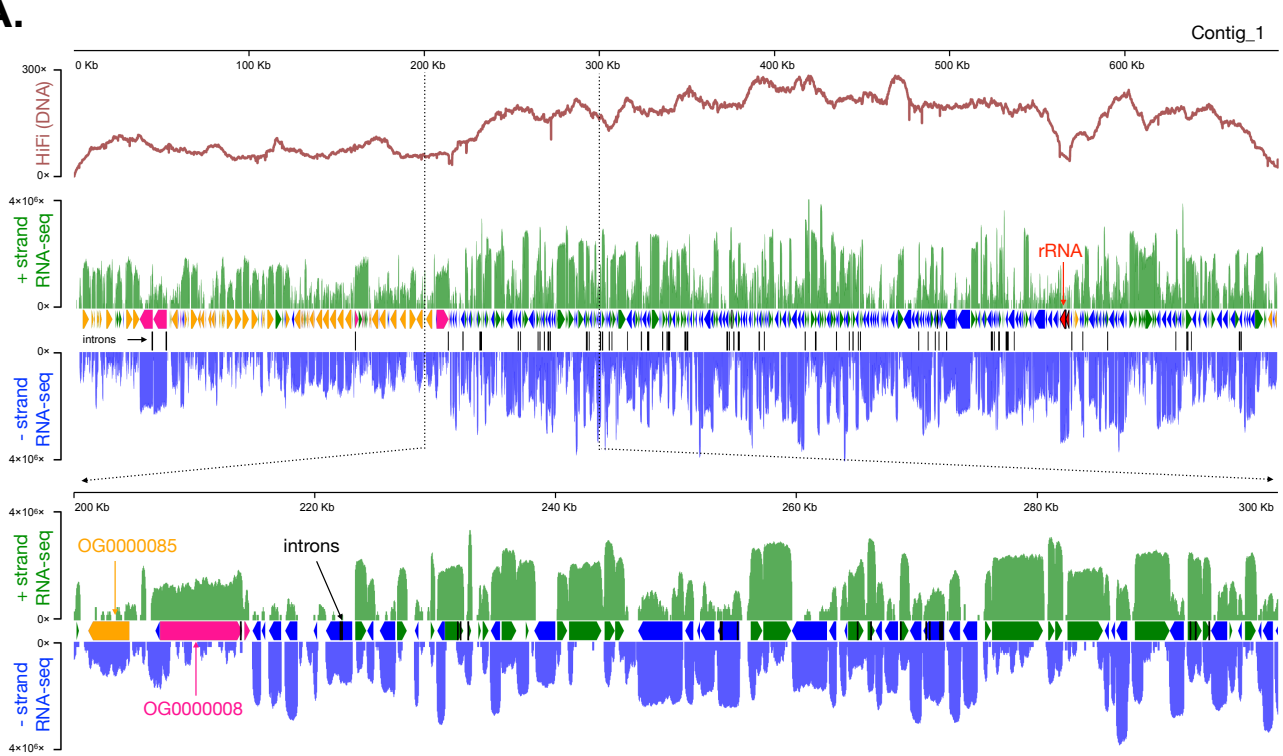

B.

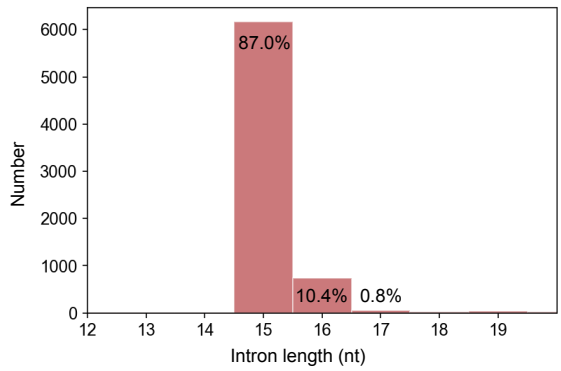

C.

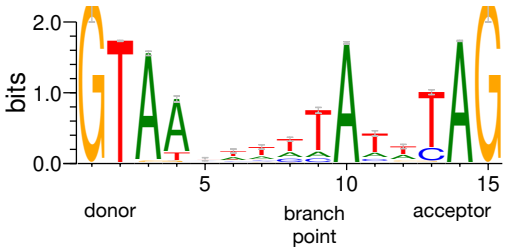

D.

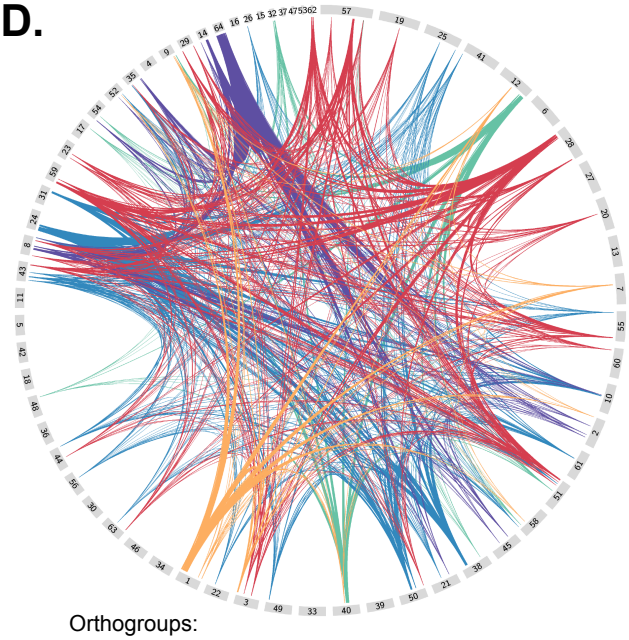

Orthogroups:

OG0000085 OG0000018 OG0000019

OG0000014 OG0000052

Figure 6.

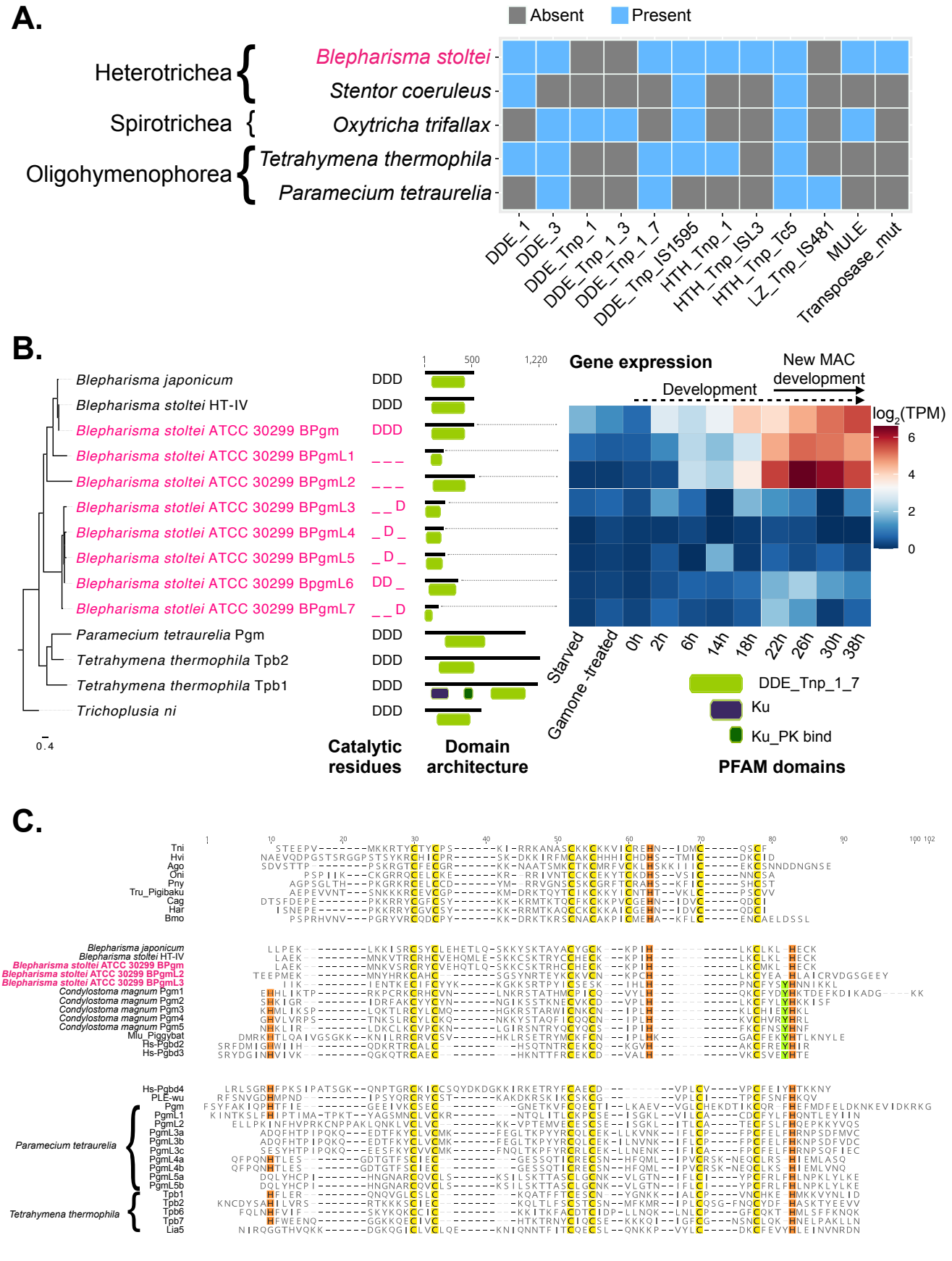
A.
Absent
Present
Heterotrichea
Spirotrichea
Oligohymenophorea
Blepharisma stoltei
Stentor coeruleus
Oxytricha trifallax
Tetrahymena thermophila
Paramecium tetraurelia
DDE_1
DDE_3
DDE_Tnp_1
DDE_Tnp_1_3
DDE_Tnp_1_7
DDE_Tnp_IS1595
HTH_Tnp_1
HTH_Tnp_ISL3
HTH_Tnp_Tc5
LZ_Tnp_IS481
MULE
Transposase_mut
B.
Blepharisma japonicum
Blepharisma stoltei HT-IV
Blepharisma stoltei ATCC 30299 BPgm
Blepharisma stoltei ATCC 30299 BPgmL1
Blepharisma stoltei ATCC 30299 BPgmL2
Blepharisma stoltei ATCC 30299 BPgmL3
Blepharisma stoltei ATCC 30299 BpgmL6
Blepharisma stoltei ATCC 30299 BPgmL7
Paramecium tetraurelia Pgm
Tetrahymena thermophila Tpb2
Tetrahymena thermophila Tpb1
Trichoplusia ni
0.4
Catalytic residues
Domain architecture
Gene expression
Development
New MAC development
log2(TPM)
Starved
Gamone -treated
0h
2h
6h
14h
18h
22h
26h
30h
38h
DDE_Tnp_1_7
Ku
Ku_PK bind
PFAM domains
C.
Tni
Hvi
Ago
Oni
Pny
Tru_Pigibaku
Cag
Har
Bmo
Blepharisma japonicum
Blepharisma stoltei HT-IV
Blepharisma stoltei ATCC 30299 BPgm
Blepharisma stoltei ATCC 30299 BPgmL2
Blepharisma stoltei ATCC 30299 BPgmL3
Condylostoma magnum Pgm1
Condylostoma magnum Pgm2
Condylostoma magnum Pgm3
Condylostoma magnum Pgm4
Condylostoma magnum Pgm5
Mlu_Piggybat
Hs-Pgbd2
Hs-Pgbd3
Hs-Pgbd4
PLE-wu
Pgm
PgmL1
PgmL2
PgmL3a
PgmL3b
PgmL3c
PgmL4a
PgmL4b
PgmL5a
PgmL5b
Paramecium tetraurelia
Tpb1
Tpb2
Tpb6
Tpb7
Lia5
Tetrahymena thermophila

Figure 7.

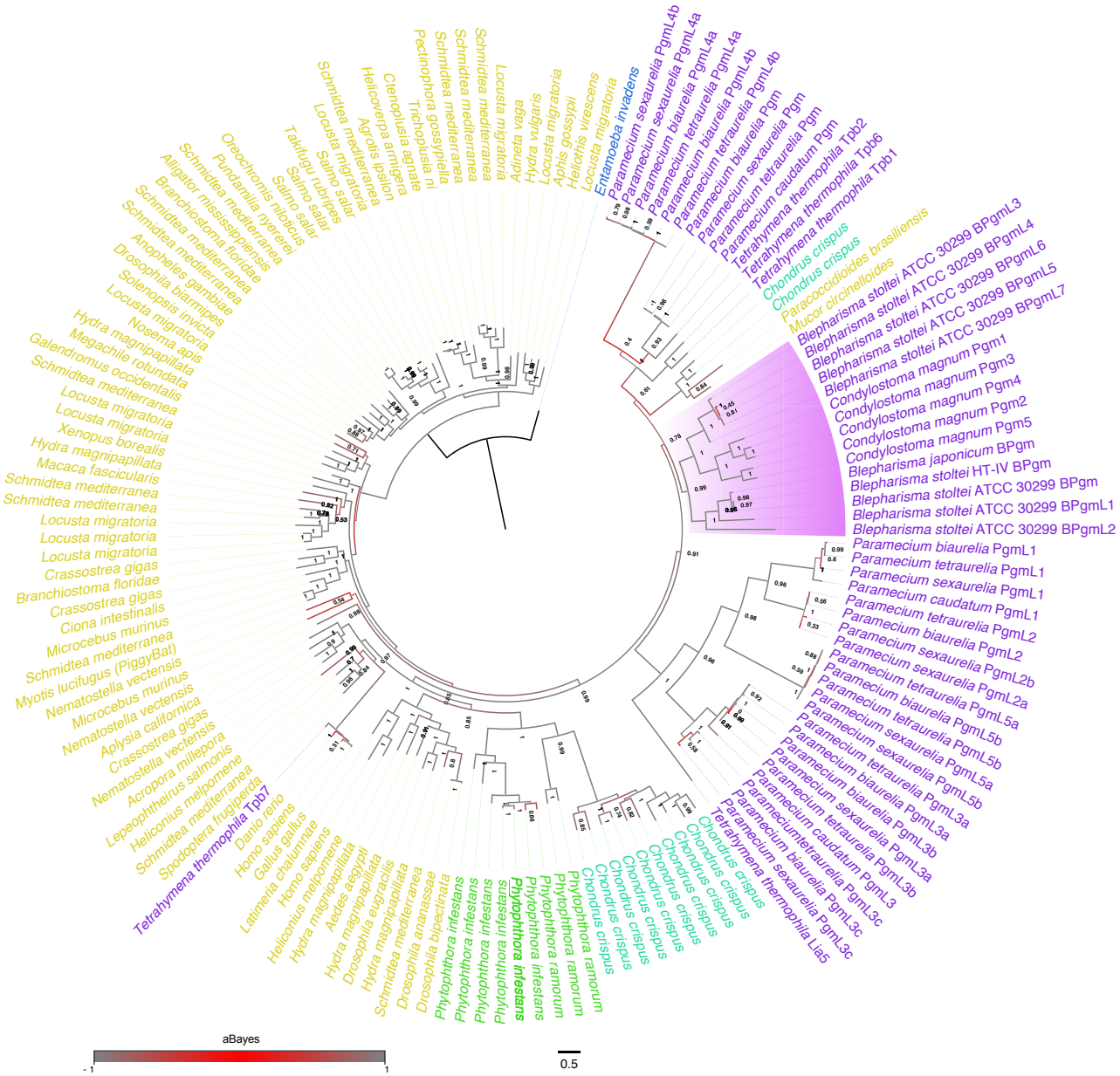

Entamoeba invadens
Paramecium sexaurelia PgmL4b
Paramecium sexaurelia PgmL4a
Paramecium biaurelia PgmL4a
Paramecium tetraurelia PgmL4a
Paramecium biaurelia PgmL4b
Paramecium tetraurelia PgmL4b
Paramecium biaurelia Pgm
Paramecium sexaurelia Pgm
Paramecium tetraurelia Pgm
Paramecium caudatum Pgm
Tetrahymena thermophila Tpb2
Tetrahymena thermophila Tpb6
Tetrahymena thermophila Tpb1
Chondrus crispus
Chondrus crispus
Paracoccidioides brasiliensis
Mucor circinelloides
Blepharisma stoltei ATCC 30299 BPgmL3
Blepharisma stoltei ATCC 30299 BPgmL4
Blepharisma stoltei ATCC 30299 BPgmL6
Blepharisma stoltei ATCC 30299 BPgmL5
Blepharisma stoltei ATCC 30299 BPgmL7
Condylostoma magnum Pgm1
Condylostoma magnum Pgm3
Condylostoma magnum Pgm4
Condylostoma magnum Pgm2
Condylostoma magnum Pgm5
Blepharisma japonicum BPgm
Blepharisma stoltei HT-IV BPgm
Blepharisma stoltei ATCC 30299 BPgm
Blepharisma stoltei ATCC 30299 BPgmL1
Blepharisma stoltei ATCC 30299 BPgmL2
Paramecium biaurelia PgmL1
Paramecium tetraurelia PgmL1
Paramecium sexaurelia PgmL1
Paramecium caudatum PgmL1
Paramecium tetraurelia PgmL2
Paramecium biaurelia PgmL2
Paramecium sexaurelia PgmL2b
Paramecium sexaurelia PgmL2a
Paramecium tetraurelia PgmL5a
Paramecium biaurelia PgmL5b
Paramecium tetraurelia PgmL5b
Paramecium sexaurelia PgmL5a
Paramecium sexaurelia PgmL5b
Paramecium tetraurelia PgmL3a
Paramecium biaurelia PgmL3a
Paramecium sexaurelia PgmL3b
Paramecium tetraurelia PgmL3b
Paramecium caudatum PgmL3
Paramecium biaurelia PgmL3c
Paramecium sexaurelia PgmL3c
Tetrahymena thermophila Lia5
Chondrus crispus
Chondrus crispus
Chondrus crispus
Chondrus crispus
Chondrus crispus
Chondrus crispus
Chondrus crispus
Chondrus crispus
Chondrus crispus
Chondrus crispus
Chondrus crispus
Chondrus crispus
Phytophthora ramorum
Phytophthora ramorum
Phytophthora ramorum
Phytophthora infestans
Phytophthora infestans
Phytophthora infestans
Phytophthora infestans
Phytophthora infestans
Drosophila bipectinata
Drosophila ananassae
Schmidtea mediterranea
Hydra magnipapillata
Aedes aegypti
Hydra magnipapillata
Drosophila eugracilis
Hydra magnipapillata
Heliconius melpomene
Latimeria chalumnae
Homo sapiens
Gallus gallus
Homo sapiens
Danio rerio
Tetrahymena thermophila Tpb7
Spodoptera frugiperda
Schmidtea mediterranea
Heliconius melpomene
Lepeophtheirus salmonis
Acropora millepora
Nematostella vectensis
Crassostrea gigas
Aplysia californica
Nematostella vectensis
Microcebus murinus
Nematostella vectensis
Myotis lucifugus (PiggyBat)
Schmidtea mediterranea
Microcebus murinus
Ciona intestinalis
Crassostrea gigas
Branchiostoma floridae
Crassostrea gigas
Locusta migratoria
Locusta migratoria
Locusta migratoria
Schmidtea mediterranea
Schmidtea mediterranea
Macaca fascicularis
Hydra magnipapillata
Xenopus borealis
Locusta migratoria
Locusta migratoria
Schmidtea mediterranea
Galendromus occidentalis
Megachile rotundata
Hydra magnipapillata
Nosema apis
Locusta migratoria
Solenopsis invicta
Drosophila biarmipes
Anopheles gambiae
Schmidtea mediterranea
Schmidtea mediterranea
Branchiostoma floridae
Alligator mississippiensis
Schmidtea mediterranea
Pundamilia nyererei
Oreochromis niloticus
Salmo salar
Salmo salar
Salmo salar
Takifugu rubripes
Locusta migratoria
Schmidtea mediterranea
Agrotis ipsilon
Helicoverpa armigera
Ctenoplusia agnate
Trichoplusia ni
Pectinophora gossypiella
Schmidtea mediterranea
Schmidtea mediterranea
Locusta migratoria
Adineta vaga
Hydra vulgaris
Locusta migratoria
Aphis gossypii
Heliothis virescens
Locusta migratoria
aBayes
-1
1
0.5

Figure 8.

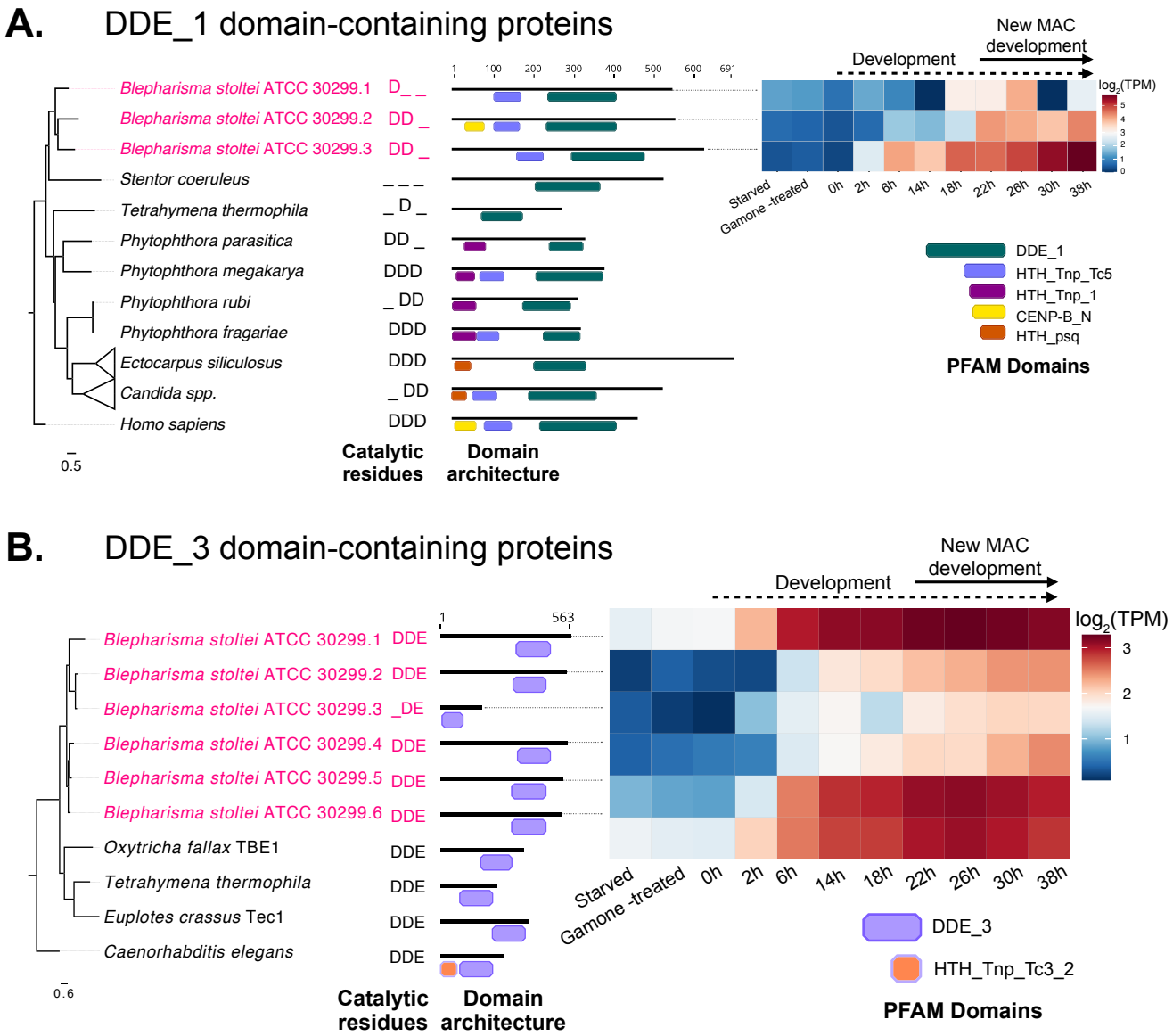
A.
DDE_1 domain-containing proteins
Blepharisma stoltei ATCC 30299.1
Blepharisma stoltei ATCC 30299.2
Blepharisma stoltei ATCC 30299.3
Stentor coeruleus
Tetrahymena thermophila
Phytophthora parasitica
Phytophthora megakarya
Phytophthora rubi
Phytophthora fragariae
Ectocarpus siliculosus
Candida spp.
Homo sapiens
D_ _
DD _
DD _
_ _ _
_ D _
DD _
DDD
_ DD
DDD
DDD
_ DD
DDD
0.5
Catalytic residues
Domain architecture
1
100
200
300
400
500
600
691
Development
New MAC development
log2(TPM)
Starved
Gamone -treated
0h
2h
6h
14h
18h
22h
26h
30h
38h
DDE_1
HTH_Tnp_Tc5
HTH_Tnp_1
CENP-B_N
HTH_psq
PFAM Domains
B.
DDE_3 domain-containing proteins
Blepharisma stoltei ATCC 30299.1
Blepharisma stoltei ATCC 30299.2
Blepharisma stoltei ATCC 30299.3
Blepharisma stoltei ATCC 30299.4
Blepharisma stoltei ATCC 30299.5
Blepharisma stoltei ATCC 30299.6
Oxytricha fallax TBE1
Tetrahymena thermophila
Euplotes crassus Tec1
Caenorhabditis elegans
DDE
DDE
_DE
DDE
DDE
DDE
DDE
DDE
DDE
0.6
Catalytic residues
Domain architecture
1
563
Development
New MAC development
log2(TPM)
3
2
1
Starved
Gamone -treated
0h
2h
6h
14h
18h
22h
26h
30h
38h
DDE_3
HTH_Tnp_Tc3_2
PFAM Domains

Figure 9.

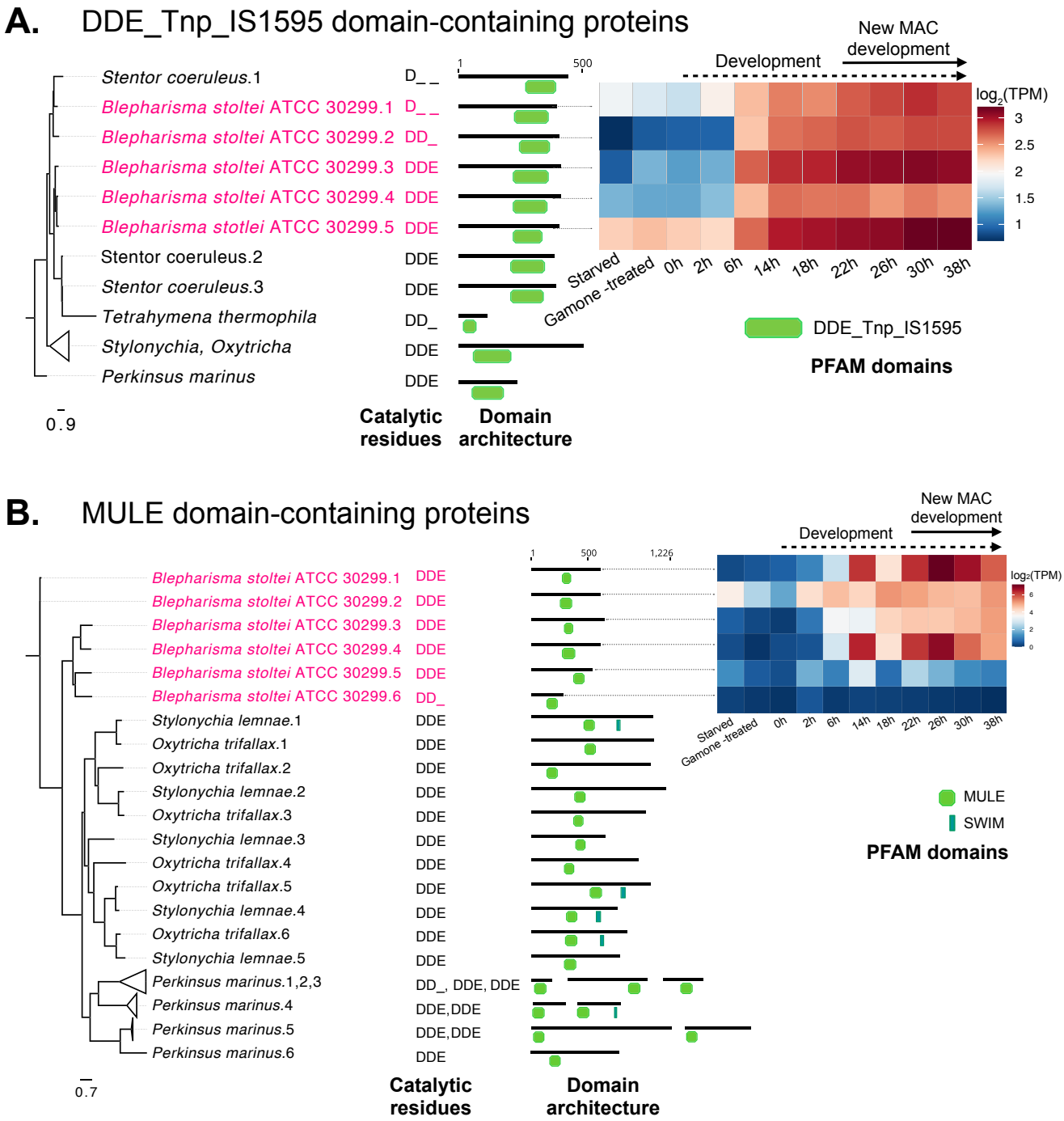
A.
DDE_Tnp_IS1595 domain-containing proteins
Stentor coeruleus.1
Blepharisma stoltei ATCC 30299.1
Blepharisma stoltei ATCC 30299.2
Blepharisma stoltei ATCC 30299.3
Blepharisma stoltei ATCC 30299.4
Blepharisma stotlei ATCC 30299.5
Stentor coeruleus.2
Stentor coeruleus.3
Tetrahymena thermophila
Stylonychia, Oxytricha
Perkinsus marinus
0.9
D_ _
D_ _
DD_
DDE
DDE
DDE
DDE
DDE
DD_
DDE
DDE
Catalytic residues
Domain architecture
1
500
Development
New MAC development
log2(TPM)
3
2.5
2
1.5
1
Starved
Gamone -treated
0h
2h
6h
14h
18h
22h
26h
30h
38h
DDE_Tnp_IS1595
PFAM domains
B.
MULE domain-containing proteins
Blepharisma stoltei ATCC 30299.1
Blepharisma stoltei ATCC 30299.2
Blepharisma stoltei ATCC 30299.3
Blepharisma stoltei ATCC 30299.4
Blepharisma stoltei ATCC 30299.5
Blepharisma stoltei ATCC 30299.6
Stylonychia lemnae.1
Oxytricha trifallax.1
Oxytricha trifallax.2
Stylonychia lemnae.2
Oxytricha trifallax.3
Stylonychia lemnae.3
Oxytricha trifallax.4
Oxytricha trifallax.5
Stylonychia lemnae.4
Oxytricha trifallax.6
Stylonychia lemnae.5
Perkinsus marinus.1,2,3
Perkinsus marinus.4
Perkinsus marinus.5
Perkinsus marinus.6
0.7
DDE
DDE
DDE
DDE
DDE
DD_
DDE
DDE
DDE
DDE
DDE
DDE
DDE
DDE
DDE
DDE
DD_, DDE, DDE
DDE,DDE
DDE,DDE
DDE
Catalytic residues
Domain architecture
1
500
1,226
Development
New MAC development
log2(TPM)
Starved
Gamone -treated
0h
2h
6h
14h
18h
22h
26h
30h
38h
MULE
SWIM
PFAM domains

Figure S1.

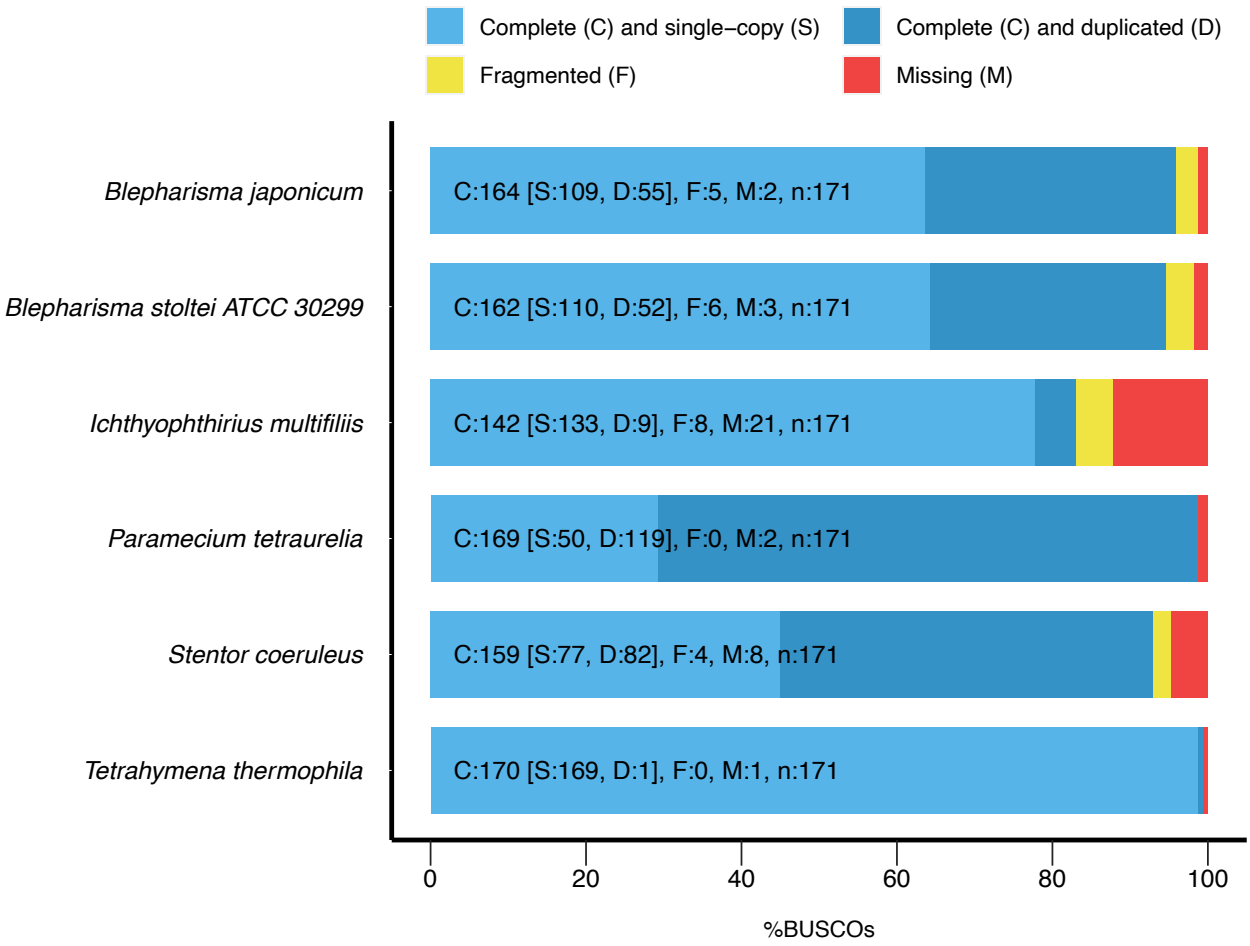
Complete (C) and single−copy (S)
Complete (C) and duplicated (D)
Fragmented (F)
Missing (M)
Blepharisma japonicum
C:164 [S:109, D:55], F:5, M:2, n:171
Blepharisma stoltei ATCC 30299
C:162 [S:110, D:52], F:6, M:3, n:171
Ichthyophthirius multifiliis
C:142 [S:133, D:9], F:8, M:21, n:171
Paramecium tetraurelia
C:169 [S:50, D:119], F:0, M:2, n:171
Stentor coeruleus
C:159 [S:77, D:82], F:4, M:8, n:171
Tetrahymena thermophila
C:170 [S:169, D:1], F:0, M:1, n:171
0
20
40
60
80
100
%BUSCOs

Figure S2.

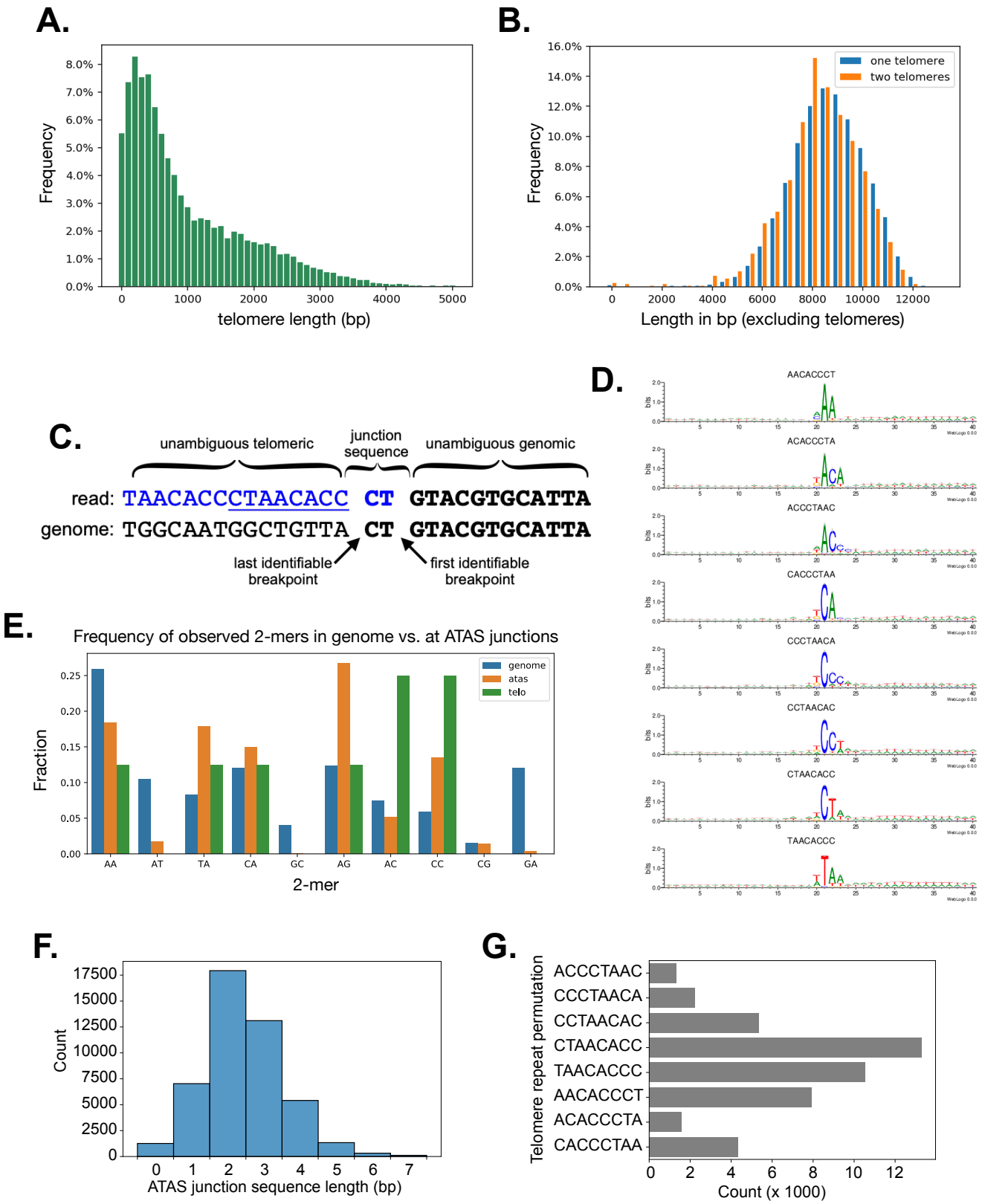
A.
Frequency
telomere length (bp)
B.
one telomere
two telomeres
Frequency
Length in bp (excluding telomeres)
C.
unambiguous telomeric
junction sequence
unambiguous genomic
read: TAACACCCTAACACC CT GTACGTGCATTA
genome: TGGCAATGGCTGTTA CT GTACGTGCATTA
last identifiable breakpoint
first identifiable breakpoint
D.
AACACCCT
ACACCCTA
ACCCTAAC
CACCCTAA
CCCTAACA
CCTAACAC
CTAACACC
TAACACCC
E.
Frequency of observed 2-mers in genome vs. at ATAS junctions
genome
atas
telo
Fraction
AA
AT
TA
CA
GC
AG
AC
CC
CG
GA
2-mer
F.
Count
ATAS junction sequence length (bp)
G.
Telomere repeat permutation
ACCCTAAC
CCCTAACA
CCTAACAC
CTAACACC
TAACACCC
AACACCCT
ACACCCTA
CACCCTAA
Count (x 1000)

Figure S3.

A.

C.

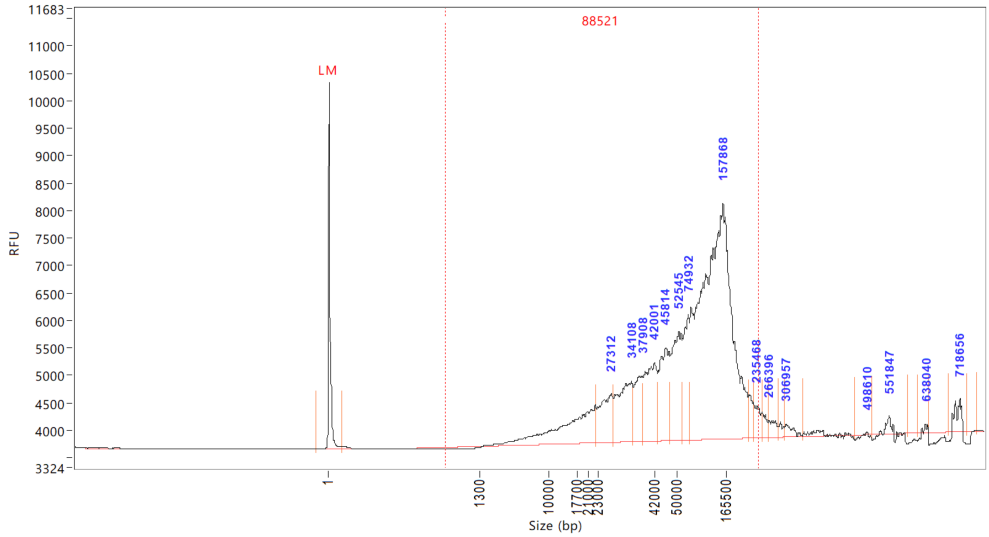

D.

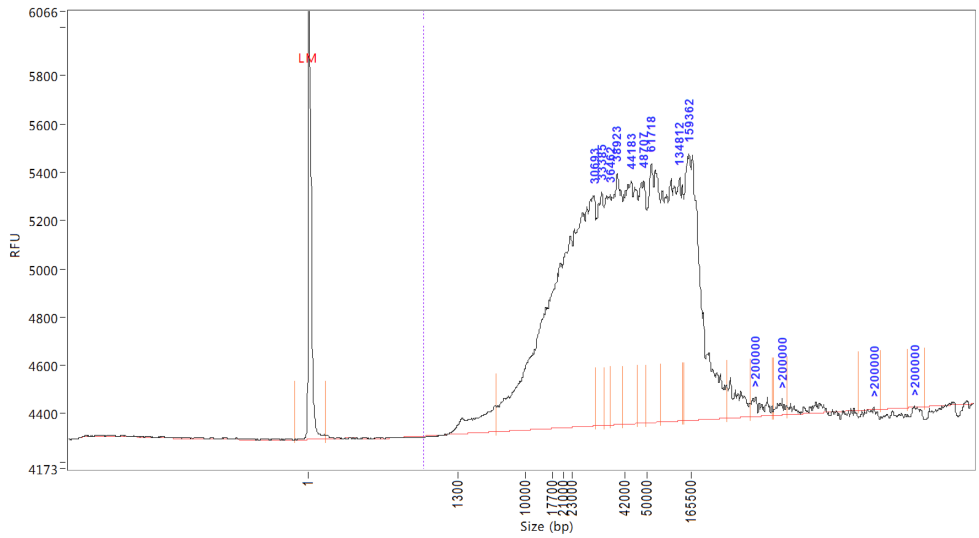

Figure S4.

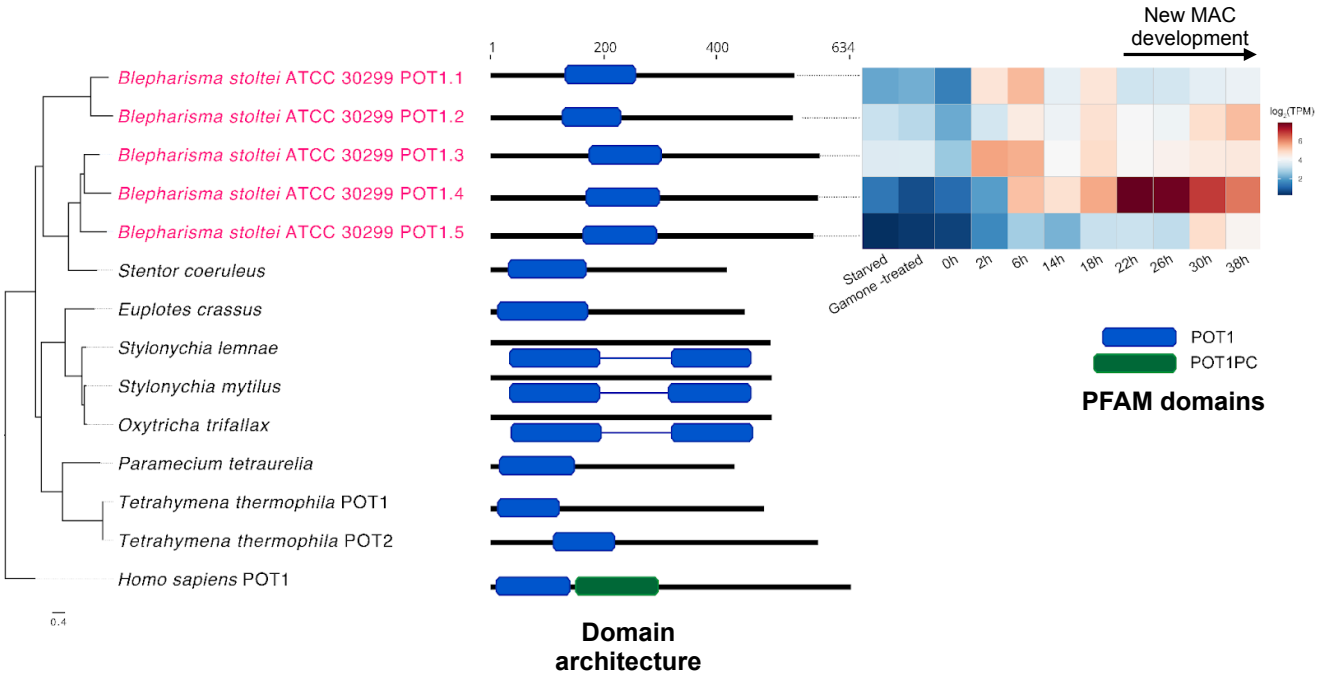
Blepharisma stoltei ATCC 30299 POT1.1
Blepharisma stoltei ATCC 30299 POT1.2
Blepharisma stoltei ATCC 30299 POT1.3
Blepharisma stoltei ATCC 30299 POT1.4
Blepharisma stoltei ATCC 30299 POT1.5
Stentor coeruleus
Euplotes crassus
Stylonychia lemnae
Stylonychia mytilus
Oxytricha trifallax
Paramecium tetraurelia
Tetrahymena thermophila POT1
Tetrahymena thermophila POT2
Homo sapiens POT1
0.4
1
200
400
634
Domain architecture
New MAC development
Starved
Gamone -treated
0h
2h
6h
14h
18h
22h
26h
30h
38h
log2(TPM)
POT1
POT1PC
PFAM domains

Figure S5.

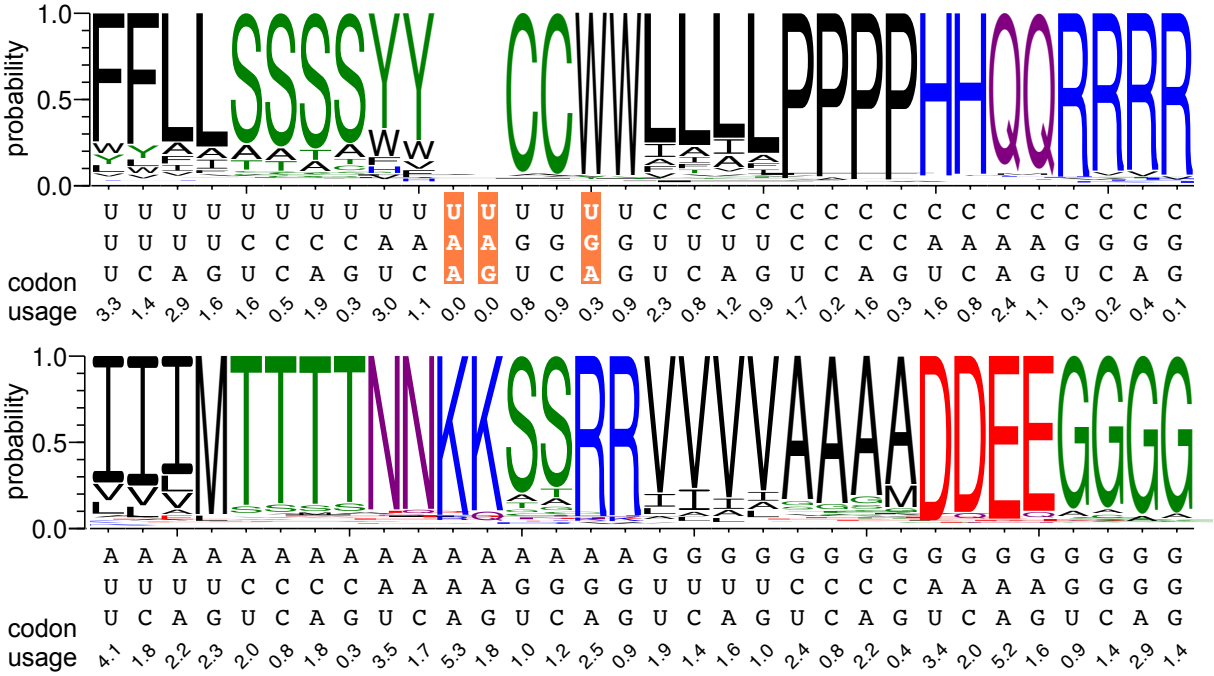
probability
1.0
0.5
0.0
codon
usage
U U U U U U U U U U U U U U U U C C C C C C C C C C C C C C C C
U U U U C C C C A A A A G G G G U U U U C C C C A A A A G G G G
U C A G U C A G U C A G U C A G U C A G U C A G U C A G U C A G
3.3 1.4 2.9 1.6 1.6 0.5 1.9 0.3 3.0 1.1 0.0 0.0 0.8 0.9 0.3 0.9 2.3 0.8 1.2 0.9 1.7 0.2 1.6 0.3 1.6 0.8 2.4 1.1 0.3 0.2 0.4 0.1
probability
1.0
0.5
0.0
codon
usage
A A A A A A A A A A A A A A A A G G G G G G G G G G G G G G G G
U U U U C C C C A A A A G G G G U U U U C C C C A A A A G G G G
U C A G U C A G U C A G U C A G U C A G U C A G U C A G U C A G
4.1 1.8 2.2 2.3 2.0 0.8 1.8 0.3 3.5 1.7 5.3 1.8 1.0 1.2 2.5 0.9 1.9 1.4 1.6 1.0 2.4 0.8 2.2 0.4 3.4 2.0 5.2 1.6 0.9 1.4 2.9 1.4

Figure S6.

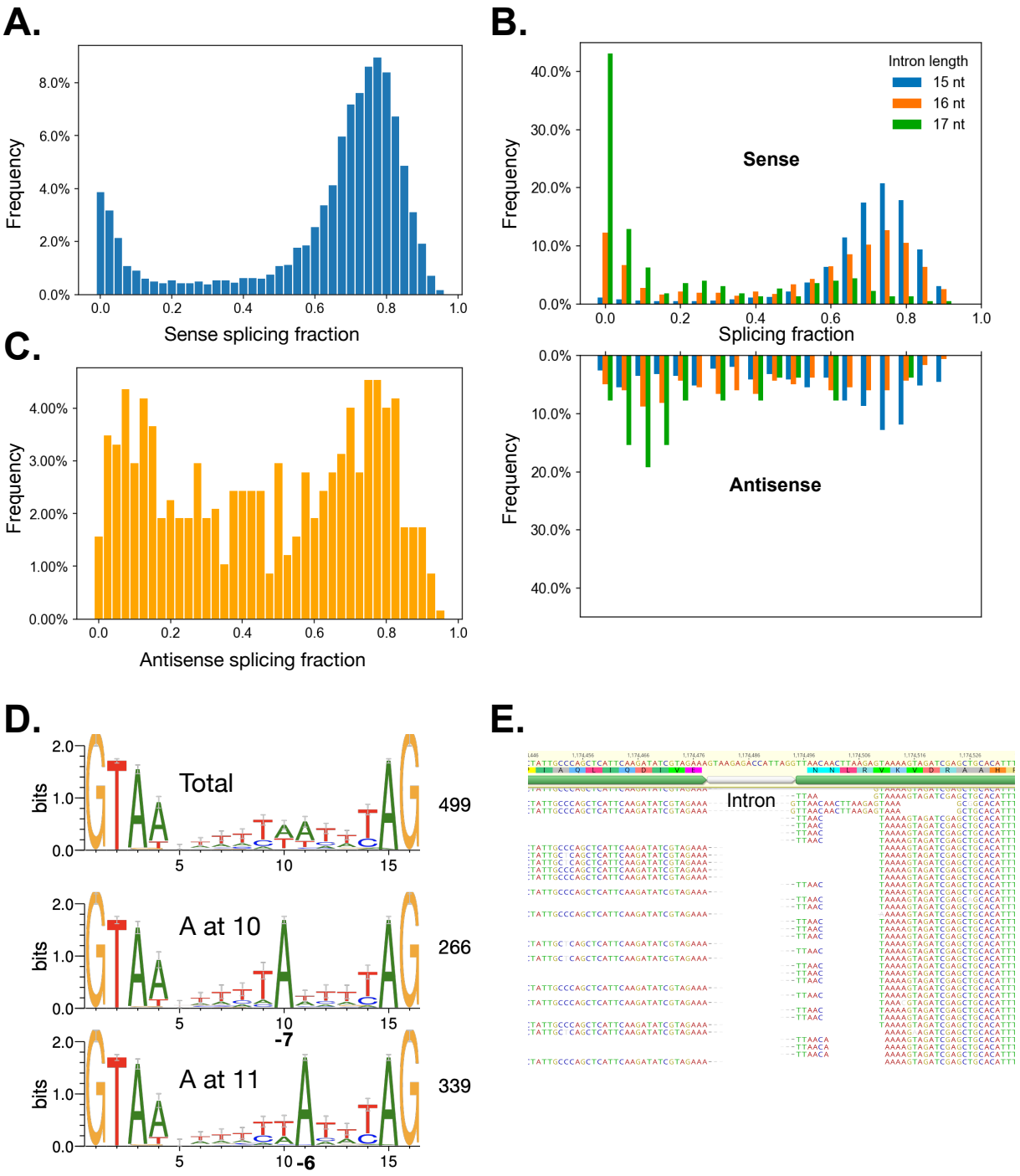
A.
Frequency
8.0%
6.0%
4.0%
2.0%
0.0%
0.0
0.2
0.4
0.6
0.8
1.0
Sense splicing fraction
B.
Intron length
15 nt
16 nt
17 nt
Sense
Frequency
40.0%
30.0%
20.0%
10.0%
0.0%
Splicing fraction
Antisense
C.
Frequency
4.00%
3.00%
2.00%
1.00%
0.00%
Antisense splicing fraction
D.
Total
499
A at 10
266
A at 11
339
bits
2.0
1.0
0.0
5
10
15
-7
-6
E.
Intron

Figure S7.

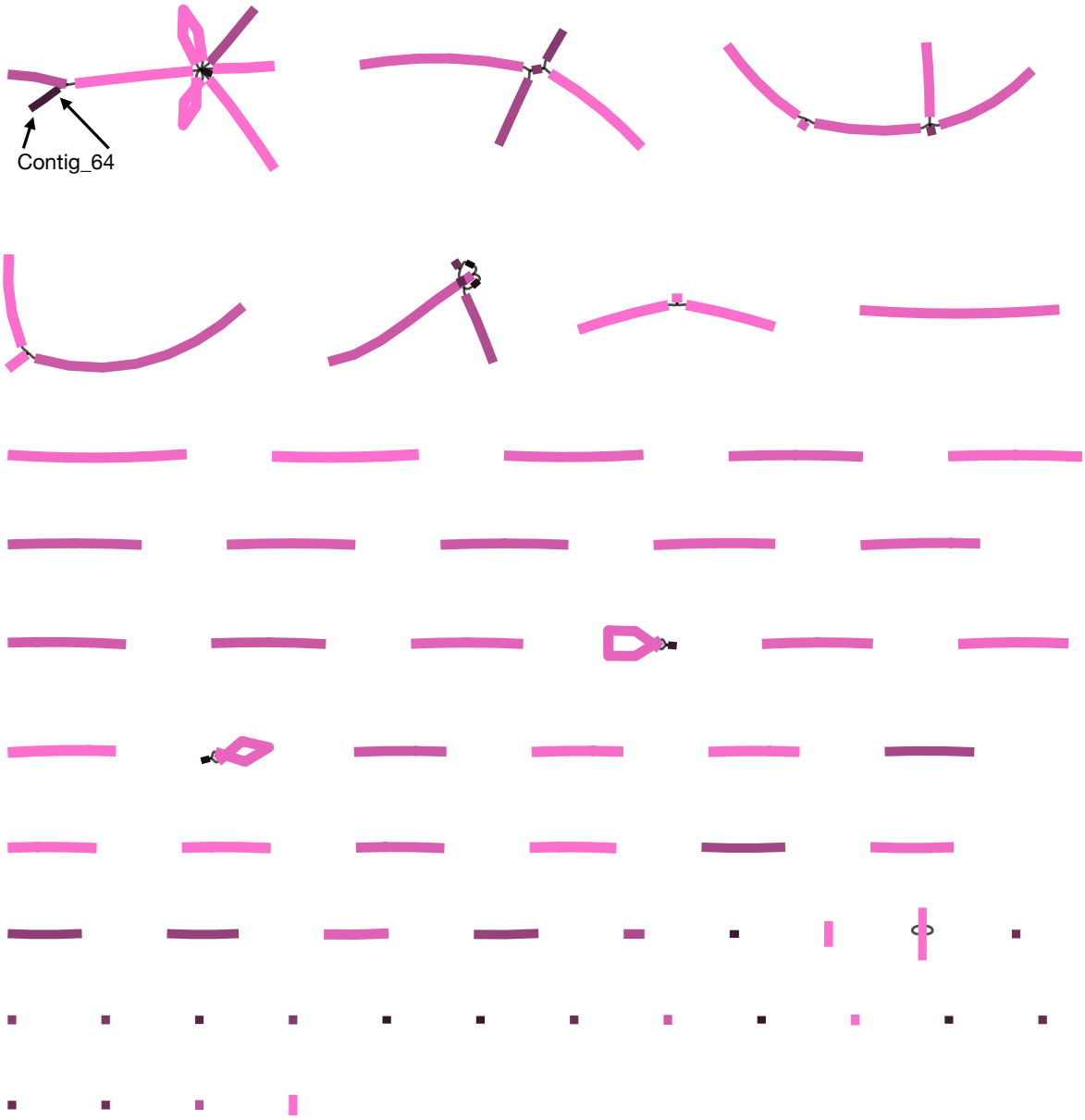

Figure S8.

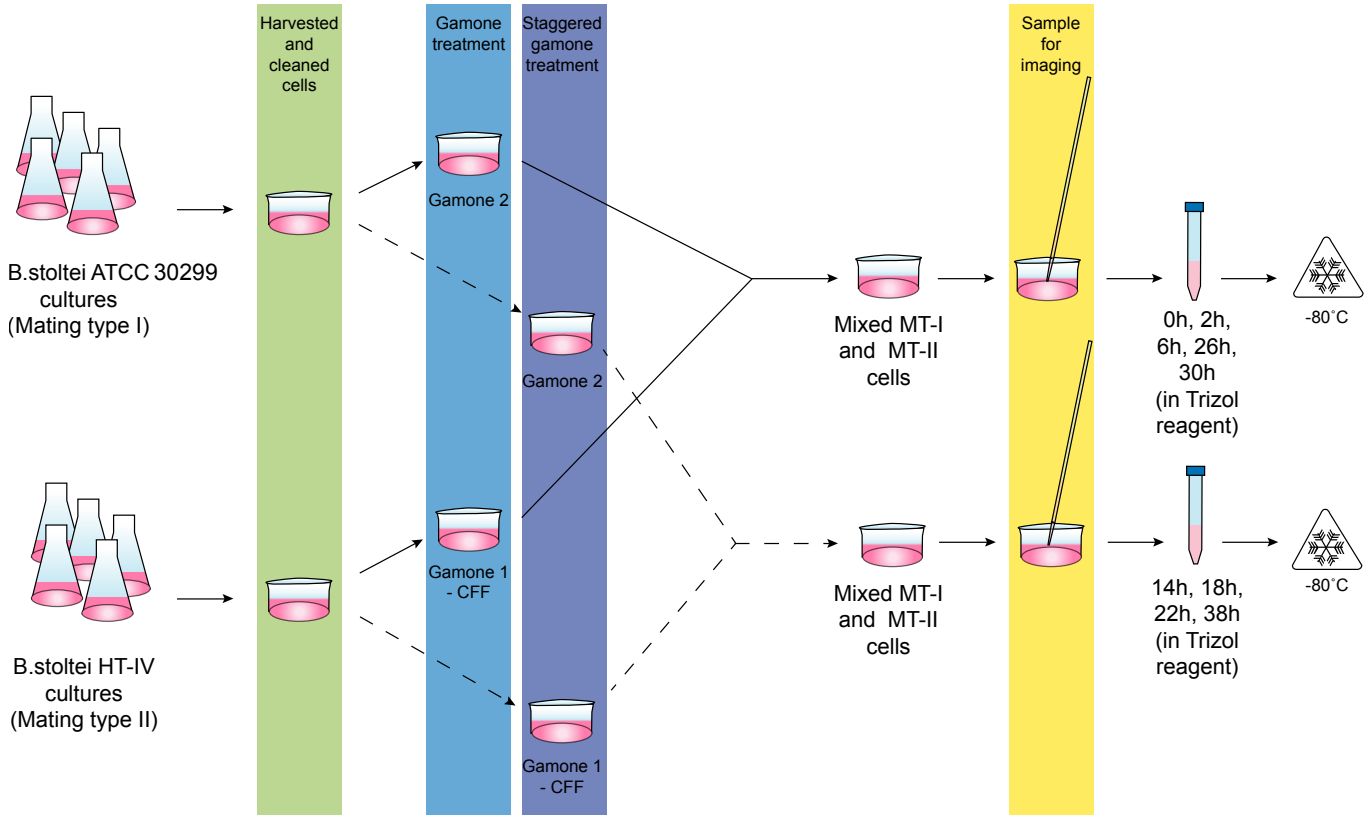
Harvested and cleaned cells
Gamone treatment
Staggered gamone treatment
Sample for imaging
B.stoltei ATCC 30299 cultures (Mating type I)
B.stoltei HT-IV cultures (Mating type II)
Gamone 2
Gamone 2
Gamone 1 - CFF
Gamone 1 - CFF
Mixed MT-I and MT-II cells
Mixed MT-I and MT-II cells
0h, 2h, 6h, 26h, 30h (in Trizol reagent)
14h, 18h, 22h, 38h (in Trizol reagent)
-80˚C
-80˚C

Figure S9.

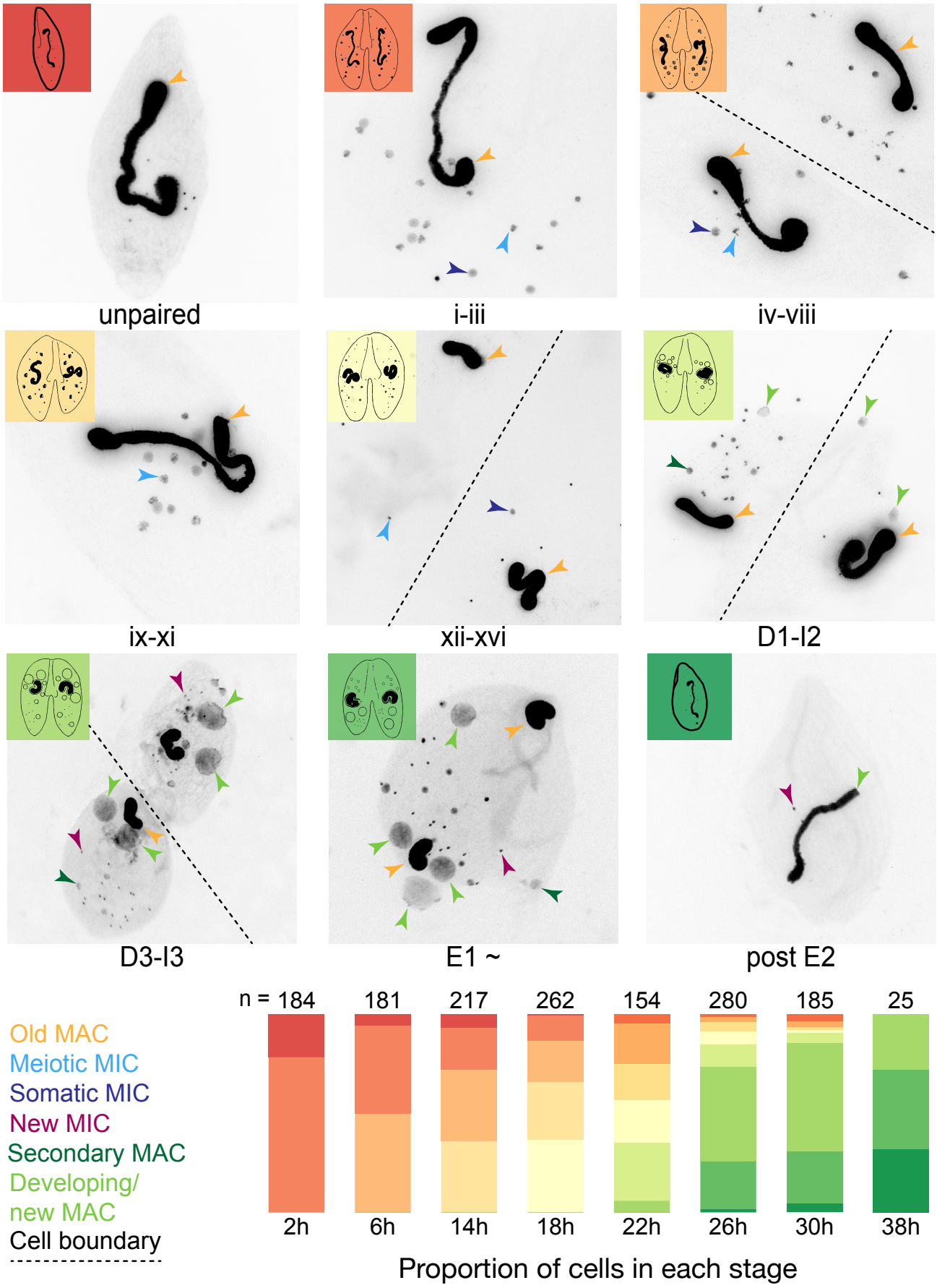
unpaired
i-iii
iv-viii
ix-xi
xii-xvi
D1-I2
D3-I3
E1 ~
post E2
n = 184
181
217
262
154
280
185
25
Old MAC
Meiotic MIC
Somatic MIC
New MIC
Secondary MAC
Developing/
new MAC
Cell boundary
2h
6h
14h
18h
22h
26h
30h
38h
Proportion of cells in each stage

Figure S10.

A. Dicers, Dicer-likes and Dicer-derivatives

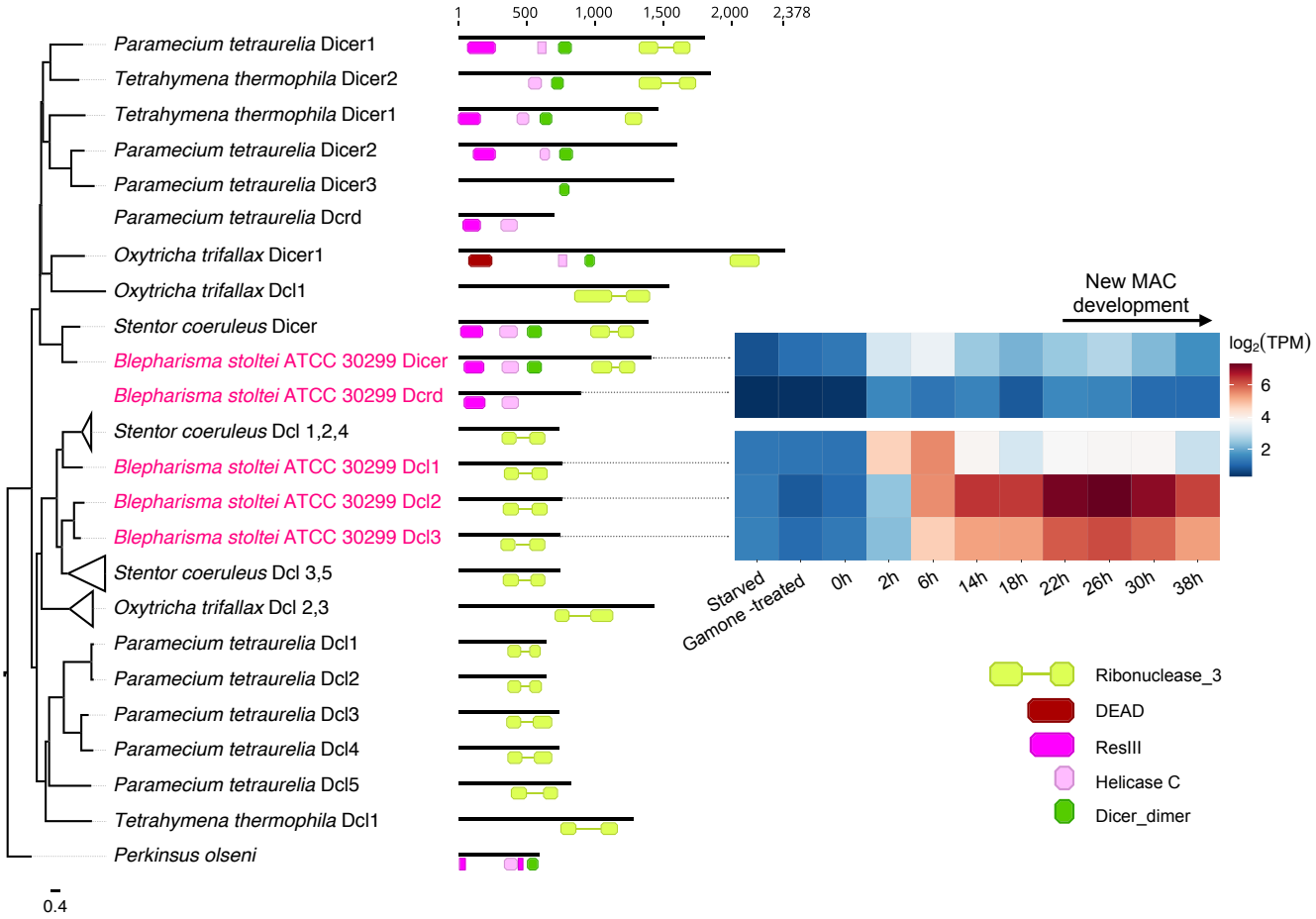

B. Piwi proteins

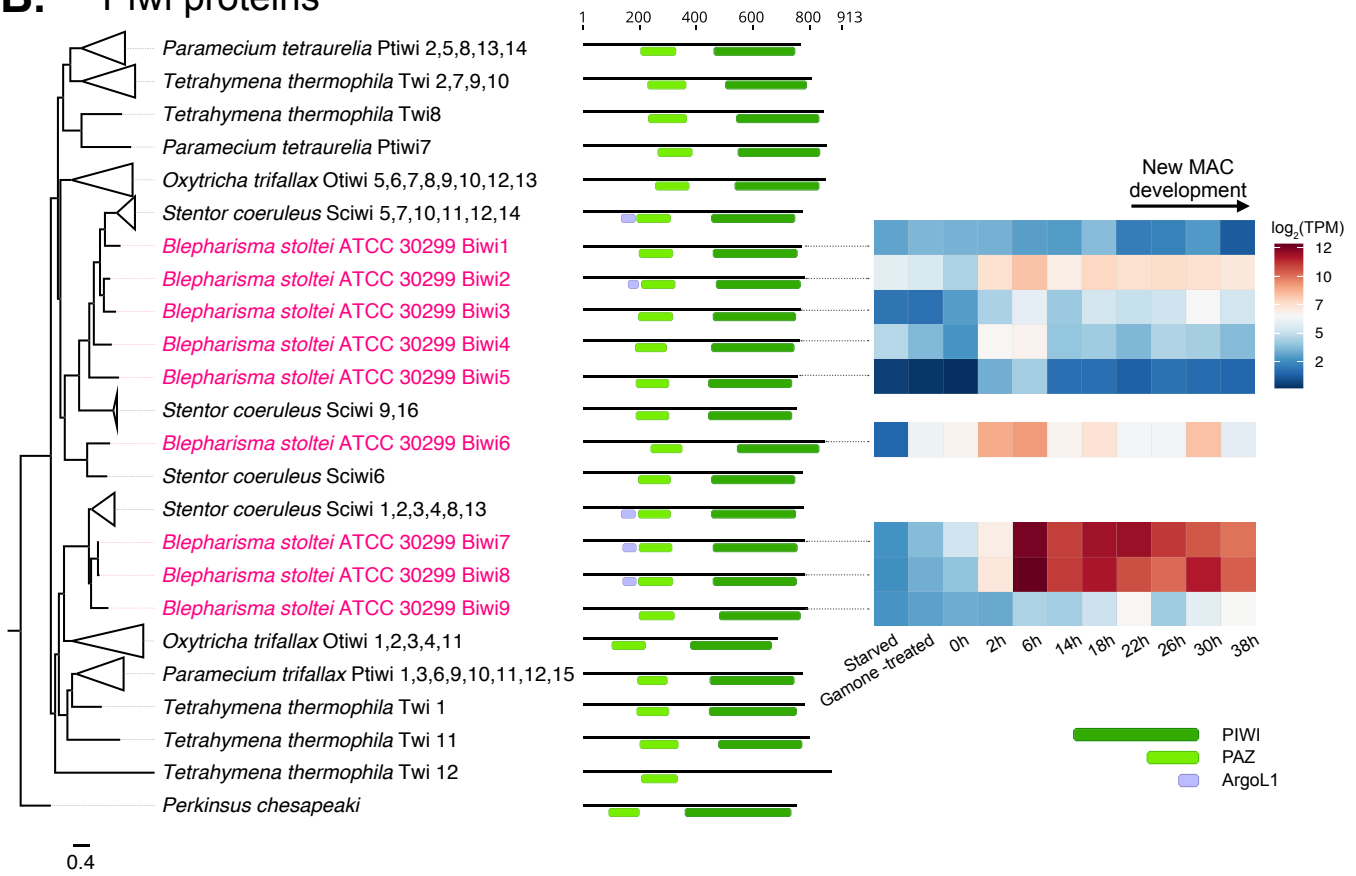

Figure S11.

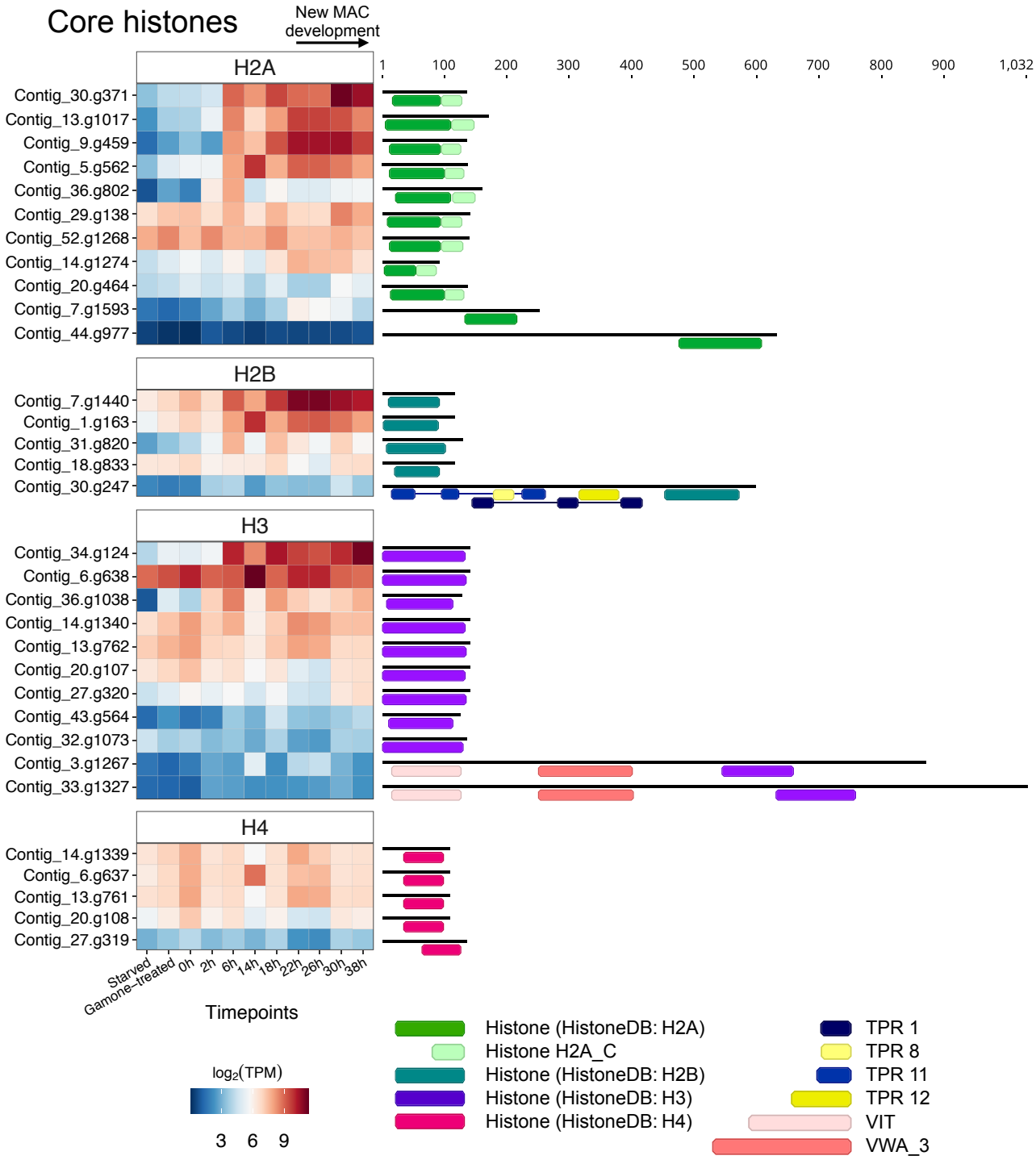
Core histones
New MAC development
H2A
Contig_30.g371
Contig_13.g1017
Contig_9.g459
Contig_5.g562
Contig_36.g802
Contig_29.g138
Contig_52.g1268
Contig_14.g1274
Contig_20.g464
Contig_7.g1593
Contig_44.g977
1
100
200
300
400
500
600
700
800
900
1,032
H2B
Contig_7.g1440
Contig_1.g163
Contig_31.g820
Contig_18.g833
Contig_30.g247
H3
Contig_34.g124
Contig_6.g638
Contig_36.g1038
Contig_14.g1340
Contig_13.g762
Contig_20.g107
Contig_27.g320
Contig_43.g564
Contig_32.g1073
Contig_3.g1267
Contig_33.g1327
H4
Contig_14.g1339
Contig_6.g637
Contig_13.g761
Contig_20.g108
Contig_27.g319
Starved
Gamone-treated
0h
2h
6h
14h
18h
22h
26h
30h
38h
Timepoints
log2(TPM)
3
6
9
Histone (HistoneDB: H2A)
Histone H2A_C
Histone (HistoneDB: H2B)
Histone (HistoneDB: H3)
Histone (HistoneDB: H4)
TPR 1
TPR 8
TPR 11
TPR 12
VIT
VWA_3